UNIVERSITAT DE BARCELONA

Observational consequences of Black Holes in the Universe: From dark matter candidates to quasars

Marc Oncins Fernández

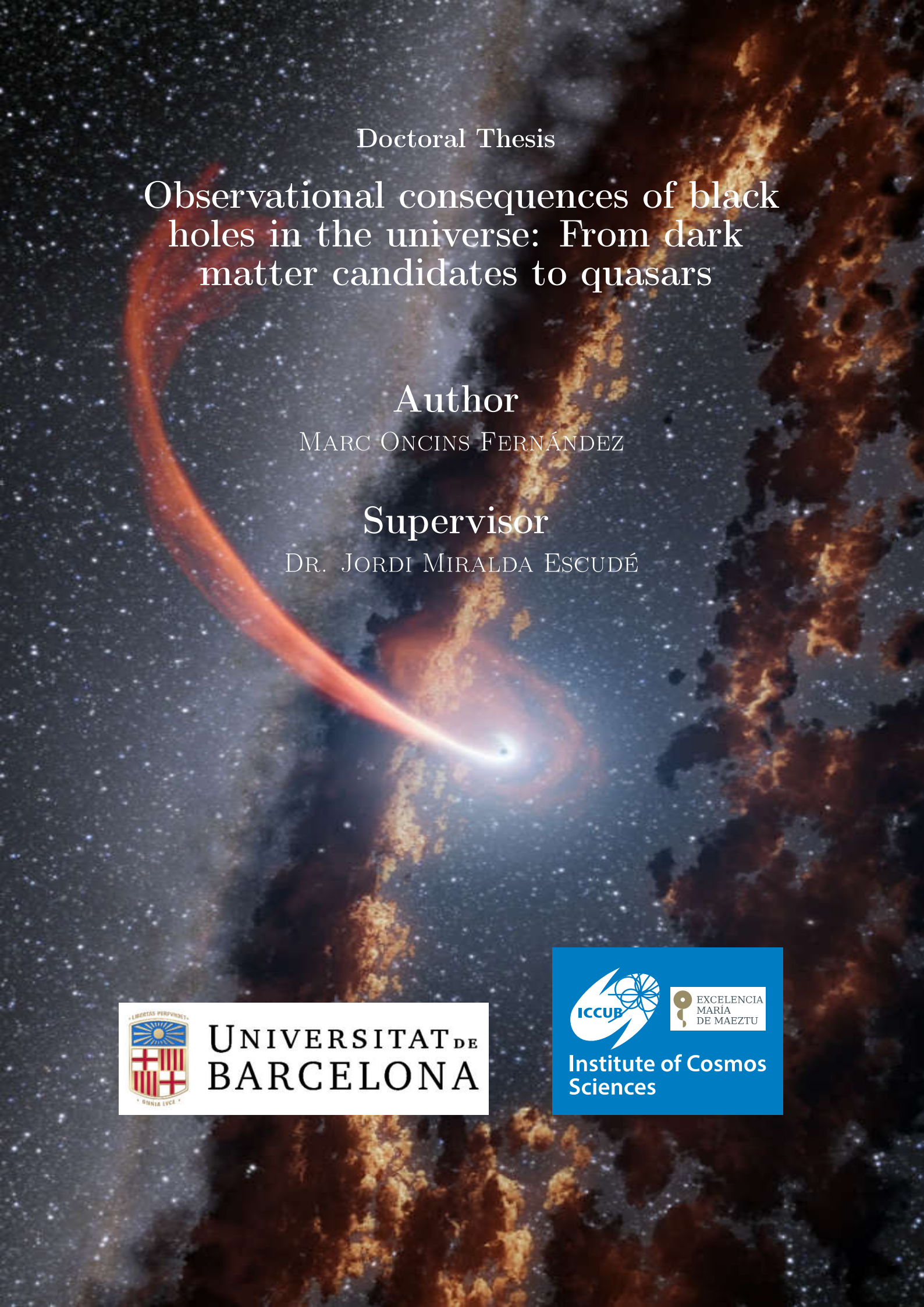

Doctoral Thesis

Observational consequences of black holes in the universe: From dark matter candidates to quasars

Author

Marc Oncins Fernández

Supervisor

Dr. Jordi Miralda Escudé

Universitat de Barcelona

ICCUB Excelencia María de Maeztu

Institute of Cosmos Sciences

Observational consequences of black holes in the universe: From dark matter candidates to quasars

Memòria presentada per optar al grau de doctor per la

Universitat de Barcelona

Programa de doctorat en Física

Autor
Marc Oncins Fernández

Director
Dr. Jordi Miralda Escudé

Tutor
Dr. Alberto Manrique Oliva

Departament de Física Quàntica i Astrofísica

Gener 2022

UNIVERSITAT DE BARCELONA

Marc

Dedicat a tots els que heu
continuat creient en mi

Mathematics would certainly have not come into existence
if one had known from the beginning that there was in nature
no exactly straight line, no actual circle, no absolute magnitude.
Friedrich Nietzsche

The better is the mortal enemy of the good
Montesquieu

"Can a man still be brave if he's afraid?"
"That is the only time a man can be brave."
Game of Thrones, 1996, George R. R. Martin

Credit to NASA/JPL-Caltech for the cover

ABSTRACT

The existence of black holes that go beyond the mass typically assigned to them by their stellar origin has been known for some time. The situation has changed however with the realisation that a subset of primordial black holes (PBHs) could form all of the dark matter with individually very low masses of up to $10^{-11}\,M_\odot$. On the opposite mass range Super Massive Black holes (SMBHs) have been found at very early redshifts, and their influence on the universe as a whole is still being discussed. Using both numerical models and instrumental techniques, we study the observational consequences of both of these extreme black holes and analyze their importance.

We start our work by studying all current existing ways there are that would result in observational evidence from PBHs being all the dark matter. Despite their varied origins, the standard PBH formation path comes from the collapse of perturbations after inflation, which permits the use of the CMB to constrain certain scales. We also make a in depth look at microlensing, which makes up the largest constraints on PBHs as dark matter, and conclude that despite its usefulness the method will not improve the constraints for lower mass ranges. We make similar analyses of gravitational waves and PBH evaporation, with the former having a lot of potential but requiring the next generation of experiments to make useful constraints, and the later being a simple case where it is unlikely further constraints will come up. We make a small aside to detail the differences between monochromatic and extended mass distributions for PBHs, before finally zeroing in the last remaining window for PBHs to be all the dark matter, concretely on its upper limits around $10^{-12}\,M_\odot$.

The PBHs in this mass range would leave very few observational results, being both too small to detect through lensing and too big to be affected by evaporation. A possible way to constrain them would be through their interaction with stars. As stars form in the very early universe in $z \sim 20$, the adiabatic contraction as the protostar is born will accrue a large dark matter density gravitational bound to the star, due to the high density and low velocity dispersion common in high redshifts. If PBHs were all the dark matter, they will orbit the star, following a flat eccentricity distribution. There is a chance some of the orbits of the PBHs naturally cross the star. While the dynamical friction of a main sequence star on the PBH is usually negligible on short time frames, it is enough to bring the PBH to the core of the star within the Hubble time, capturing it. Once at the center, the PBH will accrete the star within 10^9 years resulting in a black hole the mass of the star. This should result in a subsolar mass black hole that could not have had a stellar origin.

We compute the capture rate of a number of stars with differing masses for $10^{-12}\,M_\odot$ PBHs. We use stellar models from MENSA ranging from 0.3 to $1\,M_\odot$ for the stars, compute the dynamical friction numerically using two different types and take into account the effect of perturbations coming from the rest of the galaxy to set a maximum radius beyond which capture is uncertain. The result, which we call Ξ, is generic and can be used to compute the capture rate for any dark matter density and velocity dispersion. We apply Ξ to the case $z \sim 20$, and our models tells us that we expect all stars represented on our stellar models that are within $\sim 0.005 R_{Vir}$ of the center of their galaxies to end capturing a PBH and being accreted in turn. The capture rate lowers with distance, but it is still relevant up to $R = 0.1 R_{Vir}$. In even the worst of cases this should result in a wealth of subsolar mass black holes that would survive to this day and could be observed.

We finally study the case of quasi stellar objects (QSOs), SMBHs with very high luminosity and whose contribution to reionization is still uncertain. The presence of a Lyman α nebulae surrounding them is relevant to this matter, as the we do not know whereas it is present for every QSO and we only see the brightest of them or if they are unique cases. A good way to solve this issue is through the technique called stacking. This allows the use of multiple images of the same type of object to reach depths otherwise impossible. For stacking QSOs, the upcoming survey J-PAS and its predecessor J-PLUS are the most promising, containing a number of narrow filters, acceptable limiting magnitude and very large footprint. While J-PAS is only starting, we use stacking in J-PLUS for a total of $\sim 1,550$ QSOs and more than 3 hundred thousand stars, the later to obtain an accurate recreation of the points spread function and so to avoid mistaking it for the signal we are seeking. We find that J-PLUS does not have enough depth to reach the magnitude needed with our number of quasars, but we reach very high depths for the star stack very much inline to our projections, showing a high degree of promise for stacking. We fully expect to be able to reach the magnitude to constrain the existence of the diffuse Lyman α signal with J-PAS.

RESUM

Aquesta tesi doctoral és un estudi de forats negres amb massa extrema, i les possibles consequències observacionals que podrien comportar, enfocat des de la perspectiva de forats negres primordials [1], forats negres que no serien d'origen estel·lar sinó que haurien nascut al principi del univers [2].

En el Capítol 1 es fa una breu introducció a la cosmologia, la branca de la física que agrupa l'estudi del univers com un tot a través de models parametritzats per variables físiques. Un breu repàs històric passa a un sumari del model cosmològic actual, l'anomenat ΛCDM, incloent les part no confirmades del model, la matèria i energia fosca. Un cop situat el context, es passa a detallar la motivació física pel cas dels forats negres primordials. És fa una breu ullada a un altre forat negre extrem, els de massa supermasssiva i les seves diferents qualitats. Finalment s'acaba el capítol amb un petit anàlisi dels medis actuals observacionals que poden aportar informació sobre els dos forats negres extrems.

En el Capítol 2 es fa un estudi a profunditat del cas en que forats negres primordials serien tota la matèria fosca. Primer es descriu com seria el procés de la seva formació i les particularitats que això els comporta. Després s'exposa la idea de restringir el rang de masses en que els forats negres podrien ser la matèria fosca a partir dels efectes observacionals que tindria la seva existència i s'ensenya les restriccions actuals de massa que hi ha en aquests.

Es continua el capítol 2 amb un estudi en detall dels métodes més rellevants i que produeixen la majoria de restriccions pels forats negres primordials que són la matèria fosca. El primer és l'anomenat microlensing, del que es decsriu en detall la base teòrica però també s'utilitza aquesta per justificar les limitacions actuals i futures del microlensing que fan que certs rangs de massa de forats negres primordials siguin inabastables. Es descriu també en detall el cas l'evaporació per radiacid́e Hawking, però de forma similar es conclou que és difícl per les restriccions ja imposades de millorar. Finalment es parla de les ones gravitatòries, i de com són de forma clara el futur que pot resoldre la qüestió, però també com els observatoris actuals són força limitades i es depén de futurs projectes que trigaran com a mínim 10 anys.

Després s'analitza l'estàndard que s'utilitza per restringir possibles masses on els forats negres serien tota la matèria fosca i les seves limitacions. Finalment s'acaba el capítol estudiant la única finestra que quedaria pel cas més estàndar on forats negres primordials podrien ser tota la matèria fosca, forats negres de la massa d'asteroides entre 10^{-16} i 10^{-11} $M_\odot$.

En el Capítol 3 mirem en detall un possible métode en el que la part superior d'aquesta

última finestra, 10^{-12} $M_\odot$ deixaria un resultat observacional clar. Aquest mètode seria la captura d'un dels forats negres primordials per part d'una d'estrella de sequència principal a alts redshifts, en que un forat negre acabaria al centre d'un estel per fricció dinàmica i després l'acretaria completament. Primer s'introdueix el mètode en detall, conjuntament amb la literatura prèvia que existeix i les difèrencies principals que introdueix aquesta tesi per millorar els resultats.

Un cop introduït es proceedeix en detall a la descripció en clau matemàtica i física del processos del qual es comprén, descrivint en detall l'origen de totes les equacions i aproximacions utilitzades. En particular es millora sobre la literatura anterior en l'ús de dos tipus diferents de fricció dinàmica per analitzar possibles difèrencies, càlcul numèric la fricció dinàmica amb l'ús de models estel·lars en comptes d'aproximacions i la creació d'un métode per estimar l'efecte que pertubacions per part de la resta de la galàxia podria tenir sobre el nostre sistema de forat negre primordial i estel. Per acabar aquesta part introduim el paràmetre Ξ per descriure els nostres resultats de captura. Mentre la mitjana de captures sempre dependrà dels parametres de la posició de la estrella i la galàxia en la que està, la Ξ en canvi és un resultat quasi completament genèric, que es pot aplicar a qualsevol redshift o galàxia imaginable.

Després es proceedeix a la descripció dels resultats obtinguts en cada pas i a proporcionar gràfiques amb tots els detalls necessaris per a la seva comprensió. Concloem que tot i que en petites escales tenen difèrencies importants, els dos métodes per calcular la fricció dinàmica son equivalents pel cas que estem estudiant. En comparació, tenir en compte possibles interferències de la resta de la galàxia és extremadament important, afectant el nostre resultat final per més d'un ordre de magnitud. S'ofereix una taula amb el valor de Ξ calculats per les diferents estrelles per ús en qualsevol model, però aplicats al nostre cas particular d'una galàxia en el temps de les primeres estrelles es determina que una gran part de les estrelles similars als nostres models acabarien capturant un forat negre primodrial. Prop del centre de la galàixia quasi totes les estrelles haurien de capturar-ne un, però fins i tot en posicions similars a les del nostre Sol la proproció seria notable, de més del 1%. Finalment es conclou amb el tipus de resultats observacionals que es poden extreure d'aquest fet, i com es podrien intentar distingir per resoldre la qüestió de forats negres primordials de 10^{-12} $M_\odot$ sent tota la matèria fosca.

El Capítol 4 es mou cap a l'altre extrem dels forats negres, el cas dels forats negres supermassius. Es comença amb una petita introducció, incloent explicacions sobre el seu possible origen, i com en una teoria exòtica els forats negres primordials podien haver jugat part. Després es procedeix a detallar el cas particular dels quàsars, un subtipus dels forats negre supermassius. També s'estudia la importància de la radiació Lyman α, i com combinada amb els forats negres supermassius podria donar lloc a nebuloses brillants de forma difusa al voltant de quàsars. Aquestes nebuloses contenen informació rellevant sobre els forats negres que les generen i són una conseqüència observacional del efecte que tenen els quàsars en el seu medi, que podria tenir implicacions molt importants per la reionització del univers.

Per estudiar questes nebuloses, introduim l'stacking, una tècnica observacional que consisteix en sumar diverses imatges del mateix tipus. En sumar les imatges, la incertesa pel soroll tèrmic, anomenat Poissonià, baixa permitint-nos arribar a fluxos de llum molt més baixos. La dificultat està en que també amplifiquem senyals sistemàtics que no són aleatoris, com la Funció d'Espargiment Puntual (Point Spread Function, PSF) de la imatge. Es detalla el significat de la PSF i com es pensa estimar-la, mitjançant un stacking independent d'estrelles. També s'introdueix J-PLUS i J-PAS, campanyes fotomètriques

d'observació des del observatori de Javalambre que tenen característiques que encaixen molt bé amb el procés del stacking, una quasi finalitzada i l'altra a punt de començar respectivament.

Utilitzant totes les tècniques introduides fins ara es fa una estimació del efecte d'un possible stacking de quasars en J-PLUS per trobar la llum difusa Lyman α al seu voltant. Es troba que amb J-PLUS no hi ha prou però que J-PAS és molt més prometedor. Donat que la majoria de característiques de J-PLUS són compartides a J-PAS, es procedeix a fer un stacking per demostrar la eficacia del procés i testejar el control de sistemàtics. El resultat és que com s'esperava, amb el stacking de quàsars no hi ha prou per visulaitzar res, però un stacking molt numerós d'estrelles arriba a la profunditat necessària per testejar la lluminositat de la radiació difusa Lyman α, demostrant així que el procés és molt prometedor i que per tant futura aplicació a J-PAS podria resoldre el cas de la llum difusa al voltant de quàsars.

Finalments, es fa un resum de tots els segments de la tesi en el capítol 5. Es conclous amb les perspectives de futur sobre els forats negres primordials i el cas dels quàsars. Pels primers la solució més prometedora son els futurs observatoris d'ones gravitacionals, especialment el satèl·lit LISA, que tot i estar com a mínim a 15 anys dels llançament promet resoldre la gran majoria de les qüestions remanents. Pel cas dels quàsars la solució es molt més propera. En el pròxim any J-PAS huaria de començar a prendre dades, i els primers data releases no haurien d'estar gaire lluny. Donat que es pot traspassar la majoria de la feina fet a J-PLUS per J-PAS, en només 2 o 3 anys es podrien millorar els resultats de la literatura.

També s'adjunten un parell d'Appendixs, A explicant en detall un procés tècnic referent a un canvi de variable utilitzat en el Capítol 3 i l'altre B una justificació d'un criteri també utilitzat en el Capítol 3.

ACKNOWLEDGEMENTS

Per començar estic molt agrait al meu director, en Jordi Miralda. Un guia indispensable, que sempre m'ha donat molta independència però alhora també molt suport quan notava que em trobava perdut. Gràcies per aquelles tardes en que parlàvem de física i feiem problemes que no tenien res a veure amb la nostra tesi, perquè he aprés que la física no és una matèria sinó una metodologia i forma de pensar. També gràcies per la teva paciència i disposició aquest últim any. Perquè ajudar a preparar una tesi en tant poc temps en el teu segon any com a director científic del ICC no pot haver estat fàcil. No quiero olvidarme tampoco de Alberto Manrique, mi tutor y antiguo director del trabajo de fin de master, quien siempre me socorría cuando tenía que hacer cualquier tipo de burocracia. Tu paciencia y buen humor han sido simpre muy reconfortantes.

Agrair també a tots els postdocs, tant del grup com del departament de Física Quàntica i Astrofísica. Andreu, moltes gràcies per la teva conversa afable i la teva preocupació tant per mi com a investigador com per mi com a persona. Hamish, thank you very much for your time and calm explanations whenever I was curious. Jordi Salvadó, literalment m'has salvat més vegades de les que puc comptar. To my fellow students too. Nicola, has sido el modelo de investigador y persona que quería ser, y que me es difícil de explicar. Jose Luís, solo coincidimos un par de años pero fue un placer aprender de ti. I also want to thank everyone at the group of PhD students of ICCUB, those afternoons were always a fun moment until the pandemic. També a tu Carles, per totes aquelles reunions en les que sempre ens trobàvem, and to you Oindrilla, it was only one year but you left quite the impression on me.

Al grupo de estudiantes de doctorado del CEFCA. Me hicisteis sentir como en casa, e incluso mejor en algunas cosas. Daniele, thanks to you for your help in my research and for your kindness and patience in person, you always made me feel welcomed. Rafa, sentí que podía confiar en ti completamente solo una hora después de conocerte y el tiempo me lo confirmó. Gonzalo, David and everyone else, you were truly fantastic. Gracias también a todos los otros investigadores que estan o estaban en el CEFCA. Silvia Bonoli, Raúl Angulo, gracias por escucharme y guiarme cuando sabía muy poco. Jesús Varela, gracias por tu paciencia eterna a pesar de que estabas siempre muy ocupado. Javier Cenarro, Alvaro Orsi, Carlos Lopez y todo el resto, os estoy muy agradecido.

També donar gràcies a la Pilar Gil i el Jordi Gutierrrez. Encara em recordo com per casualitat estàveu visitant la facultat el dia que em van notificar que em concedien la beca APIF. Des d'aquell dia sempre he cregut les nostres col·laboracions serien afortunades, i crec que aquesta tesi ho demostra.

I no em puc olvidar del grup del ñam-ñam, amb qui vaig compartir probablement els dinars més divertits de la meva vida i algunes de les converses més surrealistes que he tingut mai en un espai de 4 metres quadrats. Gràcies Adrià, Andreu, Chiranjib, Claudia, Glòria, Ivan, Javi, Josep i Marc. Unes una mica més especials per l'Albert i l'Alejandro, que em van introduir al grup després d'acompanyar-me des del Master en molts dinars. Tan de bo amb la fi de la pandemia puguem tornar a fer calçotades i viatges bojos. Un record especial també pels meu tres amics de la infancia, Joan, Rubén i Marcos. Sense temps per trobar-nos m'heu demostrat que l'amistat pot durar el que nosaltres vulguem.

Moltes gràcies al Institut de Ciències del Cosmos, que m'ha donat un espai durant 5 anys i totes les eines que he necessitat per la meva tesi, així com també el suport de l'ajut APIF concedida per la Universitat de Barcelona. Voldria agrair a més l'equip que crea i manté R [3]. Un llenguatge de programació una mica diferent, però que encaixa molt amb la meva forma de treballar.

Finalment, però definitivament no els menys importants, vull donar gràcies a tota la meva família propera, el meu pare pel seu suport, a la meva mare pel seu caliu i al meu germà pels seus espaguetis. En una situació per desgracia comú, la pandèmia de coronavirus em va afectar personalment molt a pesar de no patir mai la malaltia. Durant un any i mig em vaig arrossegar sense motivació ni esperit, i va ser només gràcies a la vostra paciència, amor i fe en mi que puc presentar aquesta tesi. També a la meva cosina, la seva família i a la meva àvia, que van continuar oferint sempre la seva tendresa a pesar de veure'ns molt menys. No vull olvidar-me de la parella del meu pare, que sempre m'ha acollit amb un tracte familiar. O de la nostra gata, que tot i la meva alergia continuaré acaronant sempre que pugui. I a tota la resta de la meva família, que sempre m'ha ajudat, gràcies.

Finally, to the reader I also want to thank you. This thesis is the result of 5 years of work, but it will only exist as long as somebody reads and remembers it. For taking care of that, many thanks.

CONTENTS

CHAPTER 1

INTRODUCTION

We are currently living in years that most likely will be referred in the future as a golden age of Cosmology. For the uninitiated, cosmology as we know it today refers to the study of the Universe as whole, bringing varied fields from astrophysics to particle physics together, with the aim of creating a model of the Universe that accurately reproduces the one we live in. That is just a broad definition, but regardless of specifics cosmology has had an important role both enabling or helping a lot of the scientific successes in the last years. The LIGO detection of gravitational waves has resulted on the birth of multi-messenger astronomy, opening a new door for the future. Astronomical surveys are cataloguing our skies with increasing accuracy, each star and bright point in them being measures, both with ground based telescopes like SLOAN to space based ones like Planck.

However, looking at only the last years is perhaps reductionist, for in a way Cosmology has always been in a golden age, perhaps since its beginning. Assigning the field a year of birth is a complex endeavour though. To start, one cannot help but perhaps to think of Einstein's special relativity. Establishing the space-time as more than a background, an entity with a metric that also was affected by gravity, and setting the speed of light as a maximum velocity and a universal constant. But while special relativity is undoubtedly the foundation of almost any theoretical modelling of the universe, its first solution were used for a static unchanging universe that was forced a priori. It was not until Friedmann worked on his solution 6 years later that this assumption was relaxed, reaching the following form [4]:

$$\frac{\ddot{\mathrm{a}}}{\mathrm{a}} = \frac{-4\pi \mathrm{G}}{3}\left(\rho + \frac{3\mathrm{p}}{\mathrm{c}}\right) + \frac{\Lambda \mathrm{c}^2}{3}\ , \tag{1.1}$$

where a is the dimensionless scale factor, which measures the universe's expansion or contraction. To define a we make it so the distance between two places d_0, at a reference time t_0 where $a(t_0) = 1$, is related to the current distance by $\mathrm{d(t)} = \mathrm{a(t)d}_0$. Its double derivative measures whereas this expansion is accelerating or not and in which direction (expansion or contraction). This depends on the energy density ρ and pressure p of the universe, for in special relativity mass and energy are interchangeable, and on a possible cosmological constant Λ. From this equation expansion or contraction, with differing speeds and accelerations, all depended on parameters of the universe rather than being set a priori, a simplistic but undeniable first modelling of the universe.

But it is also true that Friedmann equations were mostly ignored. The favoured theory of the time kept being of a static universe, neglecting the possibility of a expanding one. Lemaitre found a similar solution to Friedmann independently 5 years later, and elaborated on it by reaching a possible observational result in a very simple way [5]. If we assume that the expansion of the universe dominates over any other type of velocity, then we can relate the velocity we will see the objects moving at directly with the scale factor:

$$v = \frac{\dot{\mathrm{a}}(\mathrm{t})}{\mathrm{a}(\mathrm{t})}\mathrm{d}(\mathrm{t}) \ . \tag{1.2}$$

This equation follows quickly from $\mathrm{d(t)} = \mathrm{a(t)d_0}$, you just need to derive by time on both sides and assume the velocity due to expansion is far larger than any other, which we expect to happen for far off objects like galaxies.

We can measure the velocity of far away galaxies by finding the Doppler shift of their major emission lines: if a galaxy or star moves while emitting then from our point of view will see the wave stretched or shortened, that is the Doppler shift. Because almost all galaxies were found to be receding from Earth, this resulted in the wavelength of their emission lines lengthening, shifting them to the red part of the spectrum. Thus this measure of a galaxy speed became commonly referred as redshift velocity.

Yet even Lemaitre was also initially ignored together with the implications of finding mostly receding galaxies until in 1931 Hubble published his rather famous law [6]. Based on observations he did as an amateur astronomer and previous observations, he found the redshift velocity of stars had a linear relation with their distance, just as equation 1.2 implied. The only difference with equation was that he changed the scale factor division $\dot{a}(t)/a(t)$ by a parameter, the Hubble parameter, and measured it for our current time. $\mathrm{H(t_{now})} = \frac{\dot{\mathrm{a}}(\mathrm{t_{now}})}{\mathrm{a}(\mathrm{t_{now}})} \sim 70\mathrm{km/s\,Mpc}$[1].

Backed by observations, the until then controversial expanding universe was finally accepted. Redshift became a standalone measure of an object's distance to us in an expanding universe rather than tied only to velocity. While there was a lot of previous theoretical work, it was observational evidence that tipped the balance. Some put the birth of cosmology here, when the expanding universe was adopted as the standard, perhaps a good reminder that in the end science should not only seek beautiful models but rather value observational evidence above all.

Yet the entire debate was not settled. Lemaitre continued his work and brought the idea of a expanding universe to its ultimate conclusion, a Universe that started from nothing, a Big Bang. Others believed in a steady state universe, where constant matter creation was the source of the expansion but the rest of the universe was static and eternal. The issue kept on for more than thirty years, but it was again observational evidence that solved the divide with the frankly lucky discovery of the cosmic microwave background radiation by Alpher and Herman in 1964.

A radiation coming from all sides with almost completely homogeneous and with a perfect black body spectrum. A black body is an idealized object which is both completely opaque and has no reflections, which makes a perfect model for understanding how a purely thermal emission by a very simple source would look like. In comparison stars and

[1]Due to several cosmic calibration mistakes, Hubble initially measured a Hubble parameter far above the current measurement of ~ 70. Nonetheless, him proving the linear relation between distance and redshift velocity was what mattered to settle the expanding universe issue

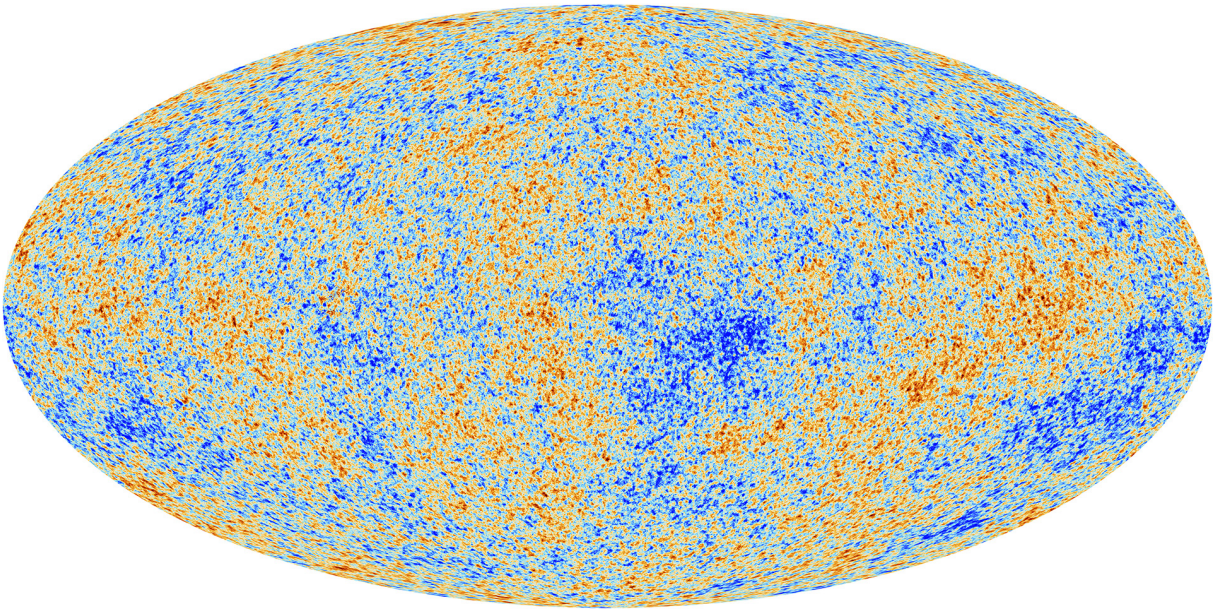

Figure 1.1: Released image of the CMB from the Planck mission, freely acessible at `www.esa.int`. The anysotropies are clearly visible, though we remind that their relative scale is extremely small. Credit to ESA and the Planck Collaboration

other astronomical object emit in more complex ways, as they are composite objects made of multiple layers and elements and are reflective and only partially opaque. The black body emission found gave a measure of the effective temperature of the Universe, but could not come from stars or other similar objects. However the black body emission fit perfectly with the CMB being the first light of the universe, the moment where protons and electrons first joined into atoms and light was allowed to roam freely through the universe.

Following this, in 1966 there were the first detailed calculations of primordial nucleosynthesis [7], which used details of the CMB and the first Big Bang models to compute the abundances of basic elements. While the exact birth of cosmology is subject to debate, what is commonly known as modern cosmology undoubtedly started with the CMB and nucleosynthesis, and there has been almost constant progress since.

A good illustration of this is perhaps the CMB itself. The initial detection settled the debate about the origin of the universe, but even 30 years after work on the small anysotropies present on the CMB is still improving our understanding of the early universe: it is expected that due to interactions in the early universe between matter and radiation the CMB is not completely homogeneous, but rather has perturbations on a relative scale of $\sim 10^{-5}$. This inhomogeneities can be seen on figure 1.1, with the redder colour being very slightly hotter and bluer very slightly cooler.

While very small in comparison to the temperature itself, of the order of microkelvin, the nature and shape of these perturbations are not random. Rather, the distance between various patches of cool and hot inhomogeneities can be analysed through their power spectrum. In figure 1.2 we show the results from Planck in 2013, a mission from the European Space Agency with help from NASA and other space agencies, where the fluctuations are shown versus their distance between them on the sky on degrees, called angular scale. The shape and peaks can inform our understanding of the early universe, including estimating parameters as specific as baryon density or the curvature of the

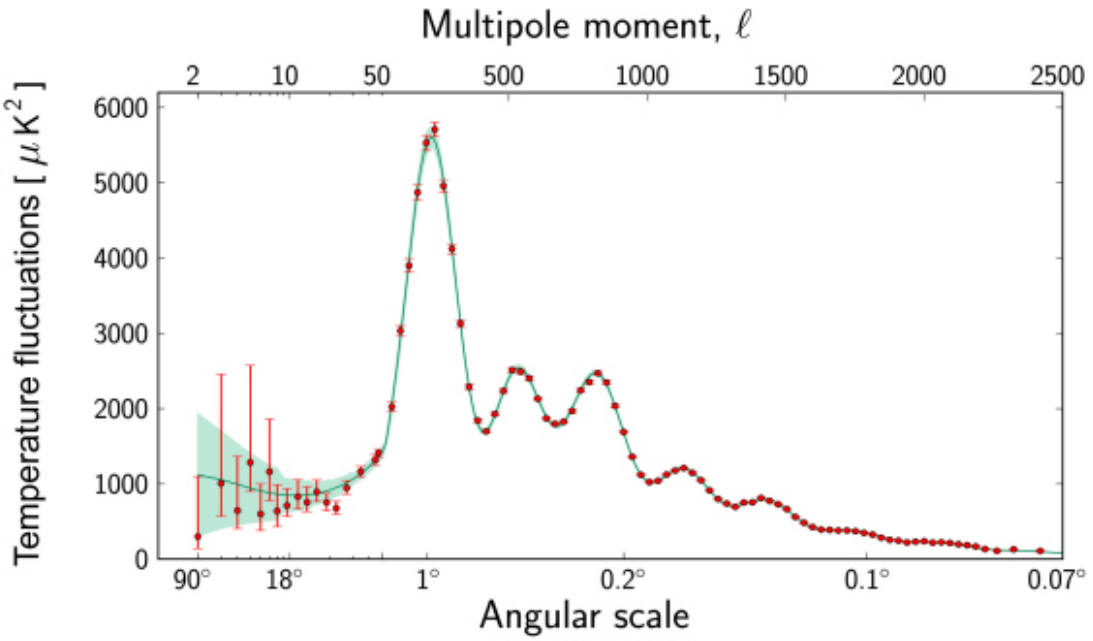

Figure 1.2: Released image of the Power spectrum of temperature fluctuations in the Cosmic Microwave Background from the Planck mission in 2013. Freely acessible at `www.esa.int`. While the shape differs a lot depending on the angular scale a set of clear peaks and tails can be appreciated. Credit to ESA and the Planck Collaboration

universe. Even today, the power spectrum of the CMB is still a focal point, every new experiment improving the accuracy or trying to shed light on poorly constrained angular scales.

All of this data has to be understood and interpreted through the current and well established standard cosmological model, ΛCDM. While there are a few tensions with observations, the latest results coming from the spacecraft Planck gave us among other things both the images in figures 1.1 1.2 and very strong support to ΛCDM. Since its conception ΛCDM has managed to tie seemingly disparate and separate issues to explain what we see.

Its name is a good example, as it comes from its two main constituents, Λ standing for Dark Energy and CDM for cold dark matter. Both are the main components of our Universe (95% according to Planck) and both have 'dark' in the name, meaning we are unable to see them, but they share little else.

Dark energy emerged from observations of supernova in 1998 [8]. Following from equation 1.2 we can estimate the Hubble parameter from observations, which can give us the scale factor and the change of the scale factor. There is another subtlety however, as light from very distant places takes quite a while to reach us, what we see is that place of the universe as it was when the light was emitted. This means very far off signals do not tell us the current scale factor, but the scale factor and its time derivative of when they were emitted. Observation of distant supernova showed that, contrary to what we expected, the expansion of the universe was accelerating. The scale factor a has increased compared to past times.

Recovering equation 1.1, the acceleration of the scale factor $\ddot{a}$ depends on the energy and matter content in the universe. But, if we hold matter and energy conservation, all factors in the first term would get lower as the universe expands and both matter and

energy dilute. For $\ddot{a}$ to increase the expansion of the universe means there is a non-zero Λ, a cosmological constant that comes to dominate the universe eventually as the expansion keeps on.

This is the nature of dark energy, which according to the last measurements forms up 68% of the current universe density[2]. Dark energy can be conceptualized as an anti gravitational force, but its nature is still being discussed. Even to this day any kind of observation beyond its effect on the scale factor remains elusive, and numerous models describing dark energy exist but there is little consensus about them. Potential experiments to try to ascertain more are currently too far off to even entertain, and would likely require venturing outside the Milky Way.

Dark matter is a decidedly different issue however. Dark Matter is self descriptive, a form of matter that barely if at all interacts with light, and so to us appears completely dark. The adjective cold comes from a description of its speed in the early universe, which is relatively slow. While simple velocity might appear trivial, this has far reaching impact on the structure of the entire universe. Unlike dark energy, we know dark matter surrounds us, its gravitational effects changing the Milky Way and allowing the galaxy to be born as we know it. Indeed, looking to our galaxy and further beyond 50 years ago illustrated the need for an unseen matter in order for the gravitational forces we observed to make sense. With the passage of time, more and more evidence for its existence has piled up, being outright needed for the ΛCDM model to explain structure formation and the power spectrum on figure 1.2. Is this precisely what has allowed us to say dark matter is cold and constrain most of its characteristics, and so exclude or include objects as candidates to being the dark matter. As a matter of fact, we do know a lot about dark matter even if we are still in the dark about its true identity.

That is perhaps why this lack of a confirmation of its identity has frustrated the scientific community for the last years. Near the change of the century the hopes of the community were focused on a series of particles called WIMP, standing for weakly interacting massive particles.

As the name said, WIMPs were fairly massive particles roughly around a 100 times the mass of the proton, though it depended on the model and could be hundreds of times above or below that. They only interact with the rest of the universe through a force with the strength of the weak interaction and gravity. While not a part of the standard model, they are a natural byproduct of what at the time were expected extensions of the standard model, like supersymmetry.

WIMP was the focus for the search of dark matter due to what was called the WIMP miracle. To put it simply, if there existed a particle with a mass roughly a 100 times of the proton and a coupling very close to that of the electroweak force, we would expect the universe to produce it thermally to the expected density of dark matter in our current universe. That would come purely from high energy scattering processes, like all current baryonic particles in the universe, without any need for special creation models and the only extension of the standard model needed being the ones that let the particle exist in the first place. Seemed like a natural fit.

However, the expected mass for that WIMP miracle was within the range of the hadronic accelerator at CERN. The LHC has failed to find them, together with multiple

[2]Note that this has not always been true. As mentioned, both matter and radiation density go down as the universe keeps expanding. In the earliest times of the universe Λ was completely negligible. However Λ is not affected by the expansion of the universe, thus it eventually dominates over all other forms of density and will keep doing so after that.

other direct detection experiments. While theoretically still possible, interactions are very much constrained and other masses become motivated, including outside the WIMP paradigm. The general attitude across the community has slowly shifted from hope to a more jaded skepticism, and the search for alternatives has become a hotly contested debate.

The axion is perhaps one of the more interesting ones. They were initially conceived as a byproduct of a mechanism used to solve a puzzling issue within the current standard model. The strong interaction, mostly known as being the basis of quantum chromodynamics (QCD), is symmetric under both charge conjugation and parity. This means that its interactions do not vary if you both flip a spatial coordinate[3] or change all particles for their antiparticle equivalent. The issue being the current standard model of particle physics, while tremendously successful, does not explain how this symmetry came to be. The strong interaction a priori should be able to ignore these symmetries. A mechanism was proposed to solve this issue, the Peccei-Quinn mechanism [9][4], which almost inadvertently results in the creation of a new type of particle, the axion [10, 11].

This axion is commonly referred as the QCD axion, and remains a very good candidate for dark matter. While the exact mass remains unknown all axion models give very light particles, of the order of less than a tenth of an electron mass. At the same time, the QCD axion itself does not have any special reason to fit the abundance and density required for dark matter. There exists a variety of experiments that are successfully constraining the parameters of the QCD axion [12], through both laboratory and astronomical searches, but its existence remains unconfirmed.

Set of particles with similar characteristics to the axion can be generated in other extension the Standard Model, like string theory. This whole class of particles are named axion like particles (ALP) after the first of their kind, but can theoretically have very different properties. Finding one that fits our cold dark matter is easy for multiple models [13]. At the same time it is hard to find extensions of the standard model as well motivated as the QCD axion, and so they remain a secondary, though interesting, candidate for dark matter.

One could try to reject the need for completely new theoretical particles, as none of the properties of the dark matter are so unique as to require it. Needing to invent a particle when standard physics might be enough is contrary to the classic Occam's razor and standard scientific thinking after all. However, in practice, primordial nucleosynthesis and the CMB strongly constrain the amount of baryonic matter within the universe.

Another possibility is to focus less on theoretical origins and more of the shape such DM could take. One of the line of thoughts was that the dark matter could be found in massive astrophysical compact halo objects (MACHOs). MACHOs would be compact objects that would not be bright enough to be observable from Earth. An example could be objects formed of standard baryonic matter like brown dwarfs to planets, as long as they are any kind of compact object whose emission is far below the scale of a main sequence star. Of course, if they were to be the dark matter there had to be more exotic objects of non-baryonic matter to fit the nucelosysnthesis constraints. The search for these objects was one of the main aims the astrophysical community 30 to 20 years ago, giving raise to the "MACHO Project" [14] from 1993 to roughly 2000 [15]. The findings looked conclusive; MACHOs, could not be the majority of the dark matter. This meant

[3]Basically the equivalent of moving the particles to where their reflections in a mirror would be

[4]The original form of the Peccei-Quinn mechanism described in the paper was ruled out by experiment, but more modern forms exist and are almost identical in mechanism and purpose

the dark matter was expected to be composed of flocks of particles rather than more massive groupings.

These last years another candidate has risen, one that was part of those MACHOs if in more unique way: black holes (BHs). They are extreme astrophysical objects and one of the most surprising consequences of Einstein's special relativity. Accepting that mass distorts the space-time and affects everything within it including light also results in the logical consequence that a big enough concentration of mass would be able to trap the light, and everything else, within its radius:

$$r_S = \frac{2GM}{c^2} \,, \tag{1.3}$$

where M is the mass, G the gravitational constant and c the speed of light. The above can be reached just by requiring an object to have an escape velocity of the speed of light using Newtonian gravity. As special relativity sets the speed of light c as the maximum achievable, this automatically traps all the objects within, including light.

Being brought to light first by Schwarzschild [16], this solution was initially highly contentious within the community. However, experimental results that are clearly in support of such, or at least very similar and factually identical objects, have constantly appeared. While black holes do not emit or reflect any kind of radiation in a substantial way, and thus cannot be observed in theory, we can measure the effect of their gravitational forces on nearby objects and see the accretion disks of matter falling into the black hole that surround them. The former warp the orbit of surrounding objects to the extent that only a mass too big to be just a planet or asteroids could be responsible. Accretion disks meanwhile shine as the matter within it heats, due to viscosity and collision within the disk. As the matter of the accrettion disk slows its orbit to fall towards the black hole proper, the energy lost heats other parts of the disk and the matter also emits a portion of its energy in the infall. This means not only the disk is visible, but also the emission of matter infalling being different from the symmetrical disk makes it a very directional and peculiar signal.

Historically a good example is Sagittarius A*, the black hole at the center of our own Milky Way. Initially catalogued as radio source, Sagittarius A* was identified as a bright and compact object in 1974 [17]. The possibility of it being a black hole was recognized in the 80s, but it was not until 1994 that the size and mass could be measured [18]. Further observations reached the conclusion that no other object but a black hole could be of that size and that mass. Similar things have happened with other black holes: with time the evidence has piled and currently their existence is as well established as that of stars and galaxies, but only at the end of eliminating all other possibilities.

This has changed however, with one of the greatest triumphs of cosmology we shared before, the detection of gravitational waves. Gravitational waves can be thought as quite literally aftershocks from strong gravitational events. If the space-time is a net affected by the mass of objects, then gravitational waves are the ripples left when something on the net moves. On 2015, LIGO detected gravitational waves for the first time in history, a merger of 2 objects of roughly ~ 30 and $\sim 35\,\mathrm{M}_\odot$ [19]. While the merger is the source of most of the gravitational waves, in the last moments of the infall, before the two objects collide, smaller gravitational waves are emitted which contain details of the individual objects. Those waves coincided exactly with simulations of black hole mergers, which together with the lack of a luminous signal to accompany the merger of two such massive

objects made it clear they were black holes. Black holes, while still not seen, were finally confirmed to exist beyond the realm of doubt.

The characteristics of black holes as being invisible to our eyes recall those of dark matter, so a connection seems natural at first. While the dark appearance is because of gravity rather than an intrinsic property, they neither emit or reflect other radiation enough for us to detect it, and they also easily fulfill the cold criteria, their speed being dependent only on gravitational interactions. It also takes advantage of them being known physics, instead of requiring introducing a whole new set of particles. However, we knew of only way for a black hole to be created, and that is being born from a giant star that has gone supernova.

This sets a priori rather strict limits on their mass and location. The collapse into a black hole requires a star to go supernova, and for the remnant to be above the Tolman−Oppenheimer−Volkoff limit of $\sim 2.3\,M_\odot$ [20–22]. There is also the issue of place, as star formation has a number of requirements, especially for stars as big as to eventually become black holes. Their big masses in the numbers required for dark matter would be very apparent in common star formation sites, which have both plenty of objects and matter to be affected. This conclusion became only strengthened by recent and improved analyses of primordial nucleosynthesis, which set rather tight constraints on the baryonic matter that existed in our universe at the very early times [23]. All these reasons make it understandable why black holes had been almost rejected as dark matter candidates.

Black Holes however are more complex than their original astrophysical context implies. From a purely theoretical point of view they are fascinating objects whose internal dynamic is completely inaccessible and even when there is a clear consensus on a particular aspect it is very hard to prove experimentally. They are effectively a black box of which we can only theorize its inner workings based on fundamental laws. A great example is Hawking radiation [24], named after the late Stephen Hawking, which is a result of the presumptive quantum nature of black holes and the only radiation they emit.

Hawking radiation will be explained in more detail in section 2.3, but is a result of the horizon of a black hole having an effective temperature from the point of view of an observer, which also means the observer will preemptively see a black body emission corresponding to such temperature. We use presumptive because despite our best efforts, the scale of Hawking radiation is currently just too small for any kind of detection on known black holes.

Another example can be its mass. From a theoretical point of view there is nothing stopping black holes from having a certain mass or another, rather they depend mostly on density. For any value of mass there is a correspondent Schwarzschild radius, as seen in equation 1.3, below which the mass will collapse unto a black hole if compressed. In practice, the black hole will only have the range of masses that the processes that can generate such extreme density value can create.

However, unlike other theoretical aspects the mass of the black hole is accessible to us both before and after the collapse. Thus, asking if stars are the only possible way to form black holes is a question that belongs to cosmology and astrophysics, and one we might be able to find observational proof rather than just ponder. While stars undoubtedly provide a way for black holes to form, there is a lot we do not know about the universe, especially in the very early times. They say the proof is in the pudding, and the easiest way to prove this alternative origin for black holes would be to find a black hole that could not form from a star. While the Tolman−Oppenheimer−Volkoff limit has some variability, a

black hole below 2 solar masses will just not form from a star.

Similarly, extremely massive black holes could exist from mergers of smaller black holes or accreting enough mass, but we normally would expect them to be much rarer than common black holes. Indeed, this is not simply hypothesizing as there already exist many examples of the so called super massive black holes (SMBHs). If there is nothing stopping black holes from being of any mass, perhaps a look at the extremes is warranted.

1.1 Super massive black holes

Super Massive Black Holes (SMBHs) are, as the name implies, extremely massive black holes, from the order of millions to even 10^9 solar masses, located at the center of galaxies. A good example is the previously mentioned Sgtr A* in our own Milky Way, with a size of $3 \cdot 10^6\,\mathrm{M}_\odot$. While it is hard to say for certain, every standard and larger sized galaxies seems to have one at its core.

This however brings a question, and it is how we have been able to identify them so readily. For Sgtr A* we have been observing it since 1974 and only 20 years later there was strong evidence that it truly was black hole. For much farther black holes identifying them should be incredibly hard, as we cannot measure the change in orbit of objects nearby to the black hole compared to what we see. We can only see the galaxy as a whole.

The answer comes from their brightness. The SMBHs are in fact the reason why we are able to see some far off galaxies, as only incredibly massive objects are able to have such high luminosity. Because of both their mass and their position, they can accrete a lot of matter. A portion of the energy lost by the matter as it falls within SMBH is emitted as radiation, and because their massive size the emission reaches brightness several orders of magnitude above even the brightest stars. Our understanding of SMBHs is also helped by the fact we can estimate the mass of such extremely bright objects.

While mostly negligible at human scale, light has associated a radiation pressure, coming from photons colliding with objects. Despite having no mass, photons carry momentum and they impart a portion of it on any object they interact with. Knowing the momentum of a single photon is $p = \frac{E}{c}$ we can derive the force for unit of time. We do not measure radiation in individual photons though, but in luminosity as the energy of the emission per unit of time and also sometimes in flux as their energy per unit of time and area.

For almost all objects we expect the radiation to be perfectly isotropic and spherical, equal in all direction, so we expect that for a single point in space and time, the emission will carry the following momentum:

$$p = \frac{L}{4\pi R^2 c}\,, \tag{1.4}$$

where R is the radius of the point from the source of the emission, and L the luminosity of the source. This follows purely from applying the momentum of the photon to the luminosity of the source divided by area.

How much of that momentum will be transmitted at any body however will depend on what we call the opacity of an object. This measures how much of the momentum carried by the photon is transferred, and depends a lot on the atomic characteristics of the object. For the particular case of our extremely bright source we do not know the exact

composition of their surroundings, but we do know that hydrogen is the most abundant element in our universe. Because we also expect these sources to have been emitting for a while before reaching this point, we can also safely assume that most of this hydrogen will have been ionized by that previous radiation, meaning most of the particles falling surrounding the source will be either free electrons or free protons. Knowing that, we can approximate the opacity using the Thomson scattering cross section of the electron σ_T. As the force is the change of momentum per unit of time, and the object will receive emission continuously, following from equation 1.4 we get:

$$F_{rad} = \frac{L}{4\pi R^2 c}\sigma_T \ . \tag{1.5}$$

This radiation force, and the pressure it causes will continuously affect all that receive the luminosity coming from the source. This applies to all kind of objects, the emission coming from a star or fainter objects, but it is most powerful for black holes, as their own accretion disks are also the source of the emission. Every individual particle within accretion disk would receive two opposing forces, the gravitational one coming from the black hole and the radiation pressure pushing them outwards. For some cases the radiation pressure wins, stopping matter from falling into the disk. The lack of accretion means the system stops emitting however, which stops the radiation force, which means matter again falls to the black hole until its own light stops it again, etc. Therefore, for any source that is accreting we can set a minimum mass, or for any known black holes a maximum luminosity, the Eddington luminosity. It is very straightforward to obtain, we just take equation 1.5 and compare it with the gravitational force from Newton:

$$\frac{L}{4\pi R^2 c}\sigma_T = \frac{GM_{BH}m_p}{R^2} \longrightarrow L_{Edd} = \frac{4\pi GMm_p c}{\sigma_T} \ , \tag{1.6}$$

where we use the proton mass m_p to assume the average mass of the object affected[5]

Using the Eddington luminosity we can easily estimate both the mass and accretion of SMBHs despite their distance, which helps a lot establishing relation with their host galaxies. We in fact call SMBHs that we can see Active Galactic Nuclei, as their scale is such that from the outside it looks as if the activity comes from the entire core of the galaxy.

Some among the AGNs containing these SMBHs are named quasars, from Quasi Stellar Objects (QSO), because their host galaxies are so far off they look point-like, similar to stars. Without the brightness from the SMBHs seeing this kind of objects would be extremely hard and a window in the far off universe would be shut down. Even more, because the speed of light is finite and the distances so large, this window is not only to large distances but also to a very young universe.

With their luminosity we can estimate their mass, and the relatively standard emission spectra of quasars also allows us to estimate the distance. While most quasars were initially found at around redshifts 1-2, current instruments have found SMBHs of even higher mass at redshift 7.5 where the universe is less than 10^9 years old [25]. Further searches have continued to find SMBHs at similar redshifts $6-7$. A controversial topic is if there would be enough time for such SMBHs to form from stellar black holes. [26]

[5]Sometimes a mean molecular weight is used, taking into account other elements like helium into the ionized soup. This can have a minor effect, but for the sake of simplicity we will not introduce it here

postulated that we would need super-Eddington luminosity, in other words ignoring equation 1.6 to achieve high enough masses, but this requires a large set of assumptions and knowledge of the formation of those SMBHs we currently do not have.

1.2 Primordial black holes

If there is this another way to produce black holes then the topic goes full circle, as smaller black holes could form the majority of the dark matter. Lower mass black holes could avoid previous searches for MACHOs and other existing restrictions.

So with that aim, are there really any alternate ways to form black holes? The answer lies at the beginning of the Universe. A period of which we know little, but there are a number of ideas with strong support from both theoretical and observational points of view. One of these is cosmological inflation, a period where just after the Big Bang the early universe expanded at exponential rate, basically enlarging and smoothing out the universe. While a very abstract and hard to grasp concept, it has grown into another strong core of the ΛCDM model, and the experimental evidence, as scant as it is with such early epochs, continues to support it. Inflation brings with it also a set of new possibilities: as inflation expands the space-time fabric itself, there is a chance quantum perturbations, inherent to everything, could escape their usual scale and grow to solar and galactic scales. Indeed, the small variability we see within the CMB in figure 1.1 is believed to correspond to a set of these perturbations and that would be extremely hard to understand without inflation. If some of the density fluctuations formed a very high peak, then the perturbations could grow enough for them to collapse into a black hole a while after inflation ended. In the case of standard gaussian fluctuations that are commonly assumed these kind of peaks would be extremely rare, but both non-gaussian and non-standard perturbations exist in a lot of the more complex inflation models.

Even assuming those the process is still not simple, as the fluctuation first has to do what we call as reentering the horizon. While the perturbation might have grown enough to collapse, because inflation expands faster than light just after it the enhanced perturbation will not be casually connected. Rather, it has to effectively wait for the universe to catch up in this process of reentering the horizon, after which the now causally connected fluctuation will finally start to collapse. As easily seen from this description, this a highly non-linear and complex process. Another layer of complexity is added in that this process happens in the radiation dominated era of the universe, so the collapse will be very unlike that of star. By special relativity matter and energy have an equivalence, so the lack of standard physical matter should not be an impediment and if the perturbation had enough energy that it would be equivalent to a mass below its Schwarzschild radius then it will collapse into a black hole nonetheless. But the accretion and collapse are still described differently than in our current matter and Λ dominated era. All of this results in that to describe this process highly complex numerical simulations are needed, and even then they have very few generalities even among superficially similar inflation models.

Still, this whole process would give birth to a group of black holes shortly after the Big Bang, a set of primordial black holes (PBHs). These PBHs would be practically as old as the universe, and because of the multiple variables in their formation they could de facto have any size we could imagine. In fact, it is not hard to theorize that they could not only give birth to a set of smaller or medium sized black holes, but also to giant seeds for the previously discussed SMBHS. While this opens a lot of possibilities, a word of

care should also be given to not just dream of infinite black holes. There are alternative models that generate PBHs, some using new fields that result in domain walls [27] or exotic phase transitions with new vacua [28], but all have in common that they make use of inflation. While very useful, as it allows the formation of PBHs with almost any mass just by fiddling with a couple of parameters, it also means adding layers of complexity to an already hard to understand epoch. Most of this complexity is also outside the standard model of physics. This is in part undeniably exciting, as finding these PBHs is one of the very few ways of probing the physics of inflation, but also should beget some caution. Creating PBHs that can explain almost everything should be subordinate to trying find what observational traces of them we can.

1.3 Detection

Of course, while finding black holes is not easy there has been a lot of progress these last 10 years. Perhaps the most visually impressive is the image obtained by the Event Horizon telescope [29], seen in fig 1.3. An image that literally required observatories from the entire world, and looked at the SMBH closest to us besides the one in our Milky Way. While very impressive, this a feat only possible because of the close proximity of the galaxy M87 and the massive scale of the black hole. For the less massive and more distant brothers of M87 there are other ways, but the most novel and promising are the gravitational wave observatories like LIGO [19, 30]. These detectors open an entirely new window and mark the beginning of multi-messenger astronomy, so called because for the first time light will not be our only messenger but another set of waves will join it.

As LIGO is only a first generation detector it is only able to catch near and relatively massive, at least for stars, mergers. However, the amount of high mass black holes detected initially took the community by surprise, as that was region of masses where very few stars were expected, and the expected numbers of mergers could fit a possible black hole dark matter in those mass ranges, despite existing constraints from MACHOs. Since then, LIGO has currently ended its third observing run and the number of mergers does not fit the one expected by a pure black hole dark matter. Still, statistical analysis conclude that a portion of the mergers likely come from a population different than that of stellar black holes [31]. This however has to take into account that black holes resulting from multiple (stellar origin) mergers are hard to model, and none of the individual events are hard to describe using stellar origin black holes. LIGO may have detected PBHs, but if so needs a lot more statistics and events to be sure.

Current first generation gravitational wave detectors, as much of an accomplishment as they are, are not perfect however, or even that good at picking up signals from possible PBHs. Earth detectors have limited sensibility, so they require the targets to be both close and massive. The seeds of SMBHs if they are PBHs would be rare and likely far off, while black holes from below one solar mass would need to be very close to be picked up, and even then assume they have mass of at least around $0.5\,M_\odot$. Masses below that are simply not detectable. Future next generation GW detectors would improve the situation a lot, especially LISA [32]. However, current plans put all these project at least 10 years away, and given how novel the technologies in use still are, further delays are not unlikely.

Fortunately we are not limited to gravitational waves to try to detect or know more about these abnormal PBHs. For SMBHs, the brightness of QSOs is an excellent way to understand their properties and further detections at even higher redshifts will only increase our knowledge. Even if there is not much progress on its possible origin as

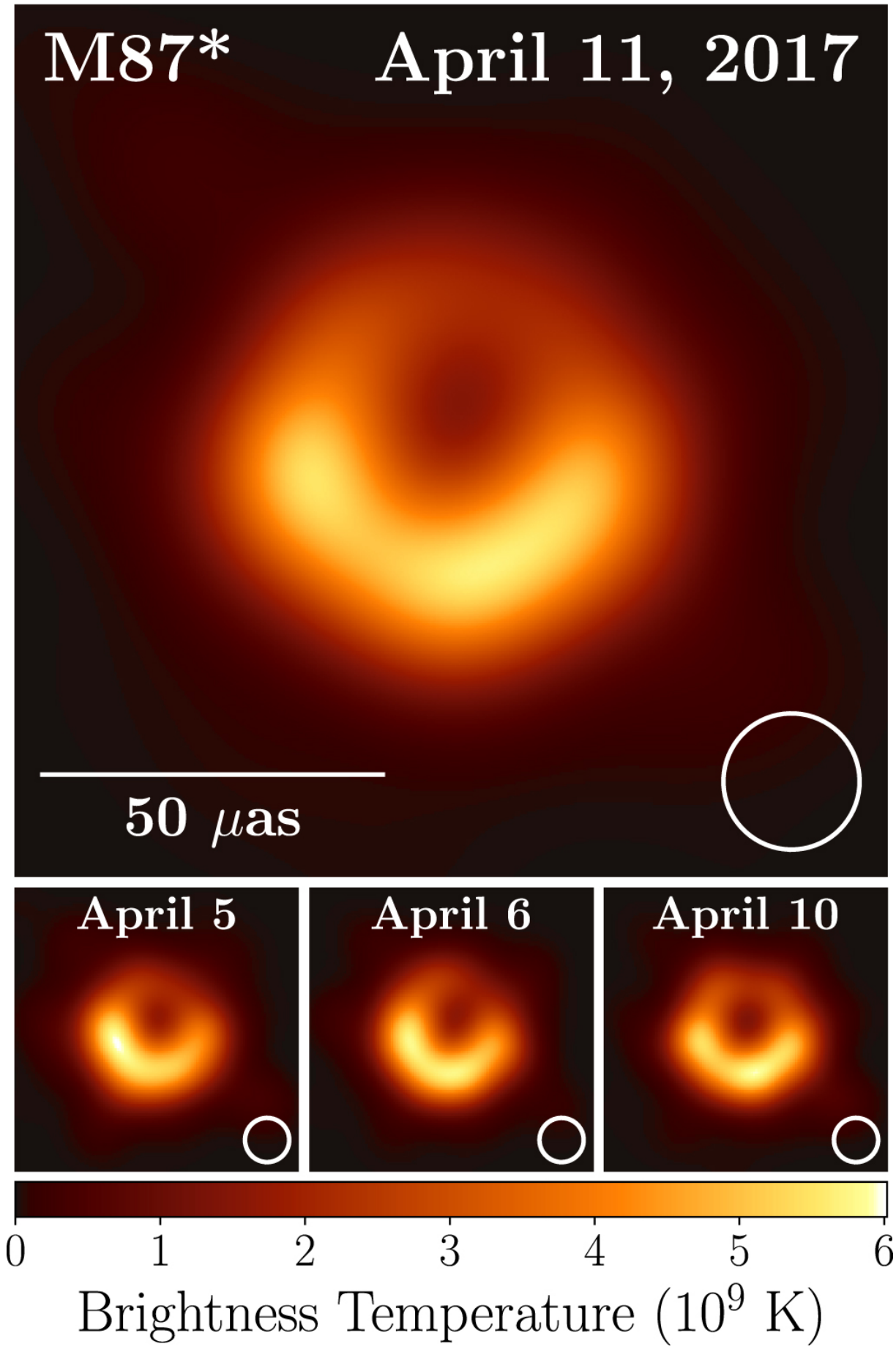

Figure 1.3: Figure 3 from [29]: EHT image of M87*, on the various observation days. It is an average of three different imaging methods after convolving each with a circular Gaussian kernel to give matched resolutions, and it is in in units of brightness temperature. For technical details check the reference.

SMBHs, just a better understanding of the early universe will indirectly help a lot, as both possible non-PBH seeds and the PBHs themselves form very early and thus depend a lot on these early epochs. While there exists a lot of theoretical work about the first stars and galaxies there is still a lot of uncertainty due to our very scant observational evidence of those times. Finding any more pieces to our puzzle will only help.

On smaller PBHs, the situation is both more promising but also much more complex. While black holes not of massive sizes are very hard to detect, the sheer scale of the dark matter means that if PBHS were the majority of it, then there would be a lot of them. LIGO despite its flaws is still enough to set harsh constraints on masses close to a bit bigger than stellar black holes. Bigger masses would have galactic consequences that we could notice [33]. For low mass PBHs however, there are a lot of issues that complicate their detection, the simplest of which that they are very hard to distinguish from planetoids or even asteroids. A number of methods have been proposed to try and help at least decide if they could be an important fraction of the dark matter, but it is still an open issue.

On chapter 2 of this thesis, we move to describe this issue in greater detail. In particular there are a lot of so called constraints, resulting from the fact that if PBHs of a certain mass were all the DM we would have noticed it in some already existing observations. Most of these constraints come from microlensing, the idea that if there were so many smaller black holes within our galaxy some would have modified the light coming from stars on their way to us. While among the most important constraints we have, very accurate estimates of both the number of stars and the type of black holes is needed for constraints on the most dubious ranges where we would only see a couple of lensing events. Another big portion of the constraints comes from Hawking radiation. While undetectable for stellar mass black holes, for the much smaller masses that PBHs can be and in the quantities needed for dark matter the Hawking radiation would produce a noticeable bump of background radiation at various frequencies we do not see. Of course, this assumes Hawking radiation exists, but on practice the models used for PBH generation already make that assumption. The question about a black hole without Hawking radiation is one worth asking, but not one suited to PBHs.

Even with all these constraints there still remain issues. In particular, most of these simply assume PBH to be of a single mass and in a very standard grouping, but as the ways for PBH to form can be very different both of these can be equally varied. Particularly the way an extended mass range (i.e. 0.1 to 1 solar masses rather than just 1 solar mass PBHs) would afect the constraints is rather complex [34], and can be used to both lighten [35] or harshen constraints [36]. Even beyond that, the clustering of these PBHs is also important. While not expected in the standard formation scenario that we described it is not uncommon in alternative ones that depend on domain walls or phase transitions. If the PBHs are very clustered together, then not only previous constraints disappear but new ones also appear [37]. It is a very nuanced topic, and while very useful, a simple constraints graph is not enough to describe the situation.

On chapter 3 we describe an observational consequence that would result if PBH of around $10^{-12}\,M_\odot$ were most of the dark matter. These PBH are too small to be detected even by microlensing [38], and are currently one of the last windows in which PBH could be the whole of the dark matter [39]. However, they are also extremely common due to being so small, so they would be constantly interacting with standard objects like stars. This would result in a lot of them crossing the stars, either free or during their orbit. While uncommon, there is a chance they are slowed enough by this crossing that they

just remain in the star, and slowly fall to the center. At the center they would accrete the star until there is no more star and the PBH now has a mass that we can detect. Previous work has been done on this idea with both neutron stars [40] and main sequence stars [41], but that was focused on globular clusters. We follow on that work by creating a model in the early redshifts, just after the first stars. While simple, we compute numerically the slowing with 2 different methods to ensure its reliability. We also add an estimate to account for third party perturbations on our system, something which has been lacking in previous works.

There are caveats to our model, but with a few exceptions it is generic and even extensible to later redshifts. This means our results are not only applicable to cases where PBHs are all the dark matter at very early epochs, but also one where they are only a small fraction and the star forms at medium redshift.

On chapter 4 we put a focus on SMBHs, concretely on a way to gain more information about their surroundings. Quasars as mentioned are very bright, but one of the biggest incognitas is how much they contributed to the reionization of the universe. Currently a mostly minor contribution is expected, but any variation on this has massive repercussions for our understanding of QSOs and then MSBHs as a collective. A related question is about the nebulaes that commonly accompany the brightest quasars, showing at least the individual contribution to their surrounding, but that we cannot appreciate for their fainter siblings. However, quantity has a quality of its own. With a technique called stacking, which we describe in detail, we can improve our sensitivity for the fainter quasars. We also bring attention to J-PLUS and J-PAS, Spanish surveys very close near that are ideally suited for this kind of work. We expect that once J-PAS is completed stacking will allow much improvement over the current results. While this is still ways off, we showcase a proof of concept with J-PLUS and workarounds the multiple issues that exist.

We finally summarize our work and present our conclusions on chapter 5. We accompany this thesis with a number of appendices. The Appendix includes technical details omitted in various sections for the sake of succinctness, and is divided in the first explaining in detail a change of coordinates we did in Chapter 3 and the second also justifying a simplification we use in Chapter 3.

CHAPTER 2

PRIMORDIAL BLACK HOLES AS DARK MATTER

Primordial black holes (PBHs) are one of the current most interesting candidates to be the dark matter. Not only they fulfill the basic criteria needed for dark matter, they do so without the need to invoke a new set of existing particles. While this might make them look ideal, their formation is not so simple and often requires some form of new physics too. As this chapter's main purpose is to detail the existing observational constraints on PBHs as dark matter, we will thus keep explanation on PBHs possible origin brief. For a more extensive review we direct the reader to [42].

The most common origin for PBHs is in the very early Universe, during radiation domination, where large curvature perturbations generated during inflation could have undergone gravitational collapse. As we are dealing with radiation domination, we are working with an energy density rather than matter density, so we will call it μ. For the case of Planck units, which take $G = c = 1$, we can simplify the Schwarzschild radius in equation 1.3 enormously, reaching $r_S = 2M$.

It is also obvious that the total mass within any spherical symmetric perturbation in Planck units would be $M \sim \frac{4}{3}\pi\,\mu r^3$, as $c = 1$. Using that with the simplified Schwarzschild radius definition means the condition for the perturbations to collapse is [2]:

$$r_S = 2\frac{4\pi}{3}r_S^3\mu \longrightarrow \mu r^2 \gtrsim 1\ , \tag{2.1}$$

where we drop the constants on the right term. While this condition might appear strange, it is in fact very close to the Jeans length for oscillations, which in natural units would be $\lambda_J \sim \left(\frac{\pi}{\mu}\right)^{1/2}$. Another possibility is simply to remember that in radiation dominated universe the radiation pressure is $p = \frac{\mu}{3}$. Matching it with the gravitational potential to see when the latter wins out and the region will collapse ends giving the same result as above.

We can introduce then a density contrast, which compares the energy density of a point μ with the background density μ_0. We will call this contrast δ and use the following definition:

$$\delta = \frac{\mu - \mu_0}{\mu_0}\ . \tag{2.2}$$

This allows us to measure how overdense or underdense a certain region is, and so

the strength of the perturbation. In an homogeneous, isotropic and flat universe, given condition 2.1, we require $\delta \gtrsim 1$ for the perturbations to collapse [43].

This condition is the threshold: if δ fulfills it by being greater than the threshold, the perturbation will collapse and form a PBH. If it is lower the pressure of radiation will win out, resulting in the perturbation continuing its spread maybe even until today, though it will so be heavily redshifted as to be extremely hard to detect.

This is all for a very idealized case though, as δ is in fact an average and not a uniform value like we assume. The density contrast will in fact be a function that we expect to peak at a certain point but also be much closer to the background on others. Numerical simulations even for symmetrical homogeneous cases have found the threshold does not depend only on the maximum of the perturbation, but also on the shape of the δ function. This is also all for the radiation dominated epoch too, an unexpected matter dominated time would result in needing an entirely different set of assumptions and change some of the equations above. All of these examples can radically change the threshold, which makes computing the collapse in any kind of generalized form very difficult.

Another way is to change our definitions a bit and use a new type of condition. Called the critical threshold δ_c, it is not a direct measure of the over-density like δ but rather of the mass excess per a unit of volume, the so called compaction function. While mathematically much more complex, this critical threshold can have a very good analytical approximation with parameters describing shape and space-time [44], which simplifies simulations enormously.

Despite this, however there is another major complication. The current power spectrum we predict for our universe and the scales we can detect from the CMB have fluctuation of the order of microkelvin, $\delta \sim 10^{-5}$. Therefore, we normally would not expect the collapse of perturbations into PBHs. There are two different solutions to this conundrum.

First some kind of enhancement of the perturbations could have happened. There are in fact lots of ways to get this kind of enhancement, from slightly modified inflation models to new physics coming from string theory, but all have in common that they are outside the standard model. The most common way is to have a modified inflation potential, the so called ultra-slow roll potential, which results in perturbations at a certain scale being enhanced up to $\delta \sim 1$ while remaining the usual value at other scales.

Another possibility is that the spectrum of fluctuations is non-gaussian. The fluctuations we find are $\delta \sim 10^{-5}$ for the average, which is too far from $\delta \sim 1$ for any kind of noticeable PBHs to form if the fluctuations follow a gaussian spectrum. We do expect a gaussian spectrum in the standard model. But if fluctuations do not follow that gaussian spectrum because we have new physics, then there could be a tail of extreme results with $\delta \sim 1$ without altering the average perturbation we expect. This could result in an important number of PBHs forming.

Something necessary to understand is that even if we are using the former way of enhancing fluctuations to obtain PBHs, non-gaussianities can still be relevant. Because PBHs are very sensitive to the values of δ, any kind of higher than expected value, like the ones that would come from an unaccounted tail of fluctuations, would affect the abundance of PBHs. Currently, in the CMB we have not detected any type of non-gaussian fluctuations, so this is why a lot of models do not contemplate them, but caution is still needed.

Even after all that, that is but the first step of PBH formation. As mentioned before, collapse does not happen immediately, it is not until the perturbation crosses the horizon that it collapses. While this might look like just a timing issue it has enormous conse-

quences. After all, the perturbation will collapse in the horizon in which it has reentered. The lower the scale, the bigger the horizon and the higher the mass it will have. We can estimate the mass within the horizon with [35]:

$$M_h \sim \frac{\mathrm{c\,t}^3}{\mathrm{G}} \sim 10^{15} \left[\frac{\mathrm{t}}{10^{-23}\mathrm{s}}\right] \mathrm{g}\ , \tag{2.3}$$

from the Planck time ($10^{-43}s$) to much later in the universe's life, this is what gives PBHs such enormous mass ranges. A perturbation generated in first instants of inflation can create tiny black holes that could could explain the whole of the dark matter. Perturbations generated later can result in massive PBHs bigger than any current stellar black holes that could be the seeds of SMBHs.

Of course, we do not expect the perturbations that make PBHs to come from the same exact instant. This will naturally result in a spread of masses for our PBHs. For the case of enhanced perturbations we do expect the enhancement to only happen at certain scales, so while PBHs will have an extended mass distribution, if there are enough for them to be a noticeable part of our universe we also anticipate them to be around a certain peak. Even then this is not a completely hard rule, as there can be extreme cases like double inflation models [45] and also models where PBH form in a completely different way that results in a more even spread [46], not to speak of the already mentioned non-gaussian cases.

Another expectation would be that they would form with spin 0 or very close, as they form in the radiation dominated epoch where the combined fluid of radiation and matter sheds angular momentum almost instantly. This can be a clear difference from stellar origin black holes, which will inherit at least a fraction of the spin of their forming star[1], though again in more exotic formation paths there could be PBHs with noticeable spin. A good example is the case where PBHs would form in a matter dominated epoch, which should result in PBH having all very high spin instead of close to 0 [49].

Something similar applies to how close or far from each other we expect these PBHs to form. In the simplest case we expect the PBHs to follow the standard poissonian matter distribution, as the perturbations they form from should also come from a homogeneous universe and the enhancement should not a priori have any specific spatial distribution. Exotic models exist however where this is not the case, in particular for alternative origins like the previously mentioned domain walls or when adding non-gaussianities to the perturbations. This adds still another layer of complexity to the whole issue.

Still, as mentioned, if PBHs are formed through perturbation collapse, then the perturbations will also be reflected on the CMB, concretely its temperature angular power spectrum. Only a number of perturbations will collapse, so the rest will transmit and appear like the other CMB fluctuations. Unfortunately, either through Planck [50] or other measurements [51], we can only constrain the power spectrum on the lower scales, equivalent to the highest masses of PBHs. Currently, no non-gaussian nor enhanced fluctuation has been found, limiting these lower scales, but only the lower scales. Saying it in another way, anything below $10^3\,\mathrm{M}_\odot$ is possible.

[1] How much is a point of contention, with very efficient angular moment transport models positing very low spin [47] while others using medium efficiency average notable spin black holes [48]. Observations of X-ray binaries always have a very high spin, but they are subset of black holes and so there could an intrinsic bias too.

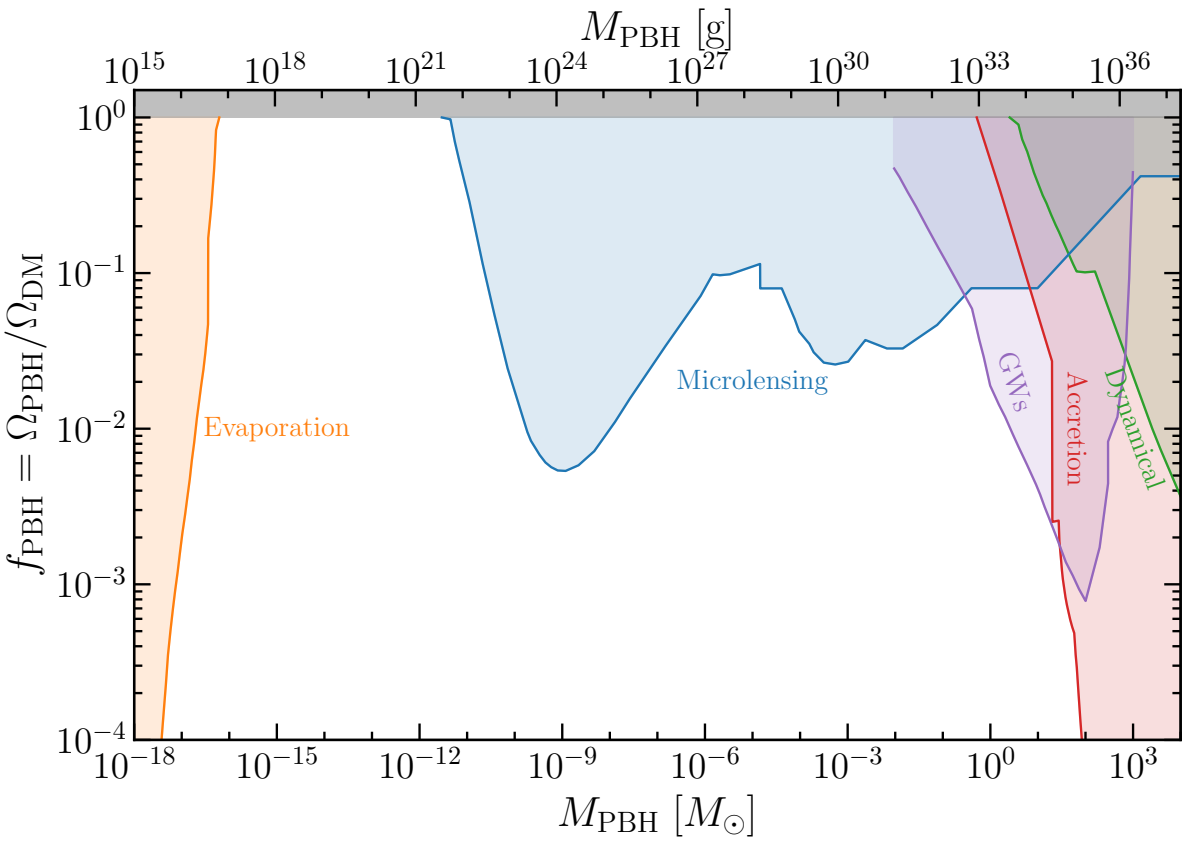

Figure 2.1: Plot with current existing strong monochromatic PBH constraints, with each color and name corresponding to a different type. The abundance on the left axis is which fraction of the dark matter they could be, while mass is given in both $M_\odot$ and grams. Obtained from [52], where other bounds and plotting codes are available.

2.1 Monochromatic constraints

PBHs could be the dark matter, but as mentioned before the properties of these PBHs could be drastically different. $10^3\,M_\odot$ black holes would warp any star or planet that is close to them, while much more smaller $10^{-10}\,M_\odot$ black holes could cross the Solar system millions of times and we would not notice them.

This means it makes a lot of sense to divide the types of PBH by mass. As mentioned above while we expect extended mass distribution we also expect the enhancement of the perturbations to result in a particular mass range with a peak. Something that helps a lot with setting constraints is taking the peak of that mass distribution and making as if all the PBHs in it had that mass. This simplifies the physics in most cases enormously, as we can avoid integrals through all the masses and make a back of the envelope calculation to see if it is even worth to pursue certain constraints. And while the final result is in practice only approximate we expect to not be it so far from the extended mass distribution as we are working with its peak after all.

The end result are monochromatic PBH bounds, which we show in figure 2.1. After a large number of such experiment we can fill an entire plot with constraints using this simplification. Of note is that the graph is logarithmic and covers more than 22 orders of magnitude. In this way it is only thanks to that approximation that we can get even close to covering all these possible ranges with different types of constraints.

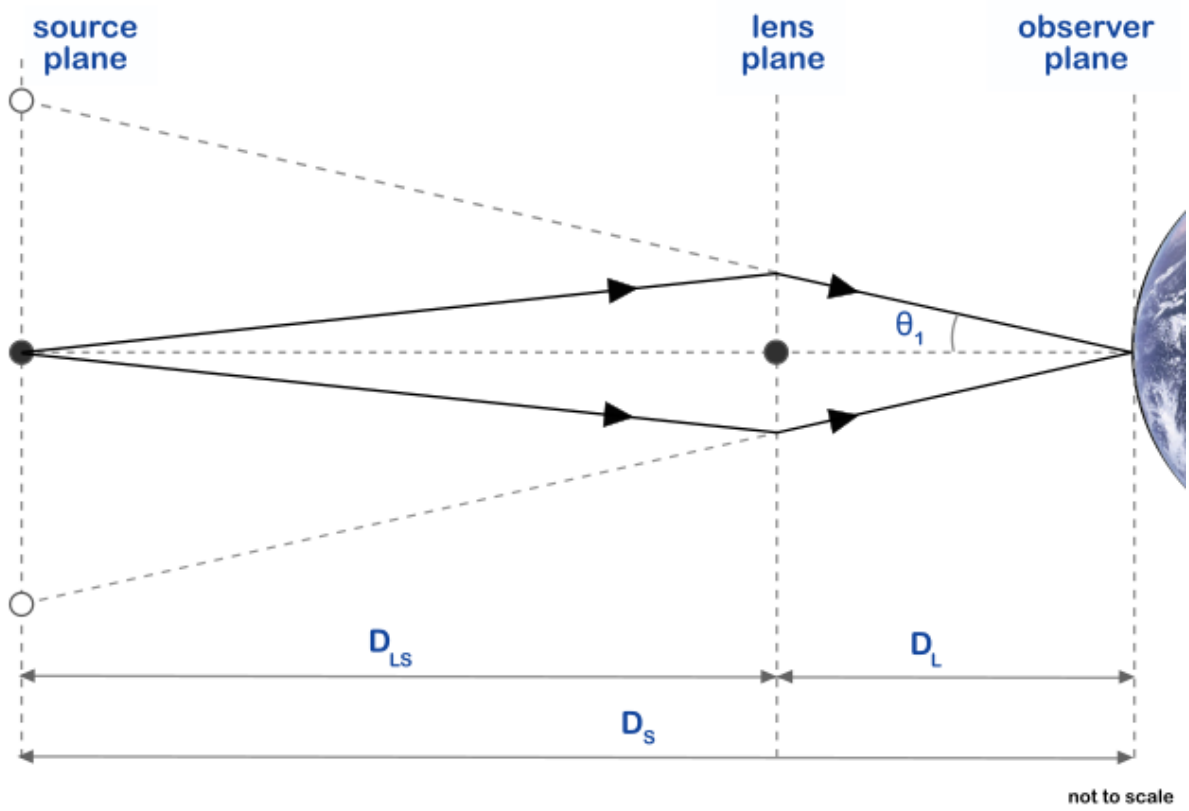

Figure 2.2: Example of the geometry of an Einstein ring. θ_1 is the Einstein radius. From Wikimedia Commons, the free media repository

There are as varied constraints as there are mass ranges, but as seen above there are 4 that dominate. The first are the dynamical and accretion constraints that were used on MACHOs before, as they work very well on very massive black holes. There are multiple sources for these constraints, but they all share that they focus on the large mass of these black holes and how they would have a large effect on their surrounding we would notice. The other three however, microlensing, black holes evaporation and GWs are more unique, so we will dedicate a section to each.

2.2 Microlensing

Microlensing is the name given to gravitational lensing on a very small scale. Gravitational lensing itself is what happens when a body projects a strong enough gravitational force so that any light that passes by nearby is distorted. In typical optical parlance, the gravity of the body acts as a lens to the light coming from behind it towards us. The most illustrative case is that the Einstein ring, which is shown in figure 2.2. There a source emits light and it typically goes through the lens. For the sake of simplicity we shall assume the lens is a black hole: then the light in the direct line of sight will not go through the black hole, but as seen in the figure two other light rays will be affected by gravity, reaching us. This will results in the viewer seeing two sources equidistant to where the source actually is (in the 3 dimensional case, a ring surrounding the source, thus the name).

The Einstein ring is an ideal case, in practice there are a lot more complications. One

is where the object and lens are so far away, or small, that our resolution is unable to separate the two images. This is the particular case of microlensing, where the lensed image appears all on the same pixel rather than as two different images. As we cannot perceive a position shift the typical measurements of angles cannot be done, and it can be hard to even detect that image has been lensed.

However, the presence of more ray beams than expected in a single pixel also means that the image will appear brighter than normal. Going from the figure above, as all rays have similar brightness receiving two will make it appear at a higher luminosity than a single one. Because all stars and galaxies appear to move for an observer on Earth, a combination of both their intrinsic orbits and the Earth's own movement, the lensing event will only happen for the short period of time that both source and lens are aligned. We can then compare the increased luminosity with the normal measured just before, noticing these kind of changes and recording them as lensing events.

To compute the expect magnification of light, a first approximation is to treat gravitational lensing similar to optic lenses, using what is called geometric optics. First of all we can get the deflection angle α, which would be how much the ray is deflected from its path :

$$\alpha = \frac{4GM}{bc^2} \ , \tag{2.4}$$

where b is the impact parameter, the shortest distance between the point-like lens and the ray it is deflecting, M is the mass of the lens, G the gravitational constant and c the speed of light.

This is the small angle approximation, which works for small α. It comes from general relativity but the result is a very simple term that reminds of newtonian gravity so it is also referred as Newtonian approximation. In fact, we can get exactly half the value of the angle just by assuming Newtonian gravity and that light is a particle with mass. Another comparison can be with the Schwarzschild radius we described in 1.3, being $\alpha = 2r_s/b$.

Another parameter of interest is the the Einstein angular radius θ_1, which is the angle at which we would see the previously mentioned Einstein ring. Using trigonometry, we can compute θ_1 from the figure above and 2.4:

$$\theta_1 = \left(\frac{4GM}{c^2} \frac{D_{LS}}{D_s D_l} \right)^{1/2} \ , \tag{2.5}$$

where we have implicitly assumed $sin\theta_1 \sim \theta_1$. In standard lensing this can troubling, but in microlensing where the angles are so small it always applies.

This would be all for the case where the source is perfectly aligned with us. In practice, these kind of cases will be rare, and we will have the source with an angle respect to the observer θ_S, and the images would appear if we could see them at an angle θ that is now different from θ_1. This is a more general case, an example of which can be seen on figure 2.3. As θ_1 is defined through the Einstein ring and not any particular image, 2.5 still works but now we do not know the angle θ at which the image will appear. However, we can still relate them by applying the lens equation of geometric optics to our case [54]:

$$\theta - \theta_S = \frac{\theta_1^2}{\theta} \ . \tag{2.6}$$

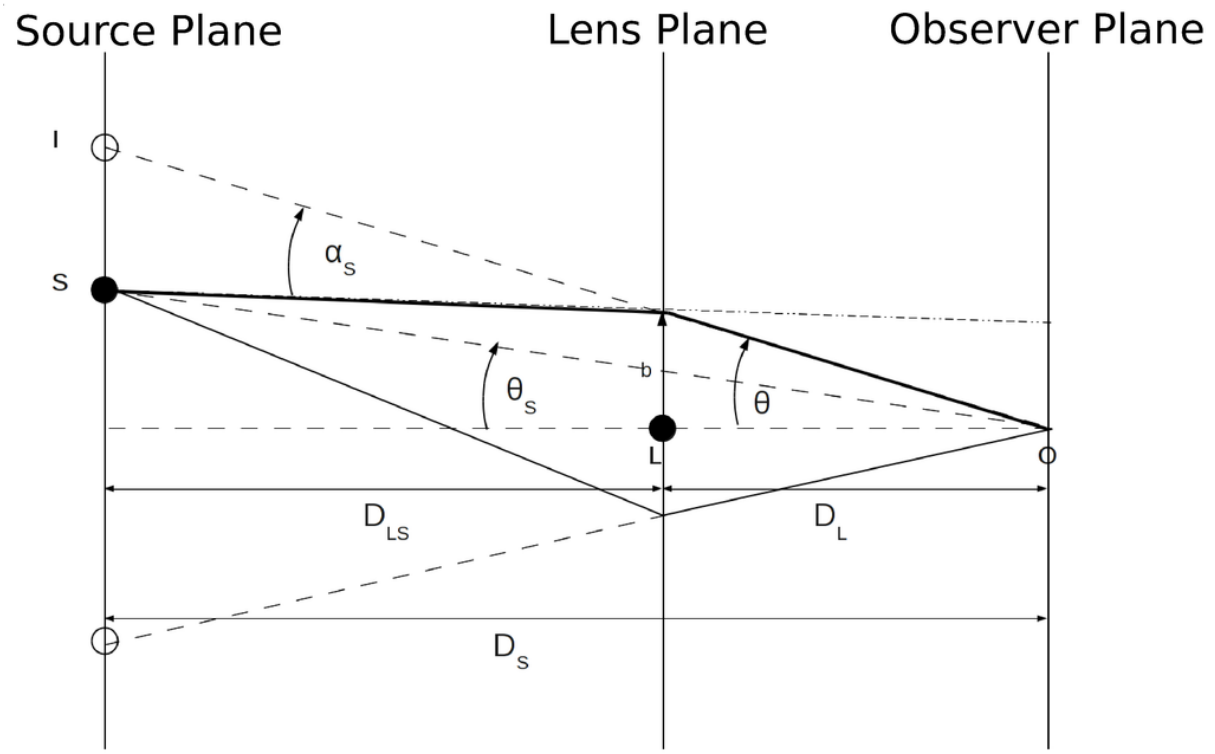

Figure 2.3: Schematics of a lensing event for a more general case. Taken from [53] Figure 1, α_s is the same as our α

As θ_S is a single value, it is easy to see we would have two solutions for θ, two images. In the case of microlensing we are unable to distinguish them, but we will be able to distinguish the increasing flux, the magnification of the source they will cause.

We can relate the two images to the flux by understanding that the flux (f [erg/sec]) results from integrating the surface brightness of the object (S [erg/sec/sr]) for a particular solid angle Ω, the width of the beam so to speak. This solid angle depends on the angle it reaches the observer. Because we are working with very small angles, we can approximate this integral as a simple multiplication $f = Sd\Omega$, and compare with the case where there would be no lensing:

$$A = \frac{f_{obs}}{f_0} = \frac{Sd\Omega(\theta)}{Sd\Omega(\theta_S)} = \frac{d\Omega(\theta)}{d\Omega(\theta_S)} = \frac{\theta d\theta}{\theta_S d\theta_S} \,. \tag{2.7}$$

Computing the magnification then is relatively straightforward if we remember the lens equation again 2.6, until we get:

$$A = \frac{\left(\frac{\theta_S}{\theta_1}\right)^2 + 2}{2\left(\frac{\theta_S}{\theta_1}\right)^2 \sqrt{\left(\frac{\theta_S}{\theta_1}\right)^2 + 4}} \pm \frac{1}{2} \,. \tag{2.8}$$

Searching for this moment of greater emission we can thus detect if a source has been lensed or not. Despite the previous complications, the final equation as seen above depends only on the source angle and the Einstein angle. If we detect a magnification of light coming from a source we can thus elucidate many details.

This makes microlensing a very attractive prospect for DM constraints. We know the mass we want to constrain and we can use the DM galaxy mass distribution to estimate the likely places where the PBHs would be. With this you can estimate the expected magnification and if it is within the sensitivity of scientific instruments. The birth of dedicated surveys like Subaru [55] has allowed to map a mass range of 10 orders of magnitude with constraints, as they have found few or none gravitational lensing events, whereas if those PBHs were the dark matter we would have expected many more.

But despite all these successes, microlensing might have ran its course. This comes from a lot of the approximations used previously. First of all, we have used standard geometric optics, but that requires light rays to work classically, thus if any wave properties are relevant during the lensing this whole scheme breaks down. Indeed, as the PBHs we are interested in are extreme objects, their Schwarzschild radius is very small and can become of the order of the wavelength of the light we are observing, triggering wave-like effects from the light we need to account for.

Fortunately even with the lack of such ideal case we can still get some information. As we do not expect the rays to be perfectly symmetrical, the rays very likely traverse different distance to reach the viewer, there will be a time delay between them. This time delay will also result on the beams not reaching on the same phase of the wave. The time delay is much more complex to compute, but an analytic expression is still possible [56]:

$$\Delta t = \frac{1}{c}\frac{D_L D_S}{D_{LS}}(1+z_s)\left(\frac{|\theta-\theta_s|^2}{2} - \Psi(\theta)\right) , \tag{2.9}$$

where all parameters are the same as previously, z_s is the redshift of the source and Ψ is the lensing potential. This lensing potential is related to the density of the lens by the Poisson equation, and can be thought as projection of the density through the plane of the lens. For point like sources, like our black hole, we can resolve $\Psi(\theta) = \theta_1^2 log\theta$ [2].

Due to wave nature of light, this time delay and the phase difference it causes between various rays will result in both destructive and positive interference. This interference fringes will make the magnification equation to grows similarly complex:

$$A = \left(\frac{W}{2\pi i}\int d^2x e^{i\omega\Delta t(x,\theta_S)}\right)^2 . \tag{2.10}$$

We can no longer avoid an integral, and even need to use imaginary numbers. W is a dimensionless frequency, related to the frequency of the light ω and the time delay Δt. For more details on the complete derivation of A we refer to [56].

While these changes might appear minor and too cumbersome, they are relevant because this mistake did in fact happen with Subaru, where an early prepublication version of the paper did not take this into account as noted in [45]. Even with the extra complications, the amplification in equation 2.10 can still be computed to get the corrected constraints as they were finally were present in figure 2.1. The integral makes it harder to compute, but the magnification is still there.

It is much more problematic however when we start finding finite source effects. These come when cannot just take the source as point-like: if the source is big in respect to the

[2]The lensing potential is the result of integrating the density through the entire plane of the lens and includes an indeterminate constant. This is normally not an issue as the time delay is used to compare with the time delay from other rays, but it will not help in computing absolute time delays for a path.

lens, emission from different points of the source will be lensed differently. This can come from the source not being small enough or far enough as to be treated as point-like, resulting in different time delays between even close by or symmetrical rays and the interference fringes being washed out the larger the effect is. The end result is that the lensing effect disappears, there being no difference with the normal luminosity. In summary, if the condition:

$$\frac{\theta_S}{\theta_1} = \frac{R_s/D_s}{R_E/D_L} << 1 \ , \tag{2.11}$$

is not fulfilled, then the microlensing effects will start disappearing.

Small PBHs have very small Schwarzschild radius. This means in effect that standard sources from lensing, stars from the Milky Way or neighbouring galaxies, are simply too big to reliably produce any constraints for PBHs below $10^{-11}\,M_\odot$. [56] estimated that we would need Gamma Ray Burts (GRB), with very distant sources and very small wavelengths, to reliably constrain this mass range but also admitted that currently GRB detection is too rare for this to be done. [57] proposed to use Pulsars, which are very far off and also smaller than stars, for this kind of purpose, but also reached the conclusion it would take a future and very ambitious observatory to reach mass ranges which are not already constrained currently. Microlensing can still remain useful for PBHs of high mass, but the much lower number of PBH means much lower expected number of events, increasing the observation time required for adequate constraints, on top of low mass PBHs being much more interesting for the purpose of dark matter as figure 2.1 illustrates.

In summary, while extremely useful, microlensing seems to have reached the limit in what it can constraint, or at least reached very diminishing results. While planet mass PBHs cannot be all of the dark matter, asteroid mass PBHs are free from such constraints.

2.3 Black hole evaporation

PBH evaporation is a process resulting from Hawking radiation. As mentioned in the introduction, Hawking radiation is the conclusion of applying quantum effects to a Black Hole's horizon and results in the emission, mostly in terms of particles, of an energy depending on the effective temperature of the Black Hole. This emitted radiation would have an almost thermal black body spectrum of the corresponding temperature, and this temperature depends mostly on the mass. The smaller the black hole is, the higher the temperature and viceversa. Of note is that while extremely useful due their analogous relation, temperature should not be taken literally and more understood as something emerging from possible quantum gravity effects and our lack of understanding of singularities.

The derivation of this temperature comes from the boundary conditions of the horizon. Assuming an observer just outside the horizon, this observer has to have an acceleration in order to not fall into the black hole. This accelerated frame of reference will see a thermal radiation by the Unruh effect, where acceleration results in a thermal bath of particles. However, this accelerated frame of reference is at local equilibrium with the horizon of the black hole, which means the horizon shares that same thermal bath. This

results in that observer seeing the black hole horizon at following temperature:

$$T_{obs} = \frac{1}{4\pi\sqrt{2M_{bh}r\left(1-\frac{2M_{bh}}{r}\right)}}\ , \tag{2.12}$$

where r is the position of the observer. This comes straight from the black hole metric, which we have assumed to be a standard Schwarzschild black hole, and the observers position. The equation is in Plank units too.

This temperature the horizon observer sees can be redshifted to infinity, to understand how a far off inertial observer like one from Earth would see the horizon. We reach:

$$T_{bh} = \frac{1}{8\pi M_{bh}} \longrightarrow T_{bh} = \frac{hc^3}{16\pi G M_{bh}\sigma} \sim 10^{-7}\frac{\mathrm{M}_\odot}{M}\ , \tag{2.13}$$

where we have returned to SI units from Planck ones on the right term: h is the Planck constant, σ the Stefan-Boltzmann constant, c the speed of light and G the gravitational constant. Of note is that this is for non-rotating (0 spin) non-charged black hole. While charged black holes are not expected to exist, as their charge will simply attract opposite charges until the black holes becomes neutral again, rotating black holes are expected in both stellar black holes and some versions of PBHs.

From the temperature we can obtain its emission, which can only come from the black hole's own energy. Therefore the black hole will evaporate when it emits all of its energy, the majority of that energy being the one stored in the black hole's own mass. For massive black holes this is extremely unlikely, not only because their temperature is much lower, but because their mass means they are constantly accreting matter unless completely isolated. For smaller black holes however, their emission might surpass their accretion, especially when not in dense environments like the usual void between stars.

This permits us to define the lifetime of a black hole as the time it will take for it to evaporate through Hawking radiation. This is only an approximation, because it does not take into account accretion. However, because as the mass goes lower it evaporates even faster and the accretion lowers, it is very hard for a black hole with a non-ridiculous lifetime (i.e. smaller than the lifetime of the universe) to jump out of it purely through accretion. A good estimate of the lifetime is [58]:

$$\tau(M) \sim 10^{64}\mathrm{yr}\left(\frac{\mathrm{M}}{\mathrm{M}_\odot}\right)^3\ . \tag{2.14}$$

The lifetime of PBHs sets the strongest constraints, they can not be the DM if they do not exist after all, but τ is not the only possible constraint. While black holes bigger than $10^{15}g$ would survive to today, the ones closer to that range would still emit a fair bit of Hawking radiation. If they are the DM this could bump the extra-galactic background light up by a noticeable amount at certain frequencies, but there is no such bump in current observations [59]. This helps set further constraints.

There are hopes for even tighter constraints in the future by improving our detectors [60], but there are vastly diminishing results. One small issue that becomes relevant is that spin now is non-negligible, as the emission and its spectra depend on if the PBH rotates or not. In practice this change is expected to be less than an order of magnitude in the mass ranges constrained, but that makes those mass ranges close to the constraints more dubious, as they might be covered or on the opposite way ranges we think are currently impossible might be where PBHs are hidden.

That might not be it all however, as one of the more curious byproducts of this evaporation might be Planck relics. They are theorized particles of Planck mass ($\sim 10^{-}6$g) left after a black hole evaporates [61]. They would be completely new physics, resulting from quantum gravity and their existence is contentious. Nonetheless, if they existed they could be the DM in the case a massive quantity of PBHs with very small mass evaporates in the early universe and leaves them behind. Due to their extremely low mass and unknown properties, it is likely if that was the case we would not be able to detect them in any way, at least not in the close future.

2.4 Gravitational waves detectors

As mentioned, LIGO opens a new window in astronomy, the possibility of using gravitational waves to detect black holes. The singular events that emit most gravitational waves are binary mergers: 2 massive objects orbiting one another that slowly inspiral until they end up colliding and fusing into a single object.

Gravitational waves are not only emitted in the merger itself. Rather, they are the reason the merger itself happens. As 2 massive objects orbit one another they will emit gravitational waves from their movement, as two massive objects perturbing the local space-time with their moving gravitational potential. These are very small and initially undetectable, but similar to radiation the emission of gravitational waves costs energy to the source. The energy stored in the orbit is slowly emitted, causing the energy to lower and so for the orbit to become similarly smaller. As the orbit decays however the tidal forces coming from the other object perturb the source further, causing more emission of GWs and further decay. This happens of course too equally for the other object. In a perfectly symmetrical case the inpiralling binaries would meet in the middle, colliding and merging despite being otherwise completely isolated. The GWs emission is what turns the initially stable binary into a future merger.

While the GWs emission peaks during the merger, LIGO has enough resolution to see the waves from just before the merger, which can give individual information from the objects. It can be used for example to constrain a neutron star equation of state. There is an important caveat however: while it can get some information of the individual members of the binary, a lot of it is degenerate with other parameters. It is also still very hard to distinguish between a neutron star and a PBH without also an electromagnetic counterpart, with currently all neutron star detections without a visible counterpart being based on mass.

This, together with the already mentioned first generation sensitivity of LIGO, limits its usefulness for PBHs in particular. Detecting PBHs or placing strong constraints on them as dark matter is very hard if you cannot detect black hole merger events with light masses. Current constraints in the mass range of LIGO exist from the fact that if PBHs were the dark matter there would be so many of them the merger rate would be much higher than the one we observe.

There are still other ways in which GW detectors can be helpful however. While LIGO cannot get any information on the individual spin of an object, it can obtain what is called as the effective spin of a Binary Black Hole [62]:

$$\chi_{eff} \equiv \frac{(m_1\chi_1 + m_2\chi_2)}{M} = \frac{c}{GM}\left(\frac{\vec{S}_1}{m_1} + \frac{\vec{S}_2}{m_2}\right) , \tag{2.15}$$

where χ_i is a dimensionless spin parameter project over the z axis, but which can be related to the angular momentum spin of the star $\vec{S}_i$ as shown in the rightmost term above. m_i is the mass of each object and M the total mass of the merger.

As can be seen, the effective spin is degenerate with individual value of each spin, and worsened by the fact that the spin can easily be negative as two black holes rotate in opposite directions. Thus, $\chi_{eff} \sim 0$ could mean low spins in both black holes or a very highly counter-rotating duo.

Currently LIGO has showed the GW events it detects have a preference for a smaller effective spin, very close to averaging 0, than expected [63], but the uncertainty is still too high and there have been individual events with indications of at least one of the members of the binaries having non-negligible spìn value. For now results on this front are ambiguous.

Another option to help distinguish PBHs are more statistical arguments: for stellar origin black holes we expect their number of mergers to peak with star formation, as they form from stars that are very massive with very short lives. This peak would be situated at $z \sim 1$ [64], while in contrast PBHs would peak at much higher redshifts and slowly decay afterwards. Unfortunately, current detectors are incapable of distinguishing stellar origin from non-DM PBHs this way. Even for the most massive binaries LIGO does not have enough resolution to resolve mergers at redshift 1 [65], so trying to see where mergers would peak in a redshift distribution is not viable.

The solution is to wait for more powerful next generation detectors, particularly LISA [66],but even with the improved resolution there is no guarantee of much better odds, particularly if we are searching for lower mass PBHs.

An interesting alternative is not searching for individual events, but for their added effect. Just how like multiple sources we cannot identify individually contribute to a background in radiation, the same applies for gravitational waves. Mergers we do not have resolution to identify are still there, and joined will create a non-zero background for our detectors. This commonly identified as the Stochastic Gravitational Wave Background (SGWB). While it is extremely hard to obtain individual values from the background, it is the addition of a lot of unidentified mergers after all, the background follows the same statistics as the mergers. This means, the SGWB will peak similar to mergers mentioned before, which could be used to put improved constraint on subsolar PBHs in the future [67].

This gravitational wave background will not only come from unidentified mergers though. As mentioned, gravitational waves are quite literally aftershocks in space-time. This does not extend only to massive objects, but also to perturbations, like the ones creating the PBHs. As the perturbations reenter the horizon and either dissipate or start the collapse, there is an emission of gravitational waves [68]. The combination of all that GW emission would result in another background that could give information about the PBH generation and abundance. Of note is that while perturbations require new physics to be produced in large enough quantities to produce PBHs, this background would depend only on the perturbations themselves and thus requires no knowledge of the specific model or physisc to simulate.

While LIGO's limitations still apply [69], this makes the future LISA mission even more interesting. Particularly, the range of LISA would cover the GW background that perturbations that would result in $10^{-12}\,M_\odot$ PBHs would make [70]. Considering this is one of the few windows remaining for PBHs to be all the dark matters, as can be seen in figure 2.1, this is a very exciting possibility. Unfortunately, all projections for the LISA

mission predict launch in 2037 or later.

2.5 Non-monochromatic constraints

With the main sources of PBH constraints discussed, it is now perhaps time to ask why monochromatic constraints have remained so popular without taking into account extended mass distributions. As can be seen directly with equations 2.8 and 2.14, adding multiple masses would likewise end up adding multiple constraints in a fairly simple way. Those mass ranges could be considered constrained by just assuming a monochromatic mass of less abundance, but using an extended mass distribution would be both more accurate and likely increase the strength of the constraints as constraints in adjacent mass ranges could contribute too.

Unfortunately, while the cases for microlensing and PBH evaporation work very well, this is because their constraints come from effects that have a direct relation with mass. Both equations 2.8 and 2.14 are analytic expressions that contain the mass (through the Einstein angle 2.5 in the microlensing case). In other constraints the effect can be more indirect, a good example being gravitational waves: we would not only see the PBHs of a certain mass, but their abundance and spread would directly affect how many mergers we expect to see if they are the dark matter. Another good example can be simulations of dynamic effects the PBHs would have. While technically possible to account for an extended mass distribution, the time and computational cost make it an impossibility. Even in cases different to those two, if no direct analytical relation exist between the constraint and mass it is much harder to deal with, as it would require integrating over different masses all the process rather than just one equation.

[34] studied the issue in a thorough way, and reached a similar conclusion. To convert a monochromatic constraint into one for an extended mass function you would need to compute:

$$g(M_{eq}, p_j) = \int dM \frac{d\Phi_{EMD}}{dM} g(M, p_j) \ , \tag{2.16}$$

where g is a function that encloses the details of the underlying physics of the particular constraint and depends on the PBH mass M and a set of astrophysical parameters p_j. Φ_{EMD} is the shape of the extended function. M_{eq} is the result we seek, the equivalent mass. It is defined as the individual mass in the monochromatic constraint that the extended function is effectively equivalent to. In summary, if an extended distribution has a $M_{eq} = 10^{-6}\,\mathrm{M}_\odot$, it would constrain the abundance of PBHs of the extended distribution to the same degree as $M = 10^{-6}\,\mathrm{M}_\odot$ is in the monochromatic constraints.

g must be determined individually for each different constraint, and should enclose both the physics of the constraints and the way the observations were taken (for more details we refer to [34]). Again, for some constraints g will be an analytic expression we know and there will not be any major issues resolving the integral above and finding M_{eq}. But for other constraints g is much, much harder to determine

Something else to note is that while this allows us to find constraints for extended mass distributions through only the monochromatic constraint, this does not work with 2 different set of constraints. Indeed, because the physics differ between 2 sets of constraints, that is where the extended mass functions causes more issues. For purely monochromatic

constraints this is no problem, as there is no addition of different types of constraints, the bigger one is the one we apply, simple as that.

However, for extended mass distributions the extremes of one could touch two different sets of constraints, so there is a temptation to just fit the extended mass distribution in the monochromatic graph above. This is a mistake however, as we should rather compute the extended constraint from each individual type and take the more stringent one, similar to the monochromatic case. Besides the one described above, other methods exist [36] to translate monochromatic constraints into extended ones, but have similar difficulties.

The type of extended function we expect is also open to debate. A lognormal mass function is the one commonly believed to be a good approximation for the standard PBH formation path of fluctuation collapse [71]:

$$\psi(M) = \frac{f_{PBH}}{\sqrt{2\pi}\sigma M} exp\left(-\frac{log^2(M/M_c)}{2\sigma^2}\right) , \tag{2.17}$$

where M_c is the mass of the peak, the one we commonly associate with the monochromatic constraint, and σ is the width of the distribution. The value of these parameters depends directly of the model used. However, as keeps repeating, particular models can result in particular mass functions, including power functions and even very sharp mass distributions that are very close to a purely monochromatic one.

Overall, extended mass distributions seem to create more stringent constraints than monochromatic ones, but it is not possible to generalize for all cases and graphs have to be individualized for each type of distribution. In comparison, the monochromatic constraints figure is generic and much easier to produce. This is the main reason it keeps being used.

While different, something similar happens with clustered distributions. These come from models where for some reason the PBHs form in a more dense distribution rather than the typical more homogeneous spread. Like before, the change in signals and constraints must be treated individually for each mass range in question. Care has to be given though, because while clustering can decrease the constraints for some mass ranges, on some cases it can also introduce new signals that should not be overlooked. A good example are binary mergers: clustering significantly decreases the constraints of LIGO, as most mergers would have occurred in the early universe due to PBHs being closer to each other, but those previous mergers also create a very significant stochastic GW background that would be within the LIGO/VIRGO sensitivity [37].

2.6 Existing windows

Among all the discussed constraints for smaller PBHs that could be all the dark matter, there still remains a sizable window between 10^{-16} and $10^{-11}\,M_\odot$. This window is extremely hard to probe with usual methods, as they are PBHs too small for either gravitational waves or microlensing events to leave a big enough signal for our current detectors, but also are too big to be affected by evaporation. Their mass, roughly corresponding to the one of an asteroid, also makes it exceedingly hard to detect them through conventional methods in big enough numbers to say anything about their abundance even if somehow a few could be found.

There have been a number of attempts to constrain them, but they have run into impediments. A good review of all attempts can be found in [72], but to summarize

most have been trying to detect the effect of such PBHs onto more standard objects like stars. One of the most noticeable would be their interaction with neutron stars. Being extremely dense objects too, their friction with the PBH's horizon would be big enough for there to be a chance for a PBH that is crossing a neutron star to be captured by it and fall towards their core. Despite the extreme high density of the core, the PBH itself would be unaffected, rather due to such high density it would accrete the entire neutron star very quickly, almost instantly for galactic and cosmological time scales. The survival of neutron stars could then be used to put a constraint on PBHs, as if PBHs are all the dark matter then those events could very common making neutron stars very rare. The possible masses in the window are both small enough so there are plentiful of PBHs to collide with, but also big enough they could accrete the neutron star sufficiently fast.

As mentioned in the review however this has run into a couple of issues. The simplest one is that even with PBHs being all the dark matter such captures would be relatively rare, as neutron stars are both uncommon and also small size wise, meaning collision is unlikely in teh first place. The second, which compounds with the first, is that there is a high degree of uncertainty on the DM density of globular clusters. Globular clusters are expected to have very low velocity dispersions, which would make the type of capture we are discussing much more likely together with high DM density. But that very high density dark matter, which the initial studies expected to have and depended upon, is very reliant on the on globular cluster's possible origin, which is currently uncertain. As such regions were the only ones from which non-negligible constraints could be extracted, any results from those initial assumptions are severely undermined.

This means that despite this rather novel idea, $10^{-12}\,M_\odot$ PBHs remain one of the very few windows where PBHs could provide all the dark matter. There exists more exotic models that avoid most of the other constraints, but if using standard inflation perturbation collapse with as few extra elements as possible they remain as one of the last possibilities. Thus, any kind of physical event that could leave a lasting effect based on such window and therefore result in observational consequences of some kind, that could lead to either constraints or evidence in favour, is of the utmost priority and worth studying.

CHAPTER 3

PRIMORDIAL BLACK HOLE CAPTURE BY STARS

Following directly from last chapter, $10^{-12}\,M_\odot$ black holes are one of the last windows where PBHs could be all the dark matter. However, part of the reason they remain possible is they are very hard to detect in any meaningful way. While finding a single $10^{-12}\,M_\odot$ black hole would be huge, as one case alone would be enough to instantly prove the existence of PBHs, a single detection alone would not say to us much about their abundance throughout the universe, meaning the dark matter question would remain open.

Thus if possible we do want to search for ways which would help us constrain that. A possible way was the one mentioned previously, where stars would capture those small PBHs. In this chapter we aim to look again at what that means and improve upon that method to obtain a way in which $10^{-12}\,M_\odot$ PBHs finally leave an observational consequence we can look for.

3.1 Capture: what it is

One of the very few ways to constrain the $10^{-12}\,M_\odot$ PBH mass range is their interaction with neutron stars [40], concretely their capture. A more advanced way of looking at it also took into account their interactions with the progenitors of such neutrons stars, which at the time would be common, if big, main sequence stars [41, 73]. As mentioned before, such attempts at constraints fail in part because the expected high DM densities at the chosen environments were not supported by evidence. But what exactly are we talking about when we use capture, what would the specifics of the method be?

If PBHs are all the dark matter then we expect them to share the characteristics of dark matter. This means mostly density but also includes velocity. The end result is that PBHs are not static, but rather they move through the dark matter halo they inhabit.

Those movements mean there is a chance they get near and then interact with other objects within the halo, like stars for example. We even expect stars to have a surrounding density of dark matter that is bound to them, as stars are much more massive objects in comparison. Just like stars gravitationally bind baryonic matter in the form of asteroids and planets, they would similarly bind dark matter. Until now nothing unusual.

However, if PBHs are the dark matter there are a range of new possibilities emerging from this. The most basic case is the one with the neutron star. If PBHs are moving through the halo, there is a chance they might cross a neutron star. Because the neutron

star is very dense, the act of crossing it would cause enough dynamical friction to affect the PBH.

As a small aside, standard dynamical friction is collisionless and comes from purely gravitational interactions [74], thus it does not matter that the object crossing is a black hole or any kind of exotic matter, they will still be slowed down in equal measure.

The end result is that if the PBH is not going very fast, then the further slowing from the dynamical friction might be enough for the PBH to become gravitationally bound to the star, and even further fall down towards the center of the neutron star and stop there. The later is what we call capture. At the center of the neutron star the density is so high that the PBH would be able to accrete it entirely in a very short time, resulting in a PBH the mass of the neutron star but no neutron star left.

The idea of [40] was that then we could use the survival of neutron stars as a proof that these kind of $10^{-12}\,M_\odot$ PBHs do not exist, for if they would exist then almost all neutron stars would have been eaten in globular clusters. As we do see some neutron stars in globulal clusters we can set up corresponding constraints on those mass ranges.

This was later expanded for main sequence stars [41]. Main sequence stars are not dense enough to stop a PBH from a single crossing, and even then the star's core does not have the high density that would result in a PBH accreting them instantly. But a subsection of those stars will end up forming neutron stars, thus previous interaction with the star can affect what happens later with the PBH and the neutron star.

This becomes more interesting because we expect most of stars to have set density of dark matter already bound to them without any initial need for dynamical friction. The bound dark matter comes from just before the start of the star's main sequence, as the progenitor molecular cloud collapses into a protostar. While complex, we can approximate this process as an adiabatic contraction, and the resulting changes in the gravitational potential from the cloud becoming more compact will naturally gravitationally bind matter that is close by and slow enough. This extends of course to dark matter, in our case PBHs.

The end result is there are a number of PBHs already orbiting the star as the main sequence starts. The orbit these PBHs will have are random, but due to this we can expect them to have what we call a flat eccentricity distribution, where for a fixed energy all possible orbits are equally probable. Some of these orbits can by chance cross the star, similar to the previous case. Stars are less dense, so a single crossing will not be enough, but for a stable orbit there will be many crossings until the end of the main sequence. The effect will be gradual, but as the PBH loses energy the orbit will also naturally end closer to the center of the star, speeding the process with both shorter orbits and higher density.

Then, once the star ends the main sequence a number of PBHs could be lodged at the center or very close. When the star becomes a neutron star, the PBHs will already be at the center and accrete the resulting neutron star just after its birth. This can give constraints in a very similar way to the previous neutron star case exposed above. While simplified, this is the method both [41, 73] were using to set improved constraints over the basic neutron star case.

As mentioned before there were issues however. Capture is very reliant in both high density and low velocity PBHs (DM). High velocity means high energy which means they will need a lot of dynamical friction before they are bound to the star. Even for the main sequence star case, high energy means larger orbits that have both lower chance to cross the star and will take longer doing so, resulting in fewer captures. Globular clusters were

the only current examples of high density and low velocity dark matter environments, that could set non-negligible constraints on the mass range. Once the high dark matter density of globular clusters became dubious, this rather interesting way to constraint low mass PBHs lacked a setting where its effects would be noticeable.

However, such circumstances of high density and low velocity are not unique to globulal clusters. High DM density are hard to achieve in our current universe, but we do not require going to globular clusters as we have high density in early redshifts. The early universe was more dense than the current one, with the highest the earlier we go, even up to the first stars at $z \sim 20 - 30$. Not only that, while not as low we also expect very low dispersion velocities in the early DM haloes that form at such redshifts.

A simple counter-proposition is that the attempt to constrain came from the survival of neutron stars. If the process was applied to early redshifts, then we would need to observe old neutron star for constraints to be valid. This is not only a problem because we would need reliable methods to determine the age of a neutron star, but also because we would expect relatively few of these old neutron stars to be in the Milky Way which means very low chance we have one nearby. Observing far off neutron stars would be extremely hard, as they are compact objects of slightly lower mass to black holes. While very bright neutron stars exist, mass is the usual way to distinguish the non-emitting ones from black holes. For distant neutron stars almost all of them we would not see, so we could not distinguish the neutron star from the PBH that might have eaten it.

Such second issue however can be settled by focusing on main sequence stars regardless of if they form neutron stars. As described above even with normal stars we expect the PBH to eventually be captured at the center (or very close) of the star. While the accretion process would not be close to instantaneous, like neutron stars, because we are talking about the early universe there is much more time for the PBH to devour the star so we can observe it currently. We also expect the majority of such stars to be low mass stars, below $1\,\mathrm{M}_\odot$.

The end result would be sub-solar mass black holes, that can only come from PBHs. Not only that, the number of objects would expand as we expect there to be a lot more low mass stars in comparison to neutron stars. This would mean a small number reaching the Milky Way would not be unexpected, and give a very easy to understand observational consequence. While the whole process of capture and accretion would take far longer, if we set the initial interactions at the early universe we would have $\sim 10^{10}$ years. Using low mass stars will also avoid issues with the end of the main sequence, such as supernova kicks possibly altering the whole process.

Using this method as a base, we will try to improve on previous results by using our own model. We will attempt to compute this PBH capture in a conservative way, so we should obtain at least a minimum to how common the process is and if we should see any sub-solar black holes at all.

We set our model in the early universe, and also look to majorly expand on a number of issues not accounted on previous papers. While our modeling of the star and the PBH is as simple as the ones before, we resolve the dynamical friction that slows the PBH numerically using low metallicity stellar simulations to avoid approximations as much as possible. We also attempt to use different types of dynamical friction to measure if there is any difference. Finally we make an attempt to compute the degree of expected perturbations outside the system that could interfere in our model and perturb the result.

3.2 Our model

3.2.1 Dark matter density profile around first stars

The first step is to find the parameters that will characterize our model of the star and PBH at early redshifts.

We start by attempting to determine $\bar{\rho}_{DM}$ around a certain star as determined by its position and redshift, and more specifically its profile depending on the radius to the star itself. While the main assumption is this DM is majorly composed of small PBHs, the profiles themselves should not differ in any major way from other types of Dark Matter, and can thus be computed similarly.

As mentioned before, we want an epoch with both high DM density and low velocity dispersion, but also where stars have already started appearing. The most common estimate for the formation of first stars is $z \sim 30 - 20$, so we will take the lower bound of $z = 20$ and start there.

For any cosmological model we can obtain the critical density ρ_c at a redshift, and from it the virial radius and density for a halo of any given mass. Taking this mass to be $M_{Vir} = 10^7\,\mathrm{M}_\odot$ we can find:

$$R_{\mathrm{vir}} = Mx \approx 200\,\mathrm{pc}\ , \tag{3.1}$$

$$\rho_{\mathrm{vir}} = \rho_c \Delta_c \approx 1.8 \cdot 10^8\ \mathrm{M}_\odot/\mathrm{kpc}^3\ \ , \tag{3.2}$$

where Δ_c is the critical overdensity needed for the halo reform, related to the δ threshold we described earlier, which depends on the redshift.

we assume the halo has a standard Navarro-Frenk-White profile, which depends on two parameters c and ρ_0, the first measuring the concentration, how clumped up the halo is, and the second a characteristic density. To obtain the average density at any R we will need to fix at least one parameter. We introduce a simplification $\mathrm{R_s} = \mathrm{R_{vir}}/\mathrm{c}$ to end up with:

$$\bar{\rho}_{DM}(R) = \frac{\rho_0}{\frac{R}{R_s}\left(1 + \frac{R}{R_s}\right)^2}\ . \tag{3.3}$$

We decide on a conservative approach and take c such that the density at a $R = 0.1R_{vir}$ is 10 times the Virial density as seen in (3.2). This corresponds to a $c = 10$, and compares favourably with observations of high redshift haloes. We can simplify further by using $s = R/R_{vir}$ and by using the universal formula definition of ρ_0 [75]:

$$\rho_0 = \frac{\rho_{crit}\Delta_c c^2}{3s(1+cs)^2\left[ln(1+c) - c/(1+c)\right]}\ . \tag{3.4}$$

Combining with (3.3), this results in:

$$\bar{\rho}_{DM}(R) \approx \frac{10^3\rho_{vir}}{44.7s\,(1+10s)^2} = \frac{4.03}{s\,(1+10s)^2}\,\mathrm{M}_\odot/pc^3\ , \tag{3.5}$$

where all the variables are the same as before.

With this we have the $\bar{\rho}_{DM}$ at any position of the halo where a star could form. However, during the star formation process this average density will be perturbed, particularly

near the future star. As the initial molecular cloud collapses into various clumps previous to a protostar, the surrounding DM will contract adiabatically with it.

We work with the most simplistic case, in which we suppose the clump is mostly isolated and will form a single star. The PBHs will have a starting density $\bar{\rho}_{DM}(R)$, and some of them will be bounded to the baryonic cloud if their speed is low enough. As the baryonic matter collapses, the bounded PBHs will adiabatically contract with it, changing the shape of the distribution.

Through Liouville's theorem we can estimate the final shape of this distribution using the phase space density. For this we have to assume the phase space density is still completely full, and also approximate the final speed as the one corresponding to a circular orbit for the bound density. While this might look overly simplistic, [73] found that even while using numerical simulations the end result had a shape $\sim r^{-3/2}$ equivalent to the one found through Liouville.

The initial maximum phase space density Q_{max} (before the contraction) corresponds to $v = 0$ for a maxwellian distribution, but it does not strictly require it, only that the velocity distribution is flat near the 0 [41]. Comparing with the phase space after the contraction:

$$Q_{max} = \left(\frac{3}{2\pi}\right)^{3/2} \frac{\bar{\rho}_{DM}(R)}{m_{DM}^4 \sigma^3} = \left(\frac{3}{2\pi}\right)^{3/2} \frac{\rho_{DM,bound}}{m_{DM}^4 \left(GM_*/r\right)^{3/2}} , \tag{3.6}$$

where r is the radius to the center of the star/proto-stellar object, m_{DM} the dark matter mass, M_* the mass of the star and σ the dispersion velocity. We stress the difference of r with R; R tracks the distance from the system to the center of the halo (and thus galaxy), and is a parameter that is constant for all the orbits, while r is the distance of the PBH to the star, depends on the orbit and will thus change with it. By continuining from equation (3.6) we eventually get:

$$\rho_{DM,bound} = \frac{\left(GM_*/r\right)^{3/2} \bar{\rho}_{DM}(R)}{\sigma^3} . \tag{3.7}$$

As it represents the good number of PBHs tightly bound to the star from the beginning, $\rho_{DM,bound}$ itself will only be affected by extremely powerful external events or outside perturbers, which we try to quantify in section 3.2.5, but will otherwise not change once the main sequence starts. This means that even if the process of falling to the star is lengthy, the $\rho_{DM,bound}$ of the star system is uniquely determined by the initial conditions of the star system within the DM halo.

Together with equation (3.5) for $\bar{\rho}_{DM}(R)$, we can thus find the profile around our star. The only remaining unknown variable is $\sigma(R)$, for which we will take the analytic estimate from [76], which contains both a symmetric case and one with velocity anisotropy that more closely resembles known galaxies.

3.2.2 Stellar models

With the conditions around our star set, it is perhaps time to ask about the stars themselves.

While the reasoning for why we would aim our model at high redshift is sound, there are still issues around it. One of it is stars. The first stars, completely metal free stars

with metallicity $Z = 0$ as they would form before supernova release metals on the void, are poorly understood [77]. They would appear in small DM haloes of $10^5 - 10^6\,M_\odot$ at $z \sim 30 - 20$, where a massive star would form at the center. This should in theory work against our simplistic case. Fragmentation that generates low mass stars is possible [78,79] and common, but the process is still poorly understood.

It is this lack of understanding combined with a rapid shift towards standard star formation that gives us confidence to pursue our model. While we expect metal free stars to form as they are normally expected, simulations also show that just giving the system a bit of metallicity, $Z \sim 10^{-4}$, starts to shift their properties closer to current stars. Current observation also expect that shift from metal free to standard star formation be very fast. Our aim is for this transition period, where we still are at very high redshifts with very dense environments and very metal poor stars, but star and galaxy formation are closer to the standard with many low mass stars, thus the lower end of the first star epoch in $z \sim 20$.

In this study we use stellar models of differing masses, which were graciously computed at our discretion using the open-source software instrument Modules for Experiments in Stellar Astrophysics (MESA) [80]. These models are given to us for various ages, from 10^8 years to exceeding the lifetime of the universe. For each age given we can obtain the density, temperature, speed of sound, mean atomic weight and pressure at all radii of the star, allowing us to directly apply all the methods we will describe after.

All the models are extremely metal poor $Z \sim 10^{-4}$ stars, to represent a star at that very high redshift. Of note is that lower metallicity stars are less compact and so less dense, so even if we move our model to start at lower redshift our results should still work as a minimum estimate for PBH capture.

Evolving the star together with the PBH orbit from its formation and ending at 10^{10} years would give the most strictly accurate results. In practice, the difference between the youngest models just after starting their main sequence and those at 10^{10} years has little effect on our final results and is not worth the extra computational cost. Thus a fixed age depending on their lifetime and flags given by MESA is chosen for each stellar model, aiming for both a similar evolution stage between the various stars and one which would closely resemble all the various stages the singular star would live through 10^{10} years.

A marked exception to this are our 2 lightest stars, with 0.4 and $0.32\,M_\odot$. Even within 10^{10} years both the stars would have just started their main sequence and have their evolution at a very early stage compared to the heavier models, with density and temperature lowering with age rather than the opposite, which we expect later in their life. As our final aim is to set our results as conservative as possible, we choose the 10^{10} years model, which also results in them having among the lowest central density of all stars, contrary to expectations. Comparing our final results in these 2 stars with ones acquired using older, 10^{12} years old versions of their models show the differences still being rather small, thus we are optimistic that none of these factors has any major effect on our conclusions. Similarly, we believe changing our models for completely standard solar metallicity stars similar to our Sun would also change little.

An example of density against radius for all the stellar models chosen can be seen in Figure 3.1, while we show the temperature versus radius graph on Figure 3.2. The stellar ages chosen are 1.5, 3.2, 1.3, 1.3, 10, 10 Gyrs for 1, 0.79, 0.63, 0.5, 0.4, 0.32 $M_\odot$ stars respectively, with stability of the model put as first priority and similar stellar age between models as second.

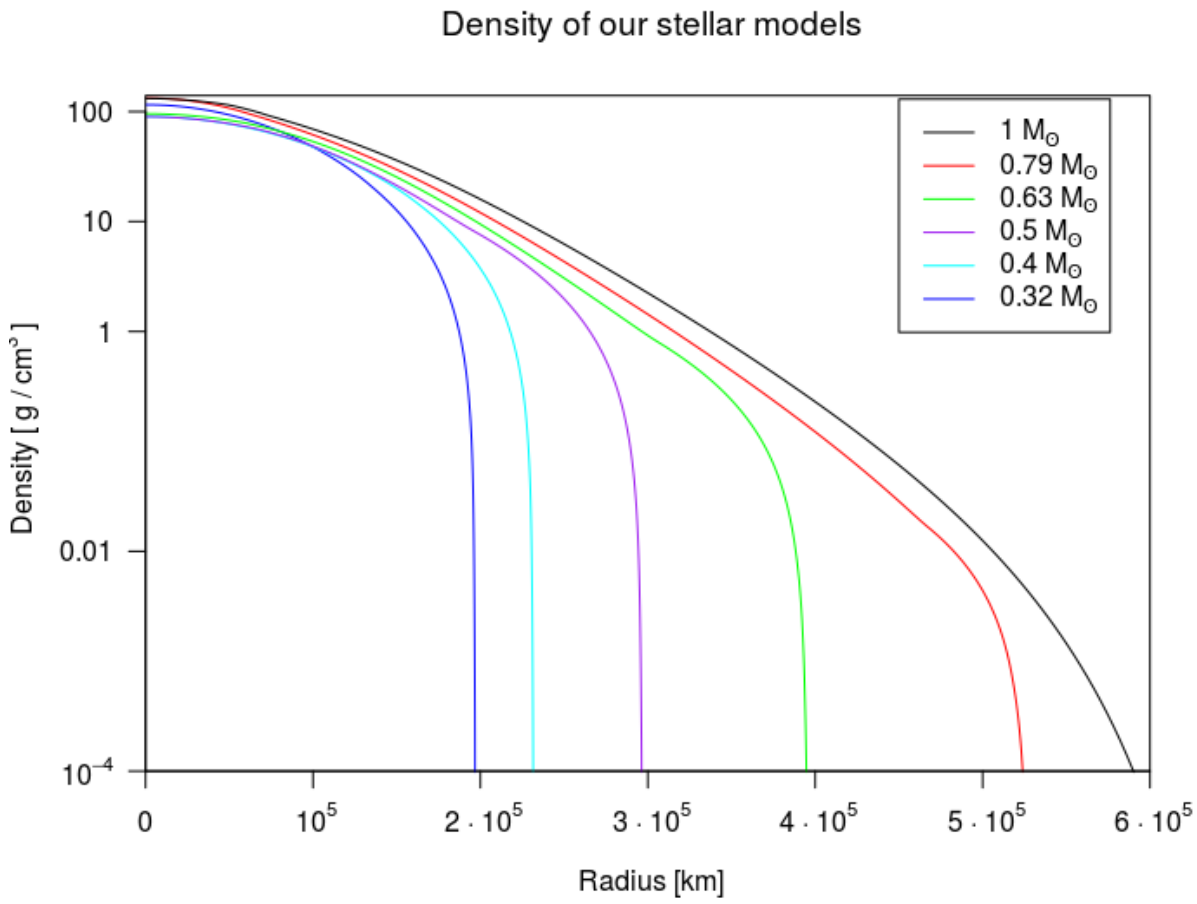

Figure 3.1: Mass density profile for our stellar models of different masses. We have chosen stellar ages that suited our objectives: 1.5, 3.2, 1.3, 1.3, 10, 10 Gyrs for 1, 0.79, 0.63, 0.5, 0.4, 0.32 $M_\odot$ respectively. In practice, as long as nuclear reactions have started in the core, variation in time of the profile is negligible to our results.

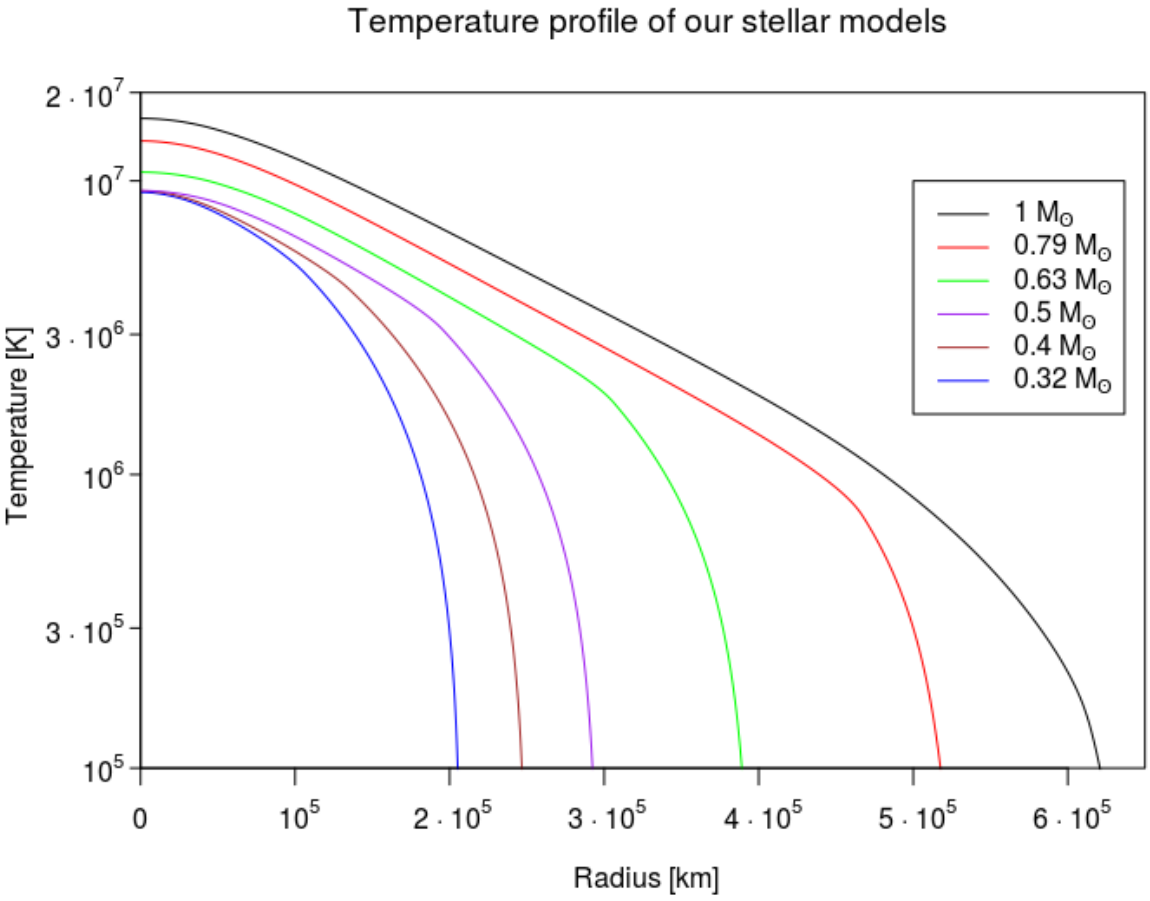

Figure 3.2: The temperature on each radius for our various stellar models. Applies the same as above for our stellar models age.

3.2.3 Black hole capture: dynamical friction inside the star

Now we can move to the main aim of this chapter, estimating the capture rate of $10^{-12}\,M_\odot$ PBHs by stars. Finding the profile and stellar models were only the first steps, the follow up is to quantify the process in which the PBH ends up in the core of the star.

The main mechanism by which the PBH might fall towards the core the star is dynamical friction, where the PBH crosses the surface of the star and gravitational and more complex interactions result in an energy loss. We will assume that friction by any other objects besides the star, or any other form of energy loss, is negligible for the most conservative approach. This is accurate for our simple model with only a star and its DM profile, but even with other possible objects the star should remain the most massive by far and our estimate reasonable. There is the possibility of capture through tidal interactions, but both [73] and [72] agree that its effect is overall negligible.

The dynamical friction depends on a number of variables. The star must be modelled accurately too. For this, we have used stellar models described previously, from which we obtain the density, temperature, speed of sound, mean atomic weight and pressure at all radii of the star.

We also need to give the PBHs both an initial energy and angular momentum, but once both are set we can evolve the system self-consistently, both in the case the PBH is in an stable orbit or the case it is just a non-bounded object passing by. We do know the effects of single cross will be extremely small (look to our results in section 3.3.1 or previous calculations by [81]), so we can ascertain that its effects on the current orbit will be negligible. Thus we assume a standard Keplerian orbit when it is not within the radius of the star, and that both the energy and the angular momentum will remain constant for that single orbit; we can thus compute the dynamical friction as 'kicks' to a orbit that result in loss of energy and angular momentum.

$$\mathrm{l} = \mathrm{b}\cdot \mathrm{v}_\infty = \sqrt{\mathrm{GM}_*\left(1-\mathrm{e}^2\right)\mathrm{a}} = \sqrt{\frac{\left(\mathrm{e}^2-1\right)\left(\mathrm{GM}_*\right)^2}{2\mathrm{u}}} \tag{3.8}$$

$$\mathrm{u} = \frac{-\mathrm{GM}_*}{2\mathrm{a}} = \frac{\left(\mathrm{e}^2-1\right)\left(\mathrm{GM}_*\right)^2}{2\,\mathrm{l}^2} = \frac{1}{2}\mathrm{v}^2 + \Phi\ , \tag{3.9}$$

where e is the eccentricity, a the semimajor axis, b the impact parameter and v_∞ is the speed the PBH had at infinity. We also use the specific version of energy u and angular momentum l which result from dividing both by mass for simplicity.

When in orbit, the angular momentum depends on both eccentricity and energy, while the energy depends on angular momentum and eccentricity too. This means fixing l and e also effectively fixes the eccentricity.

With the orbit set, we want to compute the energy loss of the PBH as it crosses the star. The dynamical friction itself can be computed through Chandrasekhar's collisonsless formula [74], or through Ostriker's variation [82] which takes into account collisional effects from the gas. For Ostriker's case in particular we will use an improved analytic estimate by [83], obtained from numeric simulations and much better suited to extreme cases like ours.

$$\mathrm{a}_{\mathrm{df}} = \frac{\mathrm{d}\,\tilde{\mathrm{v}}_{\mathrm{BH}}}{\mathrm{dt}} = \frac{-4\pi\mathrm{G}^2\rho\mathrm{M}_{\mathrm{bh}}}{\mathrm{v}_{\mathrm{BH}}^2}\mathrm{I} \tag{3.10}$$

$$\mathrm{I_{Chandrasekhar}} = \left[\mathrm{erf}\left(\frac{\mathrm{v_{BH}}}{\sqrt{2}\Sigma}\right) - \frac{2\,\mathrm{v_{BH}}}{\sqrt{2\pi}\Sigma}\mathrm{e}^{-\frac{\mathrm{v_{BH}^2}}{2\Sigma^2}}\right]\ln\Lambda \tag{3.11}$$

$$\mathrm{I_{Thun}} = \ln\left(\frac{\mathrm{R_{max}}}{\mathrm{R_{SO}}}\right) = \ln\left[\mathrm{R_{max}}\left(\frac{1}{2}\frac{\mathrm{Mach}^2}{\mathrm{Mach}^2-1}\frac{2\mathrm{GM_{bh}}}{\mathrm{v}^2}\right)^{-1}\right]\,, \tag{3.12}$$

where erf is the error function, $\Sigma = \sqrt{\frac{3kT}{\mu m_h}}$, Mach is the Mach number, $\Lambda = \left(\frac{\mathrm{R_{max}}}{\mathrm{R_{min}}}\right)$. $\mathrm{R_{max}}$ and $\mathrm{R_{min}}$ are respectively the maximum and minimum impact parameter for the interaction, while T is the temperature, m_h the Hydrogen mass, k the Boltzmann constant and μ the mean atomic weight. We take the radius of the star for $\mathrm{R_{max}}$ as is standard, while for $\mathrm{R_{min}}$ both the Bondi accretion radius and the PBH's Schwarzschild radius can work, with only a small factor of difference. We have also assumed supersonic velocities and an adiabatic index of 5/3. Given that the escape velocities at the surface is already greater than speed of the sound at the core of the star, we foresee no problems for the first case. Still, we checked for all our models and we did not find a single case where Mach < 1 (any such cases are most likely already captured deep within the star). For the second assumption, at most it would add a factor 2 to the dynamical friction for the most extreme and unlikely values, so we opt for the most conservative approach.

With $\mathrm{a_{df}}$, it is possible to find the energy lost. As the $\Delta\,\mathrm{v}$ in a single transit is very small, we can take an approximation to make it even easier:

$$\Delta\mathrm{u} = \frac{(\,\mathrm{v}+\Delta\,\mathrm{v})^2}{2} - \frac{\mathrm{v}^2}{2} = \,\mathrm{v}\Delta\,\mathrm{v} + 2\Delta\,\mathrm{v}^2 \simeq \,\mathrm{v}\Delta\,\mathrm{v} = \,\mathrm{v}\,\mathrm{a_{df}}\,\mathrm{dt}\,. \tag{3.13}$$

This result can then be integrated to obtain the total energy loss in a single transit. For details see Appendix A.

3.2.4 Average number of captured black holes

While the friction from a single pass is likely negligible [81], the time scale of the orbits compared to the lifetime of a star makes it possible for it to have an effect on the orbit of the PBH. Concretely, we will define a black hole is captured, as opposed to just gravitationally bound, when its apoapsis is below the star's radius and so the orbit is fully inside the star; it is straightforward to prove that the PBH will end up completely in the core within $t \leq 10^8$yrs once this happens, which we show on the Appendix B. This limit is also the same used in [72], where they establish it using phase space arguments instead. We can then define an eccentricity by which the PBH will end up captured in $t = 10^{10}$yrs, which we will call the critical eccentricity $\mathrm{e}_c(r)$. All eccentricities above $\mathrm{e}_c(r)$ will have smaller or tighter orbits, meaning they will cross closer to the center of the star with higher densities and so higher dynamical friction. This will result in the PBHs being captured in a shorter time than the $t = 10^{10}$yrs established, and thus might leave observable consequences.

With the energy loss, studying the evolution of the PBH orbit is straightforward. With its energy and eccentricity (angular momentum) we can determine the orbit and its period with which we can compute the energy loss for each orbit. With the energy loss we can also obtain the change in angular momentum:

$$\begin{cases} \frac{d\,\mathrm{l}}{dt} = \frac{|F|}{m}r\cdot\sin\alpha \\ \mathrm{l} = \,\mathrm{v}\cdot r\cdot\sin\alpha \end{cases} \longrightarrow \frac{\mathrm{d\,l}}{\mathrm{l}} = \frac{|\mathrm{F}|}{\mathrm{m\,v}}\mathrm{dt} \tag{3.14}$$

$$\mathrm{d\,l} = \frac{|\mathrm{F}|\cdot \mathrm{l}}{\mathrm{m\,v}}\mathrm{dt} = \frac{\mathrm{a}\cdot \mathrm{l}}{\mathrm{v}}\mathrm{dt} = \frac{\mathrm{d\,v}}{\mathrm{dt}}\mathrm{dt}\frac{\mathrm{l}}{\mathrm{v}} = \frac{\mathrm{d\,v}}{\mathrm{v}}\mathrm{l} \longrightarrow \Delta\,\mathrm{l} \sim \mathrm{l}\frac{\Delta\,\mathrm{v}}{\mathrm{v}}\ . \tag{3.15}$$

We can estimate the period for each orbit using Kepler's law, $\mathrm{T} = 2\pi\sqrt{\mathrm{a}^3/\mathrm{GM}}$, to get the total time spent [1]. Evolving each orbit, we can find the time it takes for it to fall in the center of the star, and by finding the orbit in which $\mathrm{t} = 10^{10}$yrs for different energies we also find the critical eccentricity.

As mentioned before, the PBH's orbit is determined by its angular momentum and energy, both of which can be expressed as eccentricity and semimajor axis. This means even if we fix the critical eccentricity, there will still be a degree of freedom. In other words, the critical eccentricity will be different for each starting semimajor axis. While not exactly the same, for our model we can equiparate the semimajor axis of the starting orbit to the initial radius the PBH would have, making comparing with the bound density and integrating for different radius much easier[2] Using $\mathrm{e}_c(r)$, the density distribution we found in equation 3.7 and assuming a Jeans-Ambartsumian eccentricity distribution (also known as a flat thermal eccentricity distribution) we can obtain the average number of PBHs that should be captured by the star in 10^{10}yrs.

$$\mathrm{N(e > e_c)} = \left(1 - \mathrm{e_c^2(r)}\right)\mathrm{N} \tag{3.16}$$

$$\mathrm{M_{DM}} = \int_{\mathrm{R_*}}^{\mathrm{r_0}} \left(1 - \mathrm{e_c^2(r)}\right)\left(\mathrm{GM_* r^{-1}}\right)^{3/2}\frac{\bar{\rho}_{\mathrm{DM}}}{\sigma^3}\mathrm{r^2 dr}\ . \tag{3.17}$$

As $\mathrm{e}_c^2(r)$ is not an analytic function, we will have to compute its integral numerically together with a factor $r^{1/2}$. We identify this numerical result with a parameter we will call Ξ, which we decide to make dimensionless and express in terms of both limits of the integral:

$$\mathrm{M_{DM}} = \frac{\left(\mathrm{GM_*}\right)^{3/2}\bar{\rho}_{\mathrm{DM}}\bar{\rho}_{\mathrm{DM}}\mathrm{R_* r_0^{1/2}}}{\sigma^3}\int_{\mathrm{R_*}}^{\mathrm{r_0}}\frac{\left(1 - \mathrm{e_c^2(r)}\right)\mathrm{r^{1/2}dr}}{\mathrm{R_* r_0^{1/2}}} \tag{3.18}$$

$$\mathrm{M_{DM}} = \frac{\left(\mathrm{GM_*}\right)^{3/2}\bar{\rho}_{\mathrm{DM}}\mathrm{R_* r_0^{1/2}}}{\sigma^3\Xi}\ , \tag{3.19}$$

where R_* is the radius of the star, and r_0 is the maximum radius from the PBH to the star, both constants. As all other variables do not depend on r, we can leave them out without worries (we again stress to not confuse r with R). This also means we can generalize the result:

$$\bar{\mathrm{M}}_{\mathrm{DM}} = 1.65\cdot 10^{-26}\,\mathrm{M_\odot}\left[\frac{\bar{\rho}_{\mathrm{DM}}}{10\,\mathrm{M_\odot/pc^3}}\right]\left[\frac{\mathrm{R_* r_0^{1/2}}}{\mathrm{km^{3/2}}}\right]\left[\frac{1}{\Xi}\right]\left[\frac{10\mathrm{km/s}}{\sigma}\right]^3\left[\frac{\mathrm{M_*}}{\mathrm{M_\odot}}\right]^{3/2}$$

$$\bar{\mathrm{N}}_{\mathrm{PBH}} = 1.65\cdot 10^{-14}\left[\frac{\bar{\rho}_{\mathrm{DM}}}{10\,\mathrm{M_\odot/pc^3}}\right]\left[\frac{\mathrm{R_* r_0^{1/2}}}{\mathrm{km^{3/2}}}\right]\left[\frac{1}{\Xi}\right]\left[\frac{10\mathrm{km/s}}{\sigma}\right]^3\left[\frac{\mathrm{M_*}}{\mathrm{M_\odot}}\right]^{3/2}\ . \tag{3.20}$$

[1] As the periapsis for our complex case $\mathrm{r_{min}}$ is bigger than the periapsis for its Kepler orbit $r_{min\ Kepler}$, $\mathrm{T_{kepler}} \geq \mathrm{T_{real}}$, so taking the Kepler period is both the simpler and more conservative approach to get at least the minimum capture rate.

[2] We use the semimajor axis for all computations of the orbit during the capture, this is simply to avoid having to compute the initial orbit average radius we would need when integrating by radius to the star

	1	0.79	0.63	0.50	0.40	0.32	$M_\odot$
r_{mp}	22.5	25.0	25.4	24.7	23.7	22.1	$10^{12}km$
	29.8	28.8	27.4	25.7	24.1	22.3	$10^{12}km$

Table 3.1: Values of the maximum semimajor axis that can result in a capture in 10^{10} years if the system was completely isolated. We are using a PBH of $10^{-12}\,M_\odot$ with eccentricity 1. The upper row is from colisionless friction, while the one below assumes a gaseous medium.

Besides the critical eccentricity, the capture rate also depends on r_0 both explicitly and also as the upper limit of the integral for Ξ. A priori r_0 is only defined as the maximum radius at which a PBH could be captured. From a set of simple assumptions, we expect that $(1 - e_c^2(r)) \propto 1/a$:

$$r_{min} = a(1 - e_c) \longrightarrow 1 - e_c^2 \simeq 1 - \left(1 - \frac{r_{min}}{a}\right)^2 = \frac{2r_{min}}{a} - \frac{r_{min}^2}{a^2}$$

$$a >> r_{min} \longrightarrow 1 - e_c^2 \simeq \frac{2r_{min}}{a} \propto 1/a\ , \tag{3.21}$$

where r_{min} is the periapsis of the orbit, the point closest to the center of the star. The periapsis needed to capture the PBH within 10^{10}yrs will obviously decrease for larger a, but the rate of change will be much smaller, so the semimajor axis term will dominate. So we have the numeric integral will roughly go as $\propto a^{1/2}$, meaning the capture rate will also raise significantly with an increasing radius. This is the reason we put the r_0 term explicit through the definition of Ξ, but also makes defining the upper limit r_0 very important. However, we can use this same relation for it. As mentioned, the rate of change of the periapsis will be much slower than the rate of change in the semimajor axis, as the former changes from the surface to the core of the star as the medium gets more dense, while the later spans from tens of thousands of kilometers to tens of thousands of Astronomical Units. This will hold until we reach such distances that the periapsis cannot be lowered more for we are already in the center of the star, at which point the relation above will quickly decay to 0. The quick decay comes from being impossible to capture PBHs farther away within the 10^{10}yrs given, but also gives us a very good estimation of r_0: the semimajor axis such that its orbit with eccentricity 1, crossing exactly the center of the star, will take 10^{10} years to be captured.

We showcase these maximum semimajor axis for a variety of cases in table 3.1. However, we can see that they raise up to almost a parsec, at which point perturbation by objects outside the stellar system on the PBH would be expected and our entire reasoning for $\bar{\rho}_{PBH}$ would become void, making the overall result not valid. To account for this, we need to approximate the global effect of outside perturbations on PBHs.

3.2.5 Maximum radius for black hole capture: perturbation by third objects

In our simplistic model we have assumed that we have a single star and negligible planet formation. However, we can still have perturbations on the system by objects from outside the system (third objects). Modelling in detail possible subhaloes and other stellar systems

lies outside the scope of this chapter, but we can approximate their total effect by looking at the tidal forces between the stellar system and the DM halo as a whole.

We take the orbit as the variation of position to compute the tidal force acting on the PBH. The angular momentum generated by that force can in turn deviate the orbit of the object, to the point that the PBH no longer crosses the star. Of course, the tidal force competes with the stellar system's gravitational potential, so as expected the farther objects will be much more affected. We start by estimating this competition:

$$\frac{\Delta\, \mathrm{l}}{\mathrm{l_{circ}}} = \frac{\mathrm{a_{Tidal}}}{\mathrm{a_{Gravitational}}} = \frac{\mathrm{GM_{halo}(R)r}}{\mathrm{GM_*}} \frac{\mathrm{r}^2}{\mathrm{R}^3} = \frac{\mathrm{M_{halo}(R_h)}}{\mathrm{M_*}} \left(\frac{\mathrm{r}}{\mathrm{R}}\right)^3 , \tag{3.22}$$

where l_{circ} is the angular momentum of the equivalent circular orbit. Something to note however is that the effect of the tidal forces will not be for a single orbit, but rather during all capture process. The change in both the angular momentum and orbit during the capture process is quite extreme, but we can take a first order approximation by computing the total effect it would have on the PBH if the orbit was not changed by the capture process, as that initial orbit would be the one with the highest radius and so the one the effect of perturbations will be higher.

When the change on the momentum caused by the perturbations is enough to deviate the PBH with initial e_c from the orbit that crosses the star, the semimajor axis of the starting orbit will be set r_{max}, as the effect of perturbations would be higher on farther orbits. If perturbations are enough to perturb the orbit with e_c at that radius, we expect orbits at higher radius will be even more perturbed and so not valid on our model. This is a very conservative approximation, but it suits the aim of our work. Assuming the changes in the orbit are stochastic, the total variance will then be:

$$\Delta\, \mathrm{l} = \Delta\, \mathrm{l_{orbit}} \sqrt{\mathrm{n_{orb}}} , \tag{3.23}$$

where n_{orb} is the number of orbits. This comes from assuming there will be a random perturbation from tidal forces during each orbit.

Using the definition of angular momentum in equation 3.8 and for circular orbits and that the changes in both the eccentricity and angular momentum are very small, we can derive to relate the increments of angular momentum with the increment in eccentricity:

$$\frac{\mathrm{l}}{\mathrm{l_{circ}}} = \sqrt{1-\mathrm{e}^2} \longrightarrow \frac{\mathrm{d}\left(\frac{\mathrm{l}}{\mathrm{l_{circ}}}\right)}{\mathrm{d(\,e)}} = \frac{\mathrm{d}\left(\sqrt{1-\mathrm{e}^2}\right)}{\mathrm{d(\,e)}} \tag{3.24}$$

$$\frac{\mathrm{d\,l}}{\mathrm{l_{circ}}} = \frac{-2\,\mathrm{e}}{2\sqrt{1-\mathrm{e}^2}}\mathrm{d(\,e)} \longrightarrow \frac{\Delta\, \mathrm{l}}{\mathrm{l_{circ}}} = \frac{-\,\mathrm{e}\Delta\, \mathrm{e}}{\sqrt{1-\mathrm{e}^2}} . \tag{3.25}$$

As the tidal forces will only meaningfully affect the furthest PBHs, the critical eccentricity will be very close to 1. This means even very small absolute changes in the eccentricity can deviate the orbit from capture. We therefore approximate the maximum change allowed using $\Delta\, \mathrm{e} < -(1-\mathrm{e})$ [3] and apply it to equation (3.25):

$$\frac{\Delta\, \mathrm{l}}{\mathrm{l}_{circ}} < \frac{-\,\mathrm{e}\,[-(1-\mathrm{e})]}{\sqrt{1-\mathrm{e}^2}} \simeq \frac{\mathrm{e}(1-\mathrm{e})}{\sqrt{2(1-\mathrm{e})}} = \frac{\mathrm{e}}{\sqrt{2}}\sqrt{1-\mathrm{e}} , \tag{3.26}$$

[3] We specify the sign as positive changes to the eccentricity will only make capture more likely

where we have simply used that for $\mathrm{e} \simeq 1$, $\sqrt{1-\mathrm{e}^2} \simeq \sqrt{2(1-\mathrm{e})}$. Similarly, due to $\mathrm{e} \simeq 1$ we can neglect the lineal dependency on eccentricity above, as the square root term will always dominate near 1, leaving:

$$\sqrt{\frac{1-\mathrm{e}}{2}} > \frac{\Delta \mathrm{l}}{\mathrm{l_{circ}}} = \frac{\mathrm{M_{halo}(R)}}{\mathrm{M_*}} \left(\frac{\mathrm{r}}{\mathrm{R}}\right)^3 \sqrt{\mathrm{N_{orb}}} \,, \tag{3.27}$$

where we have recovered the rightmost term from equation 3.22

This can be simplified even further. First, at the large distances which concern our case, we can approximate the critical eccentricity as the one needed in order to just enter the star within the orbit:

$$\mathrm{e} \simeq 1 - \frac{R_*}{r} \longrightarrow \frac{1-e}{2} \simeq \frac{R_*}{2r} \,. \tag{3.28}$$

Similarly, because of the large eccentricities, the energy loss per orbit plateaus, something that will be seen clearly in our results. We can then take $\Delta E_{orb} \simeq ct$. It is straightforward to show that if we derive equation 3.9 and equal it to a constant, we can then estimate the orbits decaying as $\Delta r \propto r^2 N_{orb}$, where N_{orb} is simply the number of orbits and so the number of times ΔE_{orb} was applied. We can easily absorb the other constants into a parameter we will call a_1 and which we choose to define as the distance such that single orbit will see its semimajor axis fall by half $\Delta r = r/2$, leaving:

$$\Delta \mathrm{r} = \frac{\mathrm{r}^2}{2\mathrm{a_1}} \mathrm{N_{orb}} \longrightarrow \mathrm{N_{orb}} = \frac{2\mathrm{a_1}}{\mathrm{r}} \,, \tag{3.29}$$

where we have used that, as we are talking about possible captures with at least initial e_c, $\Delta r = r$. Applying both of these changes to equation (3.27):

$$\sqrt{\frac{\mathrm{R_*}}{2\mathrm{r}}} > \frac{\mathrm{M_{halo}(R)}}{\mathrm{M_*}} \left(\frac{\mathrm{r}}{\mathrm{R}}\right)^3 \sqrt{\frac{2\mathrm{a_1}}{\mathrm{r}}} \tag{3.30}$$

$$\mathrm{r_{max}^3} = \frac{\mathrm{M_{halo}(R)}}{2\mathrm{M_*}} \sqrt{\frac{\mathrm{R_*}}{\mathrm{a_1}}} \mathrm{R}^3 \,. \tag{3.31}$$

As seen in the equation above, the r_{max} we are searching for is cubed and both the number of orbits and eccentricity terms have square roots, so even in the worst case we expect these simplifications to not have any major effect while making the estimation much simpler.

From this we obtain a r_{max} after which the condition above will stop being fulfilled and perturbations from the galaxy would interfere in the capture process. We showcase the results for $R = 1/10 R_{Virial}$ in table 3.2. We can compare it with the maximum possible radius of capture, discussed in the previous section, which are in table 3.1. It can be easily seen that the r_{max} obtained from perturbation effects are as expected much lower than the maximum capture radius. To be sure, we computed it for various R and found that even at very large distances from the halo like $R = R_{Virial}$ the same happened. We can thus conclude that perturbations are the main effect limiting the PBH capture, and so should always be taken into account, even in a simplified matter. [73] for example obtained constraints by integrating up to a radius of $5,000$ AU, but, as we have showcased, for a lot of stellar systems such orbits would be perturbed far before the PBH could be captured.

	1	0.79	0.63	0.50	0.40	0.32	$M_\odot$
r_{max}	0.142	0.133	0.124	0.115	0.110	0.104	$10^{12}km$

Table 3.2: Values of the maximum semimajor axis taking into account perturbations coming from the galaxy/halo (but not planet formation or binaries). It only depends on the halo mass, and the radius to both the center of the halo and the star of the system. In this table here we assume $R = 0.1R_{vir}$.

A final caveat is that, from equation (3.31) it can be easily understood that r_{max} will evolve with time, as both M_{halo} and R will increase while the stellar parameters remain constant. In this work we neglect this effect: while change in r_{max} can be important, the total effect of this evolution is more mild, as the perturbations need a large number of orbits to start having an effect, and so the changed perturbations will only have an effect a bit< after the change itself. This means that only the orbits surviving to that point will be affected, not affecting the PBHs that have already been captured. From equation (3.31) it is obvious that r_{max} will only increase with time, thus the main effect will be orbits stopping being perturbed. How to treat these half-perturbed orbits is a difficult question, and in this work we are aiming for conservative and stringent lower bounds on capture rate. If we implemented the evolution of r_{max}, we would also need to divide the capture time in various bins, and integrate (3.17) for each of them in turn, making the whole process much more complex and expensive computationally wise for only a dubious increase in accuracy. Overall setting a constant r_{max} allows us to simplify the process, meaning we only need the initial conditions, and gives a minimum value of the capture rate.

3.2.6 Black hole growth after capture

A reasonable doubt about all this process is if such a small PBHs with $\mathrm{m} = 10^{-12}\,\mathrm{M}_\odot$ can really have an effect on a star of $\sim 1\,\mathrm{M}_\odot$, maybe even accreting it whole. This computation was done previously in [72, 84, 85], and [86] looked in detail at how the parameters of the star could change the type of accretion and its emission. Here we will reproduce it, but with very conservative approximations: we assume the PBH will start accreting only once it has settled in the core of the star and an Eddington limit with a radiative efficiency of $\eta_{\mathrm{rad}} \sim 0.1$, the standard for astrophysical settings. We note that this is overly conservative, as accretion luminosity inside a star could also be carried primarily by convection in very optically thick stellar cores, bypassing the Eddington limit and avoiding the creation of torus-like accretion disk. Indeed, that was the conclusion of [86] for a wide range of masses, including our initial mass $10^{-12}\,\mathrm{M}_\odot$ and any mass above $10^{-2}\,\mathrm{M}_\odot$. This would result in a standard Bondi accretion, which as seen both below and in the previous references would be much faster. Nevertheless, we keep on with this calculation to show its robustness, even in a worst case scenario:

$$\dot{\mathrm{M}}_{\mathrm{Bondi}} \approx \frac{\pi \left(\mathrm{GM}_{\mathrm{BH}}\right)^2 \rho_*}{\mathrm{c_s^3}} \tag{3.32}$$

$$\dot{\mathrm{M}}_{\mathrm{Bondi}} \approx 8.75 \cdot 10^8 \left[\frac{\mathrm{M}_{\mathrm{BH}}}{\mathrm{M}_\odot}\right]^2 \left[\frac{\rho_*}{1\mathrm{g/cm^3}}\right] \left[\frac{\mathrm{c_s}}{10\mathrm{km/s}}\right]^{-3} \mathrm{M}_\odot/\mathrm{yr} \tag{3.33}$$

$$\dot{M}_{Edd} = \frac{4\pi G m_p}{c\ \eta_{rad}\ \sigma_T} M_{BH} \approx 2.2 \cdot 10^{-8} \left[\frac{M_{BH}}{M_\odot}\right] M_\odot/yr\ . \tag{3.34}$$

Looking at our typical case, with $M_{BH} = 10^{-12}\,M_\odot$, taking the ensity of the star's core as $\rho_* \sim 100 g/cm^3$ and speed of sound $c_s \sim 500 km/s$:

$$\dot{M}_{0\ Bondi} \approx 7 \cdot 10^{-19}\,M_\odot/yr$$

$$\dot{M}_{0\ Edd} \approx 2.2 \cdot 10^{-20}\,M_\odot/yr\ .$$

If the Eddington limit applies, the accretion is limited from the start. With a squared dependence on the mass in comparison to the linear Eddington dependence, the Bondi accretion will increase more than the Eddington limited as the PBH accretes, and thus if the Eddington limit applies at the beginning the resulting accretion will always be Eddington limited. Therefore we can just integrate the Eddindton limited accretion rate:

$$\frac{dM}{dt} = \frac{4\pi G m_p}{c\ \eta_{rad}\ \sigma_T} M_{BH} \longrightarrow \frac{dM}{M_{BH}} = \frac{4\pi G m_p}{c\ \eta_{rad}\ \sigma_T} dt \tag{3.35}$$

$$\int_{10^{-12}}^{1} \frac{dM}{M_{BH}} = \int_{t_0}^{t} \frac{4\pi G m_p}{c\ \eta_{rad}\ \sigma_T} dt = \ln\left(\frac{1}{10^{-12}}\right) = \frac{4\pi G m_p}{c\ \eta_{rad}\ \sigma_T} \Delta t \tag{3.36}$$

$$\Delta t = \frac{c\ \eta_{rad}\ \sigma_T}{4\pi G m_p} \ln\left(\frac{1}{10^{-12}}\right) \approx 1.25 \cdot 10^9 yrs\ , \tag{3.37}$$

where we have used that most of the parameters are not affected by the PBH's growth, and thus we can take them out of the integral.

There are 2 important factors to note about this result. The first is that the exact final value of the mass is not relevant. The logarithm suppresses both increase and decrease, so even if we changed the mass of the star to $0.1\,M_\odot$ or $3\,M_\odot$, the total time would only change by $\sim 10\%$. The second is the possible change of the parameters that affect the two types of accretion rates during the accretion process. In particular, the Bondi accretion rate depends on the sound speed and density of the core, both of which will be heavily affected as the PBH grows larger. However, this worries are unnecessary. A look at the starting accretion rates clearly shows the lengthiest process are the first steps, as the exponential nature of the equation means it will take around the same time to double its mass at $10^{-12}\,M_\odot$ and at $0.5\,M_\odot$, despite the later being $5 \cdot 10^{11}$ times more massive. The change of parameters will only start mattering when the PBH's mass is comparable to that of the core, at which point the accretion rate is already large enough that even a suppression around a factor 10 would not alter the final result. While some amount of ejecta escaping could affect the final mass of the PBH, by similar reasoning it would only occur right at the end, when the PBH's mass is already of the order of the star, and ejecta escaping would only lower the final mass of the PBH, not interfering with our observational result of a subsolar mass PBH at all.

Indeed, [86] concluded that the star would only start being dynamically affected by the black hole inside it at maximum 6 days before being completely accreted. [29] studied in depth a similar case but with a neutron star, and reached even more strict results: besides a transient electromagnetic pulse and gravitational wave emission there would be no other observational remain or result of the process outside the PBH, including no ejecta. Extending this study to main sequence stars is the obvious step forward, but lies outside the scope of this thesis.

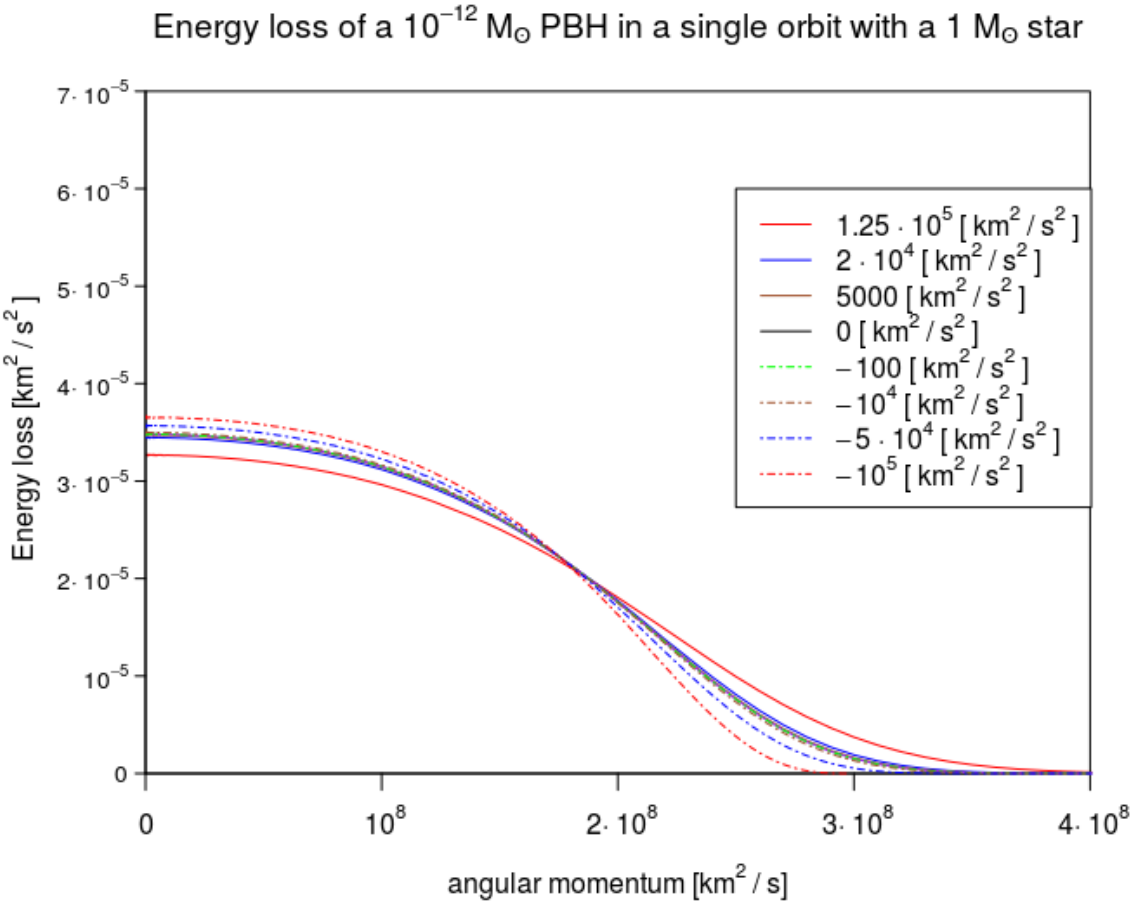

Figure 3.3: Energy loss of a $10^{-12}\,M_\odot$ PBH when crossing our model $1\,M_\odot$ star, as a function of the orbital angular momentum. Each curve is for a different value of the specific energy of the initial orbit (positive for unbound orbits and negative for bound orbits). The Chandrasekhar dynamical friction formula for collisionless matter is used.

3.3 Results for six stellar models

To compute the various results we have created a set of unique programs using the previous equations and stellar models. We now describe the steps it takes, together with its immediate results.

3.3.1 Energy loss by dynamical friction

Following equations (3.10) and (3.13), we integrate numerically to find the loss of energy over a single pass depending on the PBH's energy and angular momentum, for both the collisionless (3.11) and gaseous (3.12) cases, and for a variety of energies including both bound PBHs and free ones that just collided by chance. The results for a star of $1\,M_\odot$ are shown in Figures 3.3 and 3.4.

While the energy loss increases the more tightly bound the PBHs are, for a single pass it is negligible as expected. The difference between the different types of dynamical friction is quite mild too. However, the value is still enough that the accumulated effect

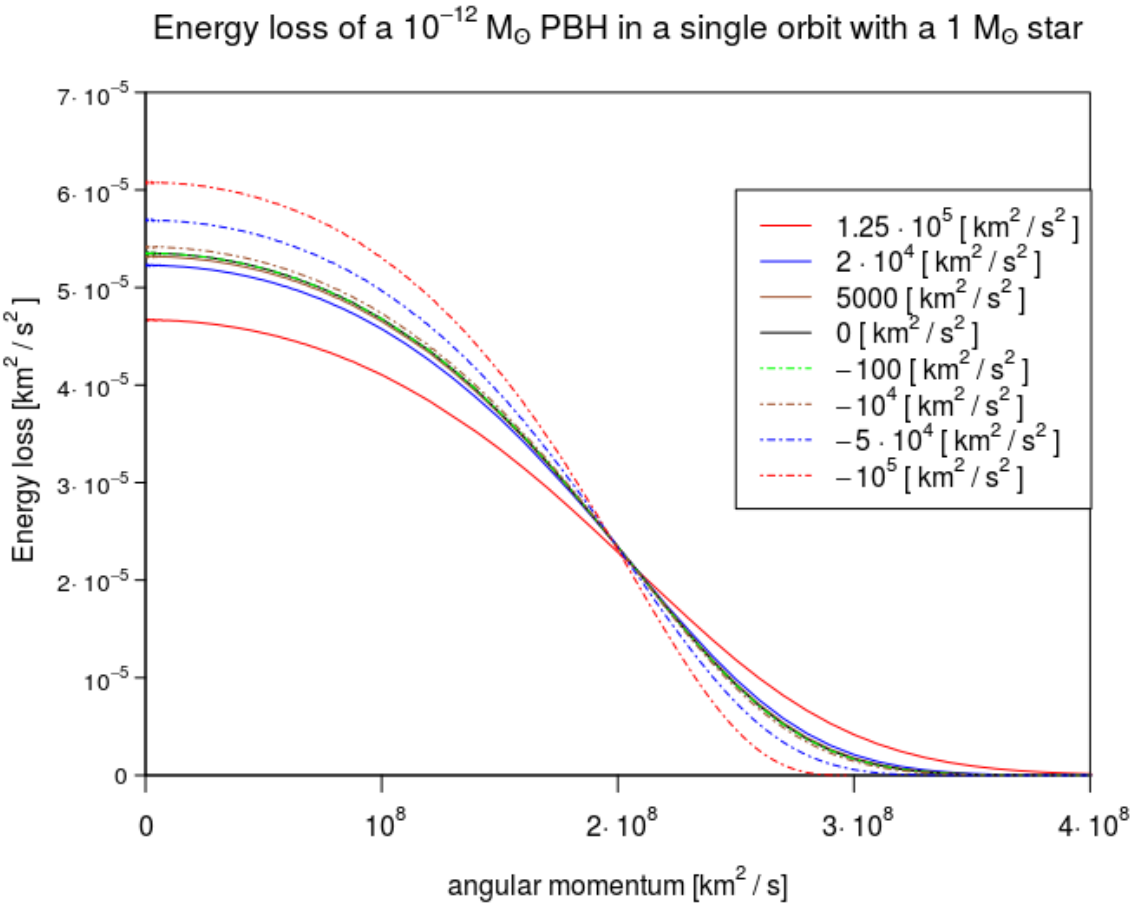

Figure 3.4: Same as Figure 3.3, but for the hydrodynamic formula based on [83] and [82]

after a number of orbits could force a bound PBH deep into the core of the star. We take our simplistic model, in which the PBHs orbits a single star and effects by individual distant bodies are mostly neglected. We estimate the global effect perturbations by tidal forces could have by establishing an upper radius r_{max} above which we assume orbits will not contribute to the capture rate (for more details, see section 3.2.5), but besides that the PBH is unperturbed. These assumptions can be optimistic, especially in very dense environments and the more common binary systems. However, in more isolated cases our simplistic model gives a very good approximation, and thus is ideal to establish a base case upon which to later improve upon. Further work on studying the effects of these perturbers would also benefit from establishing accurate models of inner system objects like planets or binary stars.

3.3.2 Critical eccentricity for capture

Following this model we can compute a 'time of capture' for a set energy depending on the eccentricity/angular momentum. We follow the evolution of the PBH orbit using equation (3.15) and the energy loss, computing the energy loss per orbit again after any of the parameters changes by at least 1%, and use the criterion described in section 3.2.3 and in the Appendix B to determine when the PBH has been captured. The more eccentric the orbit the quicker the PBH will be captured and below a certain eccentricity the orbit will simply not cross the star so the time of capture will be infinite. Above a certain eccentricity, meaning lower angular momentum, we also expect the capture time to plateau, reflecting the behaviour seen in figures 3.3 and 3.4. As mentioned in the previous sections, we define the *critical eccentricity* as the eccentricity by which the PBH will be captured in 10^{10} yrs. Thus, any eccentricity equal or above the critical eccentricity will result in the PBH being captured by the Star (and in turn, accreting it) within the lifetime of the Universe.

Assuming a flat thermal eccentricity distribution we can convert the critical eccentricity into how many of the PBHs at that SMA will end up being captured, which we showcase multiplied by semimajor axis in Figure 3.5 for our various stellar models. As from this point onward all the differences between the two types of dynamical frictions we are working with become negligible, all results shown below are using the gaseous case (3.12). The SMA also gives us a very good approximation of the radius to the star, which we can use to compare with the density distribution as we did in equation (3.17) to get the total mass accreted. As discussed in section 3.2.3, the maximum radius of integration (r_{max}) is perhaps the most important parameter in that integral. Figure 3.6 illustrates its importance; it represents the average number of PBHs captured against the maximum radius of integration. While not exact, there is a rough $M \propto r_0^{1/2}$ relation, especially at larger radii, originating from the relation between the semimajor axis and the critical eccentricity showcased in equation (3.21). As mentioned before, we use equation (3.31) for the maximum radius, which depends on the position of the system within the halo, R. Of course, $\bar{\rho}_{DM}$ will also depend on that, so R will be one of the major factors deciding the capture rate. The r_{max} we found for our particular DM halo can be seen on Figure 3.7 for various stellar masses and R.

Finally, we use the analytic estimate of σ from equations (13) and (19) of [76]. As can be seen in equation (3.17), σ is cubed, so the final result is very sensitive to its possible changes. To appreciate these differences, we use the two different models mentioned above, one being an idealized case with completely isotropic velocity dispersion, and the

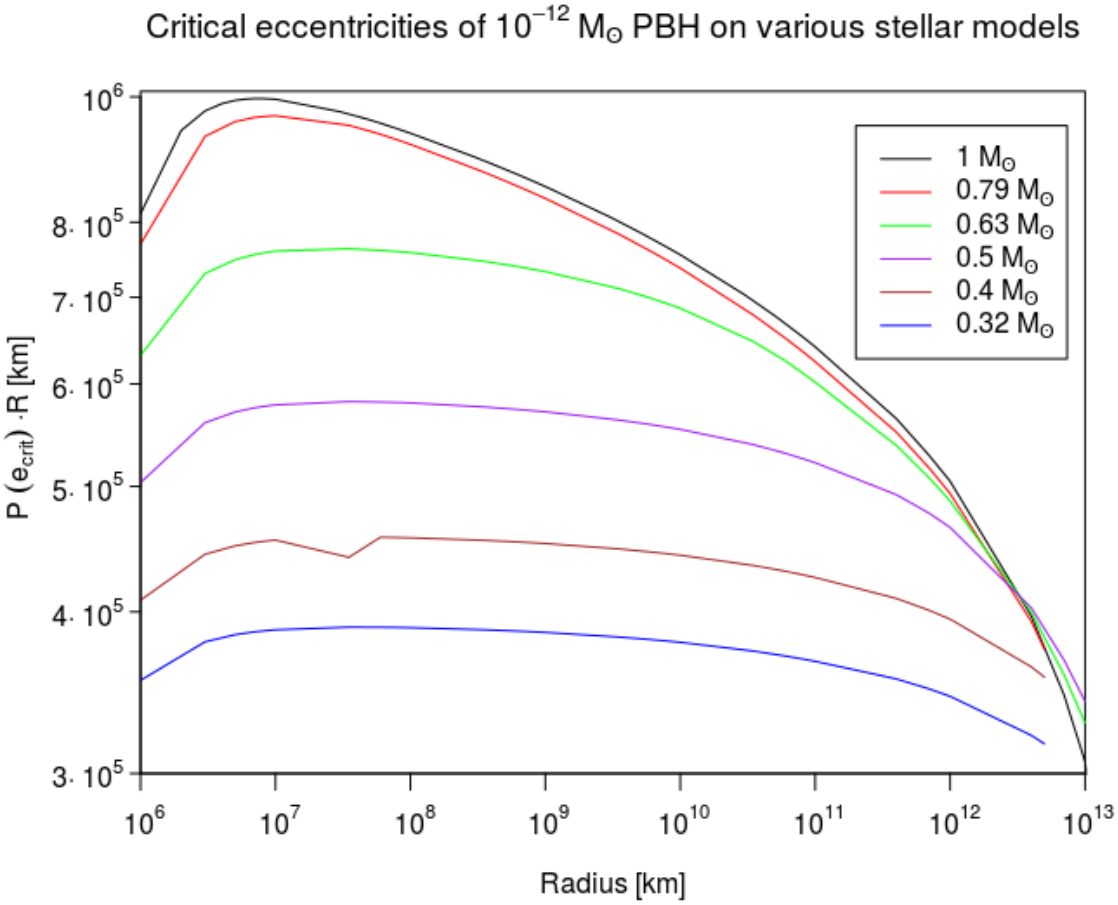

Figure 3.5: Probability for a randomly captured PBH of $10^{-12}\,M_\odot$ to have the critical eccentricity or above for all semimajor axis and various stellar models. For visibility we have multiplied the probability by the semimajor axis. Following equation (3.21) we should expect the value to be roughly constant until close to the maximum semimajor axis, something which fits the figure above.

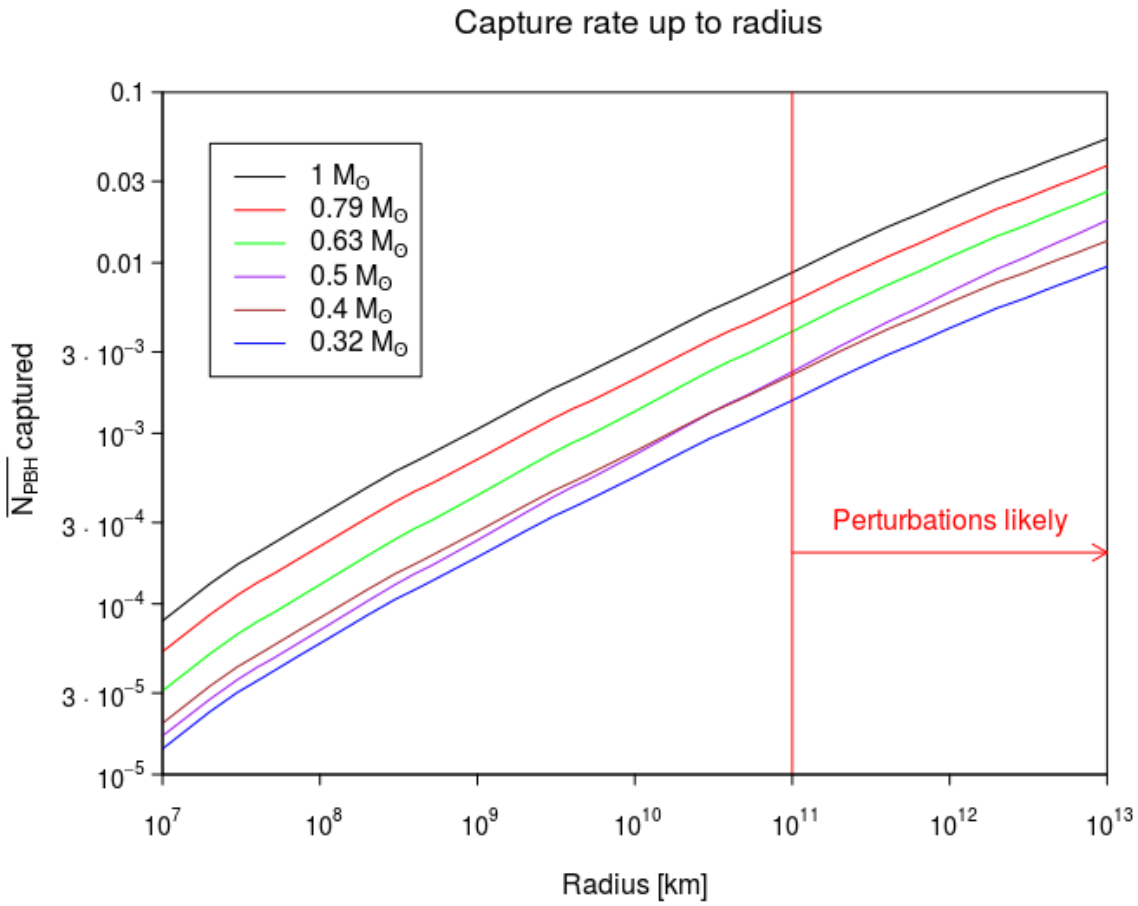

Figure 3.6: Average PBHs captured by the star up to that radius. While at some point the density distribution will naturally go to 0, our simplistic model (which assumes no interactions by third objects) breaks down much earlier, and so the choice of the maximum radius of integration is an important one. The star is situated at $R = 0.1R_{Virial}$ of the center of our DM halo.

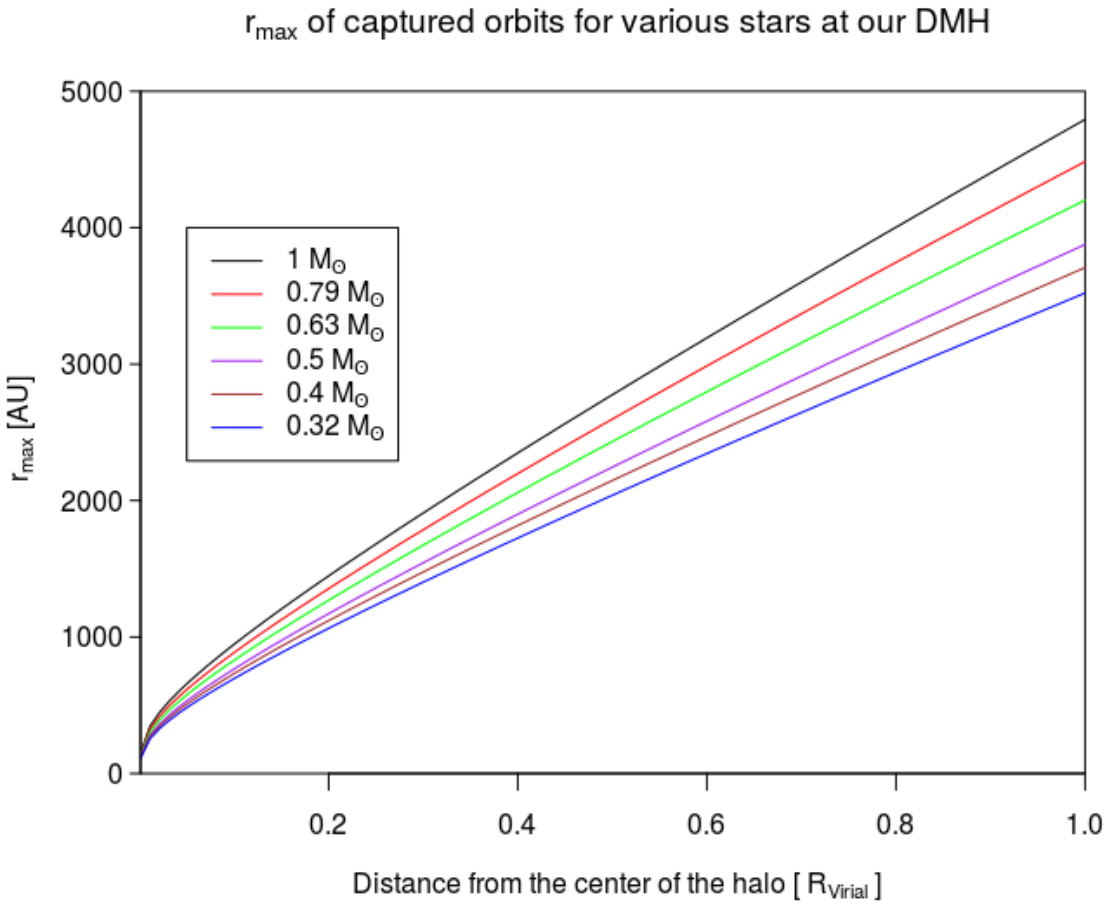

Figure 3.7: The upper limit of the integral we found according to equation (3.31) for the case of our particular DM halo and the various stellar models we are working with.

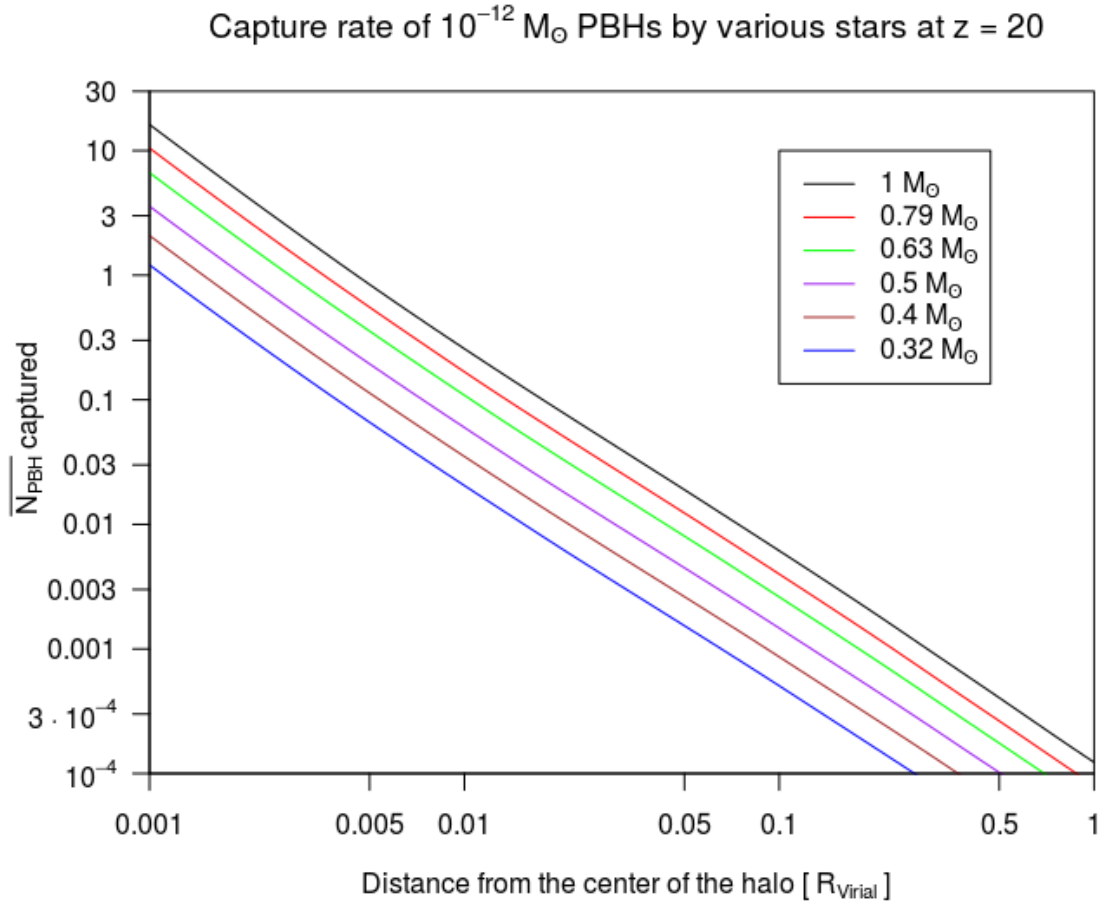

Figure 3.8: Average PBHs captured by the star depending on the distance of the system from the center of the DM halo with purely isotropic dispersion velocities.

other a more realistic approach with a variable anisotropy parameter[4]. We showcase the final results depending on the position of the star within the DM halo with these two dispersion velocity models on Figures 3.8 and 3.9 respectively and for all our stellar models. Interestingly, while the capture rate peaks near the center as expected, where we would average 30 PBHs per system being captured and accreting the whole star, even at larger distances, in the more isolated systems which more closely resemble our idealized model, the capture rate is still notable, having an average of 1 in 100 systems capturing a PBH at distamces $R \sim 0.1 R_{virial}$.

3.3.3 Results for captured primordial black holes

While we have been talking about the early universe, as that is the most interesting case, a single glance at equation (3.20) shows that the Ξ that we compute is generic, completely separate from $\bar{\rho}_{DM}$ and σ. This comes from the fact that our model first works around the capture process, and then adjusts the final number based on the number of available PBHs. Thus, our results are not only extendable to other redshifts but also to cases where

[4]In observations, the anisotropy parameter is very close to 0 in the center but grows with distance up to 0.5 near the virial radius [87]

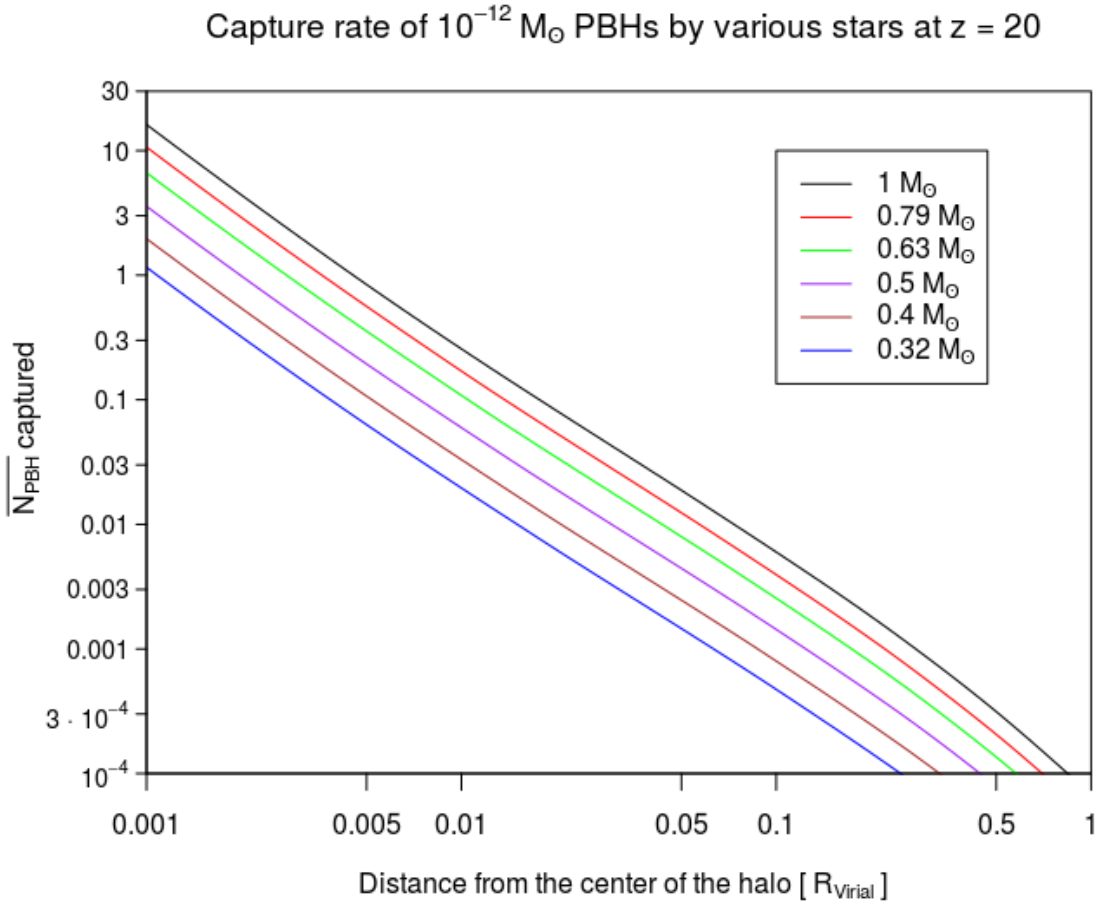

Figure 3.9: Average PBHs captured by the star depending on the distance of the system from the center of the DM halo with anisotropic velocity dispersion.

PBHs are only a minority of the DM.

An important caveat is that the upper limit of the integral, r_{max}, does affect Ξ and is also explicit on the average number of PBHs captured, and that depends on the DM halo itself. As can be seen on equation (3.31), at lower redshifts r_{max} should raise and capture rate with it. Similarly, even more dense regions would indirectly result in a lower capture rate as perturbations affect objects earlier. Unlike the mean density and velocity dispersion, of which we only need the initial conditions, r_{max} can also evolve, though in this work we have neglected the evolution for reasons explained in section 3.2.5.

Therefore, rather than just use the r_{max} we have computed, we are showing Ξ for various r_{max} and stellar models in table 3.3, which should allow anybody interested to find the value suited to their particular case.

3.4 Observational consequences

If all the DM is composed of PBHs there is only a small range of masses that are not constrained by current observations. However, on the bigger side of this range, $10^{-12}\,M_\odot$, interactions between these PBHs and stars could have an observational result, with PBHs falling into and later accreting the much larger objects [81].

In our study we have made use of the primordial nature of the PBHs, which would interact with the star since the moment of its formation and could fall into orbits that cross the star. The strength of the dynamical friction would usally be negligible, but within 10^{10} years it ends up being enough for the PBH to end up in the core of the star. There we have shown the PBH can accrete the star in less than 10^9 years, for a grand total of 11 gigayears in comparison to a an age of 13 gigayears from $z \sim 20$ to our current universe. We therefore expect the process to be easily completed by now, even leaving a few gigayears to spare for safety.

We made an in depth analysis of the main elements contributing to the possibility of PBH capture, reaching a generic solution for a simplified model that can compute the average number of PBHs captured by a star from a set of parameters and a numeric integral. While the type of dynamical friction used can vary the energy loss of a single orbit a substantial amount (see figures 3.3 and 3.4), it has only a very small effect on the critical eccentricity and a negligible one on the capture rate. This is due to the extreme eccentricities we are already starting with for most orbits to cross the star, as even big differences in energy loss will only translate to very small critical eccentricity changes

However, following the limitations of our model we also reached the conclusion that external perturbers will easily affect the outer layers of the system. This outer layer is where PBHs are more numerous, due to their density scaling as $r^{-3/2}$ meaning their total number scales as $r^{3/2}$. We showed that the effect of external perturbations is important for our final results, as there are PBHs with an orbit that would result in them being captured but that are instead perturbed by the tidal forces of the DM halo. This is something that has not been taken into account in previous studies [40, 73] but that is of major importance, changing our results by an order of magnitude.

Once taken into account, our main results are the average PBHs captured by a star depending on its position within a $10^7\,M_\odot$ DM halo at $z \sim 20$, shown in figure 3.9. As can be seen in the figure, our final conclusions are very exciting. According to our model almost all the stars within the central part of the galaxy would eventually capture a PBH and be accreted by it within the Hubble time. If $10^{-12}\,M_\odot$ PBHs are all the dark matter, this should result in an abundance of black holes with $m_{PBH} < 1\,M_\odot$ but still big enough

$M_*(\mathrm{M}_\odot)$	1	0.79	0.63	0.50	0.40	0.32	$\mathrm{M}_\odot$
$R_*(km)$	634134	528054	395880	296642	231579	196870	km
$r_{max}(km)$			Ξ				
$7 \cdot 10^6$	0.53	0.44	0.42	0,41	0.40	0.40	
$9 \cdot 10^6$	0.49	0.41	0.39	0.38	0.38	0.37	
10^7	0.48	0.40	0.38	0.37	0.37	0.36	
$3 \cdot 10^7$	0.38	0.32	0.31	0.30	0.30	0.30	
$5 \cdot 10^7$	0.38	0.33	0.30	0.29	0.30	0.29	
$7 \cdot 10^7$	0.36	0.30	0.29	0.29	0.29	0.29	
$9 \cdot 10^7$	0.36	0.31	0.29	0.28	0.28	0.28	
10^8	0.36	0.31	0.29	0.28	0.28	0.28	
$3 \cdot 10^8$	0.35	0.30	0.27	0.26	0.26	0.26	
$5 \cdot 10^8$	0.35	0.30	0.27	0.27	0.27	0.26	
$7 \cdot 10^8$	0.36	0.30	0.27	0.27	0.27	0.26	
$9 \cdot 10^8$	0.36	0.31	0.27	0.27	0.26	0.26	
10^9	0.36	0.31	0.27	0.27	0.26	0.26	
$3 \cdot 10^9$	0.36	0.31	0.27	0.26	0.26	0.25	
$5 \cdot 10^9$	0.37	0.32	0.27	0.26	0.26	0.25	
$7 \cdot 10^9$	0.38	0.32	0.28	0.26	0.26	0.26	
$9 \cdot 10^9$	0.38	0.33	0.28	0.27	0.26	0.26	
10^{10}	0.38	0.33	0.28	0.26	0.26	0.26	
$3 \cdot 10^{10}$	0.40	0.34	0.28	0.26	0.26	0.25	
$5 \cdot 10^{10}$	0.41	0.36	0.29	0.27	0.26	0.26	
$7 \cdot 10^{10}$	0.42	0.36	0.30	0.27	0.27	0.26	
$9 \cdot 10^{10}$	0.43	0.37	0.30	0.27	0.27	0.26	
10^{11}	0.43	0.37	0.30	0.27	0.27	0.26	
$3 \cdot 10^{11}$	0.46	0.40	0.32	0.28	0.27	0.26	
$5 \cdot 10^{11}$	0.48	0.42	0.33	0.28	0.27	0.27	
$7 \cdot 10^{11}$	0.50	0.43	0.34	0.29	0.28	0.27	
$9 \cdot 10^{11}$	0.51	0.44	0.34	0.29	0.28	0.27	
10^{12}	0.52	0.44	0.35	0.29	0.28	0.27	
$3 \cdot 10^{12}$	0.60	0.51	0.39	0.32	0.29	0.29	
$5 \cdot 10^{12}$	6.39	5.34	4.18	3.33	2.99	2.92	
$7 \cdot 10^{12}$	6.74	5.70	4.36	3.44	3.09	3.01	
$9 \cdot 10^{12}$	6.97	6.39	4.48	3.52	3.39	3.28	

Table 3.3: Values of Ξ for $10^{-12}\,\mathrm{M}_\odot$ PBHs for various r_{max} and stellar models. Note that Ξ is roughly constant for a sane stellar model until the larger r_{max} where it starts decaying. This comes in part from the relation originating from equation 3.21, as Xi is defined by dividing the numeric integral of the critical eccentricity and $r^{1/2}$ by $r_{max}^{1/2}$ and R_*, heavily reducing the dependence on r_{max} until that relation falls off.

to be detected with our current means, and a noticeable lack of old stars. This lack of old stars does fit with the current lack of very old very low metallicity stars on observations, though we stress large uncertainties in both the measurement and the expected number of extremely metal poor low mass stars make it still an open and contentious issue. Furthermore, because the capture itself only depends on the initial conditions just before star formation, the stellar system of star and black hole could also migrate freely from the DM halo or maybe even survive galaxy mergers, meaning the resulting subsolar black hole end up in younger galaxies, such as our Milky Way.

There are caveats to the result. First of all, our model is very simple and does not take into account binary stars or multiple systems. The existence of another star would complicate our model massively. We a priori expect the results for binary stars to be in a similar order of magnitude if not higher capture rate, but the need to account for much more complex combined potentials and orbits makes saying anything more without an specialized simulation very uncertain. Similarly, our model does not take into account possible planet formation or specific outside perturbers beyond tidal forces, like the mentioned galaxy mergers. More work on how to model these kind of perturbations is the simplest way to improve on our results.

We have also assumed that there would exist this low mass stars just after the first stars, something we have discussed more in detail in section 3.2.2. We however remark that shifting our results to further generation stars would not change them by much, and that the Ξ we give at Table 3.3 is universal, and so can be used for any redshift.

While at lowers redshifts we expect our results to not be as spectacular, considering the large number of stars in galaxies this should still end up as a noticeable amount of subsolar black holes that similarly to the previous case could also end in our Milky Way.

The most evident observational result of the captures would be that, an abundance of PBHs under the Chandrasekhar mass. This alone would prove the existence of black holes with a primordial origin. Unlike primordial black holes that are formed directly with $0.1\,\mathrm{M}_\odot < \mathrm{m_{PBH}} < 1\,\mathrm{M}_\odot$ as result of perturbation collapse, the results of the capture would also take the star's position and momentum, leaving PBHs with very close properties to black holes of astrophysical origin but with masses below the Chandrasekhar mass.

Observing sub Chandrasekhar mass black holes could challenging, especially if they are alone. Any non-luminous object with low mass can be confused with a cold white dwarf. Lensing would be an option, as would be binary systems where we we could see the black hole tidally stripping a fellow star. The biggest difficulty however would be differentiating our PBH that started as a $10^{-12}\,\mathrm{M}_\odot$ from other $0.1 - 1\,\mathrm{M}_\odot$ PBHs.

The are a few ways they could be differentiated from these other low mass PBHs. The spin would be the easiest, as our resulting black hole would inherit at least portion of the angular momentum from the star they have just accreted and we expect PBHs resulting from perturbation collapse to have negligible spin. This is not a hard rule though, as mentioned previously in Chapter 2. Another, if harder way to differentiate them would be by their statistics. If we detect enough their statistical values should be much closer to the stellar population they have replaced in contrast to PBHs, and there would be no GW background from mergers of subsolar PBHs.

Another possibility comes from binary systems. Depending on the final stages of accretion and interaction with multiple systems, we might also have binary systems of a star with one such small black hole, or planets surrounding it. Primordial black holes of $0.1 - 1\,\mathrm{M}_\odot$ can pair with a star to create a binary system, but they will not share an origin and so are likely to perturb any planet formation on the system in the process of

pairing up. We also expect the occurrence of close pairs to be small. In contrast, because our PBH start as very small they will not perturb any surrounding disks of material, and they will simply take the place of one of the stars of the system, making close pair binaries more common than in the directly primordial case.

In all cases our black holes could still explain all the dark matter through their $10^{-12}\,\mathrm{M}_\odot$ progenitors, unlike the $0.1 - 1\,\mathrm{M}_\odot$ PBHs. On the contrary, if such black holes are not found then it places a very strong constraint on $10^{-12}\,\mathrm{M}_\odot$ PBHs of any origin, because our results show there should be many of them. Finding them or not can thus close these PBHs being all the Dark Matter, one of the very last windows still remaining.

CHAPTER 4

DIFFUSE LYMAN α EMISSION BY MATTER AROUND SUPER MASSIVE BLACK HOLES

Some of the brightest objects currently known to men are active galactic nuclei(AGN), which are galaxy cores so luminous they outshine the rest of their host galaxy combined. This massive luminosity allows us to measure far off galaxies that otherwise would be too faint to be detected with current instruments, and so are an extremely useful tool to explore the early universe. While today they may appear well established objects, it has only been 30 years since the Active Galactic Nuclei unified model, which joined a set of extra-galactic objects of unknown origins in differing wavelengths as coming from the same type of object, an AGN just seen at different orientations. A showcase of this can be seen on figure 4.1.

This unified model could be theorized in the first place because AGN themselves were expected to be the result of active super massive black holes, as only massive accretion could justify the luminosities measured and the various frequencies and phenomena seen depending on the orientation. Super massive black holes themselves are, as the name implies, massive individual black holes found at the center of galaxies, going from 10^6 to $10^9\,M_\odot$. While their specifics depend on their host galaxy, SMBHs were from the beginning understood as the natural solution to the AGN's high luminosity [89].

As the center of the core has the highest density present in the galaxy, any possible object more massive than their surroundings would constantly accrete matter. Even if the objects radiating the AGN started as only a dense star clusters or a single super massive star, the high density environment would continually feed mass to that object, starting a runaway process where more mass would result in increased gravitational potential, increased accretion and so increased mass again. This is compounded because we also expect dynamical friction to play a significant paper in the core. In a very analogous process tp the one detailed in section 3.2.3, we expect friction to push any massive object to the core of the galaxy. The friction rises as the mass of the object rises too, so the increased mass not only will increase accretion, but also friction.

The difference is that massive object need not to start as a black hole. As long as it is massive enough, it will end up on the center of the galaxy, the place of hightest density, and it will eventually become so massive that it can only collapse gravitationally into a black hole[1]. After that, either by normal accretion or by other similar massive objects

[1]After a certain mass threshold, stars are expected to be so unstable that they collapse directly,

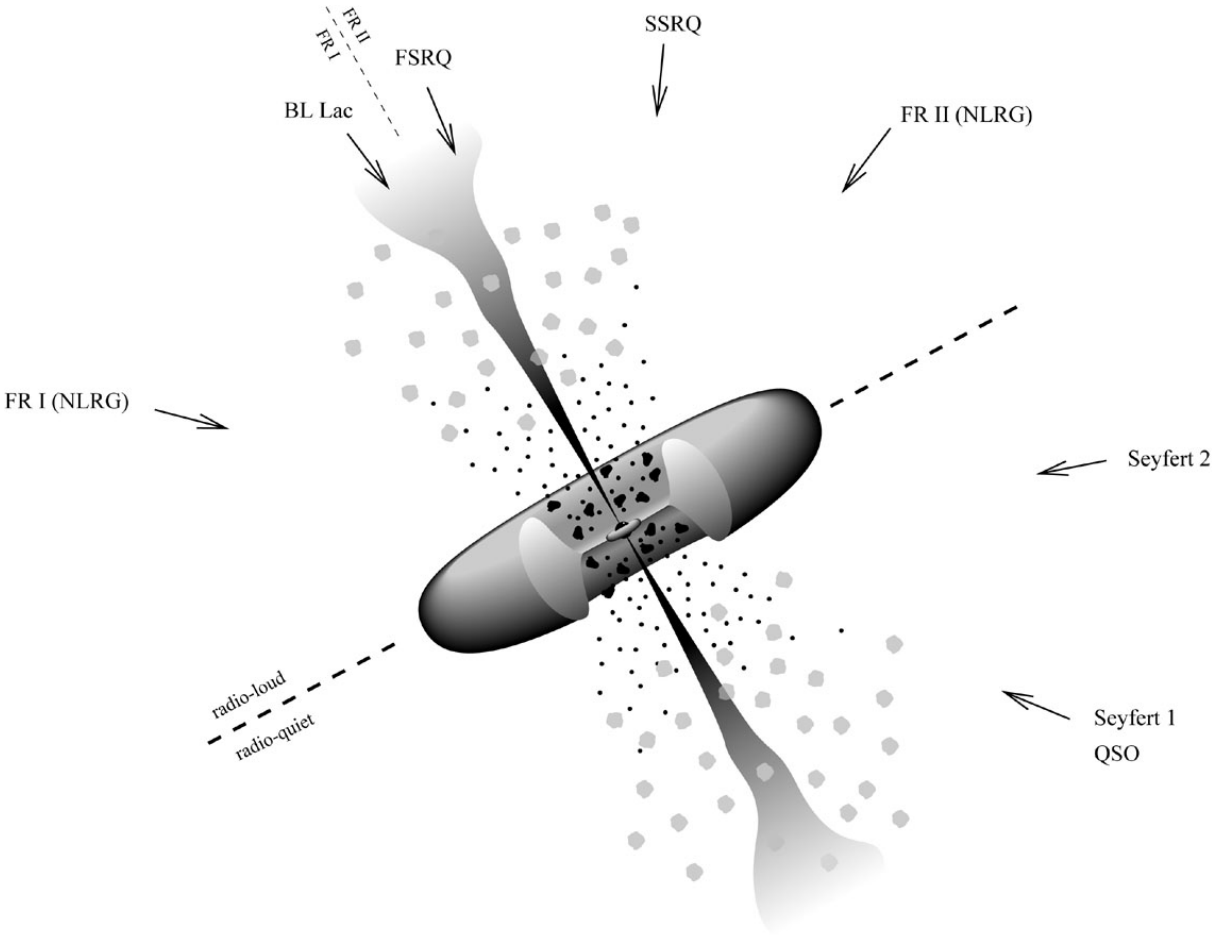

Figure 4.1: The AGN unified model. Extracted from figure 5 of [88]

that also fall to the core by friction, the black hole will eventually reach the size of our SMBHs.

We can in fact estimate this process by recovering the Eddington luminosities and accretion rates we showed before. As we defined in equation 3.34, the Eddington limited accretion rate depends on the mass of the object and a radiative efficiency. This radiative efficiency measures how much of the accretion results in emission, and is highly uncertain as it depends a lot on the geometry of the accretion: if there is an accretion disk, if its spherical and symmetric, etc. The standard for astrophysical processes is $\eta_{\mathrm{rad}} \sim 0.1$, which also works as a conservative approximation. By assuming that and that we are starting with an object of M_{seed} we have an initial accretion rate of:

$$\dot{\mathrm{M}}_{\mathrm{Edd}} = \frac{4\pi \mathrm{G m_p}}{\mathrm{c}\ \eta_{\mathrm{rad}}\ \sigma_{\mathrm{T}}} \mathrm{M_{seed}} \approx 2.2 \cdot 10^{-8} \left[\frac{\mathrm{M_{seed}}}{\mathrm{M_\odot}}\right] \mathrm{M_\odot/yr}\ . \tag{4.1}$$

Integrating in a process analogous to that in section 3.2.6 we end with a total time:

$$\Delta \mathrm{t} = \frac{\mathrm{c}\ \eta_{\mathrm{rad}}\ \sigma_{\mathrm{T}}}{4\pi \mathrm{G m_p}} \ln\left(\frac{\mathrm{M_{SMBH}}}{\mathrm{M_{seed}}}\right) \approx 4.5 \cdot 10^7 \ln\left(\frac{\mathrm{M_{SMBH}}}{\mathrm{M_{seed}}}\right) \mathrm{yrs}\ . \tag{4.2}$$

If we input a seed mass of $\sim 100\,\mathrm{M_\odot}$, even for the highest expected mass of our SMBHs ($10^9\,\mathrm{M_\odot}$) we would get total times below 1 gigayear. This would leave plenty of time for SMBHs to form even with pure accretion without needing to input multiple or larger seeds. While constant Eddington limited accretion rate can seem a big assumption, the high densities of the galactic core make it reasonable. We also only need one SMBH per galaxy, so the process do not need to be common, just feasible.

The biggest uncertainty is how much it would take for the object to reach the core. This is however easily solved as star formation can happen close to the core. Because the most massive stars will also leave the most massive black holes, the SMBHs being the result of these first big black holes is the simplest solution, with other objects feeding into it later.

There has been some controversy recently, as SMBHs as massive as $10^9\,\mathrm{M_\odot}$ have been found at redshift 7.5 [25]. This could leave the timeline above a bit strained, with some models having difficulty reproducing SMBHs [26]. This is however very far from conclusive. Not only the timeline above comes from assuming $\eta_{\mathrm{rad}} \sim 0.1$, but this also depends on the formation and death of the first stars which are still poorly understood. Even within these limits, we are also assuming constant Eddington limited accretion, while even within this model we would also expect plenty of other black holes to fall down to the galaxy core, where they would merge in a shorter more violent events not affected by the Eddington limit.

Still, one of the alternatives are PBHs, which could form the seed of SMBHs both earlier than the first stars and more massive up to a $1,000\,\mathrm{M_\odot}$. While monochromatic constraints bar them from being all the dark matter, only a very small abundance would be needed to act as seeds. Because of their low abundance the only way to constrain them however would be to improve our understanding of AGNs and SMBHs and solve their origin, as they would be otherwise too rare.

One of the objects within AGNs are Quasi stellar Objects (QSO). As mentioned previously, when matter falls in the black hole, it loses energy in the form of radiation.

skipping even the supernova

Depending on the angle and dust obscuring it we can see in different forms from Earth, as seen in figure 4.1. A Quasar is one of them, in which we see a very bright emission across the optic and ultraviolet spectrum coming from a point like source within a host galaxy. Overall quasars are rare, but because of their high luminosity we can observe them at medium to high redshifts ($z \sim 5$), in which they are a great tool to understand the early universe.

One of the most important contributions of quasars is to the reionization of the Universe, a process around $z \sim 7 - 8$ that saw the intergalactic medium shift from cold molecular gas to heated ions. It is commonly expected that star forming galaxies should dominate and provide the grand majority of the contribution, but quasars can be bright enough to contribute a portion. This is relevant, because due to both their rarity and the bias in observations, where we only see the brightest among them, there is a fair degree of uncertainty on their more generic statistical properties.

This issue is also compounded by the relation of QSOs with Lyman α emission, a type of ionizing radiation. Not only is very easy to confuse QSOs with Lyman α emitting galaxies, but among the brightest quasars it is very common they have a bright Lyman α nebula surrounding them [90]. A higher than expected brightness of this diffuse emission implies more active AGNs and higher contribution to ionization and other processes. Similarly, a missing nebula where it is expected also carries its own set of implications on both the luminosity of the AGN and the density of the intergalactic galactic medium (IGM). An overall better understanding of the nebulae would help with deepen our knowledge of both AGNs and their surroundings.

4.1 Lyman α emission

4.1.1 Lyman α line

The Lyman α line is a spectral line of hydrogen in the Lyman series of 1215.67 angstroms of wavelength. It is emitted when the atomic electron transitions from its second orbital to the first orbital, the ground state. As the first excited state of Hydrogen, is thus a very important marker of the most common atom in our universe.

Technically it is a doublet, as there are two quantum states depending on the projection of the electron's spin angular momentum along the z-axis that change the wavelength of the emission very slightly. However, in practice the width of the line we see in the spectrum is large enough that we are not able to differentiate them in our instruments.

This width of the line, commonly measured through the equivalent width, results from the source's own movement and temperature. While we can measure the expected wavelength we will see a line from Earth through the redshift, $\lambda_{obs} = (1 + z)\lambda_{em}$, this does not take into account that beyond the expansion of the universe the source might have their own peculiar velocity. With extended sources different parts can have different velocities, and temperature will mean even within the same region of the source particles will also have differing speeds. Each differing speed will mean different Doppler shift to that particular ray. As our instruments do not have infinite resolution, we will see all those differing spectra as coming from the same source, and rather than multiple sets of sharp lines we will see a broad line with wings, the size depending on the intensity of the emission. The wings also combine with the adjacent continuum, the normal spectra (usually close to a black body) we expect purely from the temperature without individual spectral lines. The overall effect is what looks like a broadening of the line. This broadening can carry

its own advantages though, as the wings can give us information on the dynamical state of the system, but also results in the doublet being treated as a single line in almost every case.

There is another question referent to the Lyman α line however. The one we described corresponds to the decay of second orbital (n=2), but also concretely the non-zero orbital angular momentum (l=1), commonly called quantum state p. The second orbital has another state with l=0, s. However, this second orbital cannot simply decay to the ground state, as both share the same orbital angular momentum. Such decay would require emitting a photon with 0 angular momentum with respect the hydrogen atom, which is not possible. A possibility is instead emitting two photons, which would allow for a net zero angular momentum. This would result in two different lines that can differ for each each individual case of 2 photon emission, meaning in practice they would be contributions to the continuum rather than a set spectral line and thus be much harder to measure. However, two photon emissions are also less likely to happen [91] than more simple one photon decays. Therefore, the Lyman α line dominates the transition from the second orbital, the most common excited state for the electron, to the ground state of the Hydrogen atom.

Being the most common emission of the most abundant atom in the universe, Lyman α lines are a good reference line in most spectra. Also they are a typical tracer of star formation, as the line is on the ultraviolet spectra which is also strongly present in young big stars. There is another degree of value however, as we can see Lyman α lines not only in emission, but also in absorption spectrum. Radiation equally or even more energetic than the Lyman α is still light and will interact with the objects that it crosses. As there is plentiful of atomic Hydrogen in most systems, this atomic Hydrogen has good chance of absorbing the radiation, moving their electrons from the ground state to the second orbital, the same transition as the Lyman α line but in reverse. Having been absorbed, this Lyman α emission will not be on our spectra. However, because radiation gets redshifted as it travels, the emission that was for the system equivalent to their Lyman α we will see at different wavelengths than the original Lyman α line of the source, in effect leaving clear gaps in our spectra at different wavelengths. Thus we can not only get information on the Lyman α emission, but also on objects between us and the source, the foreground.

Absorption lines are then very commonly used as a sign of baryonic matter presence. Because of the abundance of Hydrogen, any kind of non-ionized matter that receives strong enough radiation will absorb the Lyman α line with the higher density resulting in a higher degree of absorption. An example of spectra that focuses on the foreground is the Lyman α forest, which is called so because the multiple absorption lines in a row look like trees in a forest. The Lyman α forest is not only a measure of the density of various objects, but also of the ionization state of matter at various redshifts, as only atomic Hydrogen will leave a Lyman α absorption line. There are more layers of complexity to the Lyman α forest too, as similar to in emission lines there can also be wings on absorption spectra, coming from differing peculiar velocities and also radiation damping helping give more information about the foreground.

On the intersection of both these phenomena there is another interesting case. Emission is in most cases isotropic and spherical, therefore surrounding objects not on our line of sight will receive radiation that would not normally reach the Earth. This includes Lyman α and more energetic wavelengths, resulting in the surrounding matter absorbing it in a similar case to the Lyman α forest, but without any kind of observational sign reaching us. A natural consequence of that however is that the now excited Hydrogen

will eventually decay, re-emitting the line. This reemission will be similarly spherical and isotropic, the hydrogen surrounding the source shining with this same line. This results in a diffuse emission with increasing intensity the higher the density of hydrogen is with a maximum set by the brightness of the central source. Characterizing and understanding this emission gives useful complementary information to the main object, giving us information on the surroundings of the source we were initially missing. If the spectra gives us information about the emitting object and the foreground it goes through towards us, the diffuse emission gives information about the surroundings of the object.

In this simplistic case of diffuse emission by recombination radiation, radiative recombination cascades (emssion from the electron decaying) are the main reason for the emission of Lyman α. The Lyman α emissivity will be simply proportional to the hydrogen recombination rate times the ionized hydrogen density squared. The Hydrogen recombination rate depends in a mild way of the temperature [90], and the Lyman α we see will also depend on how many of the cascades to the ground state produce Lyman α photons instead of more energetic emission or the two photon case. While exact modelling is complex, a good approximation is to take ~ 0.65 Lyman α photons per recombination for temperatures between 10^4 and 10^5 K [92]. This method can most of the times reproduce the luminosities we observe in Lyman α nebulae, but require densities several times higher than in common haloes, of the order of ~ 1 atom per cm^3.

That is only an ideal case however, as there are other possible ways for the matter to emit Lyman α photons and contribute to the diffuse emission. One of the ways is through scattering. Rather than being ionised and then decaying, reemitting the photon, in this case the surroundings scatter another photon that originated from the central source towards Earth. Another name for it is continuum pumping, as the matter scatters photons increasing or reducing their wavelength, thus pumping photons that were originally in the continuum on the Lyman α line.

One important difference from recombination is that the scattering is with neutral hydrogen rather than ionized, and it depends only linearly on the column density of neutral hydrogen. This is because we are working with Lyman α optical depth rather than recombination rates, the optical depth being a dimensionless measure of the energy loss after crossing a specific medium. For our case it is roughly equivalent to the rate of interaction with the medium, said interaction being the scattering. Therefore the optical depth also depends logically on the distance from the source, as more material to cross will result in a higher rate of loss. As the Lyman α optical depth gets closer to 1, we expect the scattering to start giving an important contribution to diffuse emission. Simulations however have shown that the requirements for this to happen are steep [93], and scattering is expected to contribute only in a minor way. The scattering process itself also affects the polarization of the light however, so it remains a useful way to explain one off nebulae with strange polarization profiles.

Another factor which can contribute to the diffuse emission is simple cooling. As the temperature increases, collisions excite electrons to higher orbitals. If the temperature is very high, the atoms will directly ionize and then decay later in a recombination cascade, thus contributing to the first case. If the temperature is not so high however, the collisions will not be enough, only exciting the electrons to jump one or two orbitals. This is the collisional excitation case. For Hydrogen, the temperatures are between $2 - 5 \cdot 10^5$ K [90], which is very close to the temperatures we expect to see in the intergalactic medium. While re-emitting the Lyman α line will cool the matter, if there is a heating source like the original source of the Lyman α nearby, an equilibrium can be reached, allowing collisional

excitation to contribute to the diffuse emission. An exact value of this contribution is however unknown, as unlike the previous cases cooling has few analytic simplifications and mostly requires either simulations or specialized numeric models

Overall, we expect recombination, also sometimes called fluorescence, to be able to explain almost all cases of diffuse emission, but care has to be given as cooling can add a significant degree of uncertainty on the densities derived and scattering can have an undue effect on the polarization of the light.

4.1.2 Diffuse emission observations

However, this understanding does not change that diffuse emission is very hard to observe. Galaxies are surrounded by dense filaments of matter and can be very bright, but their emission is not even, with the dust in the galaxy itself obscuring a lot of the ultraviolet radiation. This problem gets even worse at higher redshifts, so only the surroundings of exceptionally bright or unobscured galaxies can be seen. Standard point-like objects are also generally not bright enough to power a surrounding nebula, though highly energetic transients are possible but still very hard to observe due to their fleetingness.

The most common example of diffuse emission can be found near the center of clusters of galaxies. The very dense environment is grouped with a number of very high luminosity objects which allows the Lyman α emission between the galaxies to be observable.

Another good example are the already mentioned quasars. Most discovered nebulae surrounding quasars are on the brightest most massive ones. However there has been doubt if nebulae could be a generic feature of quasars, where their brightness combined with their dense surroundings would result in all quasars having some form of diffuse emission. Such emission would be just too faint to be seen in most quasars due to distance. As more and more quasars are discovered with nebulae and without it, this idea of studying them and their diffuse emission statistically rather than looking for each nebula individually has gained weight.

One of the strongest ways to do so is through stacking, which we will explain in detail in the following section. This seems to have worked in fact too well, as [96] found that the Lyman α emission surrounding quasars at large distances was several order of magnitude above the expected, indicating either clustering above the expected or a much higher emission. A follow up study [95] found a degree of systematic effects had bumped up this result above the reasonable, but it still found that surface brightness to be on the higher end.

This can be appreciated on the lower image of figure 4.2. Note that the solid lines are the Lyman α emission coming form individual giant nebulaes, which we expected to be significantly brighter than the average one. For comparison the upper figure is from [94], who stacked 15 quasars without an apparent nebula and achieved some if very uncertain results. The difference in both surface brightness between both is notable.

While the very large scales of [95] are extremely hard to prove, stacking the lower distances could improve on the work of [94] and prove the presence or absence of these generic nebulae, before moving onto larger scales.

4.2 Stacking

Imaging in astronomy was revolutionised by the invention of CCD cameras, and the current state of the art is only possible thanks to them. These devices are able to detect

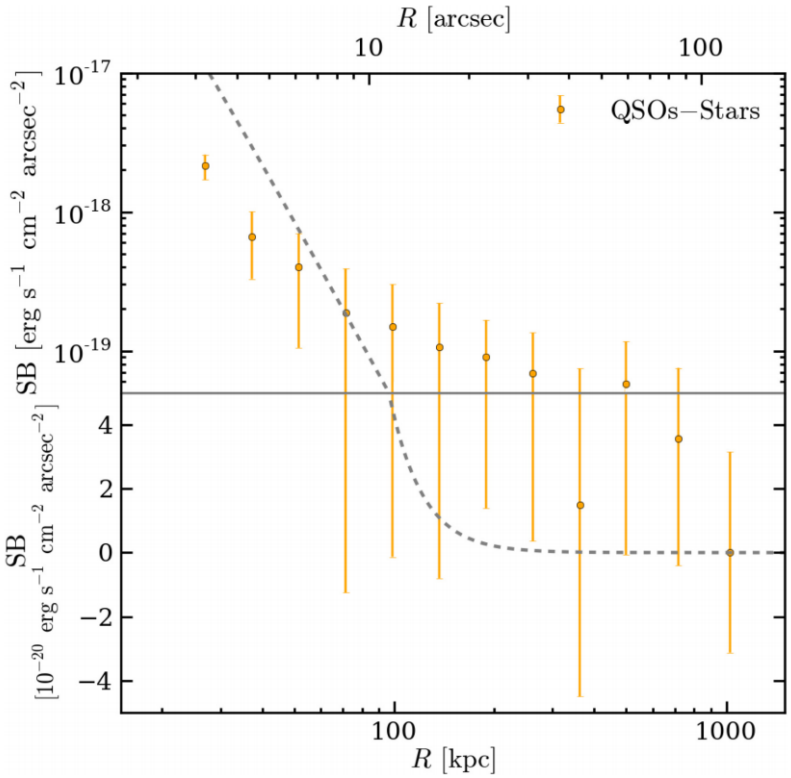

(a) Battaia et al.

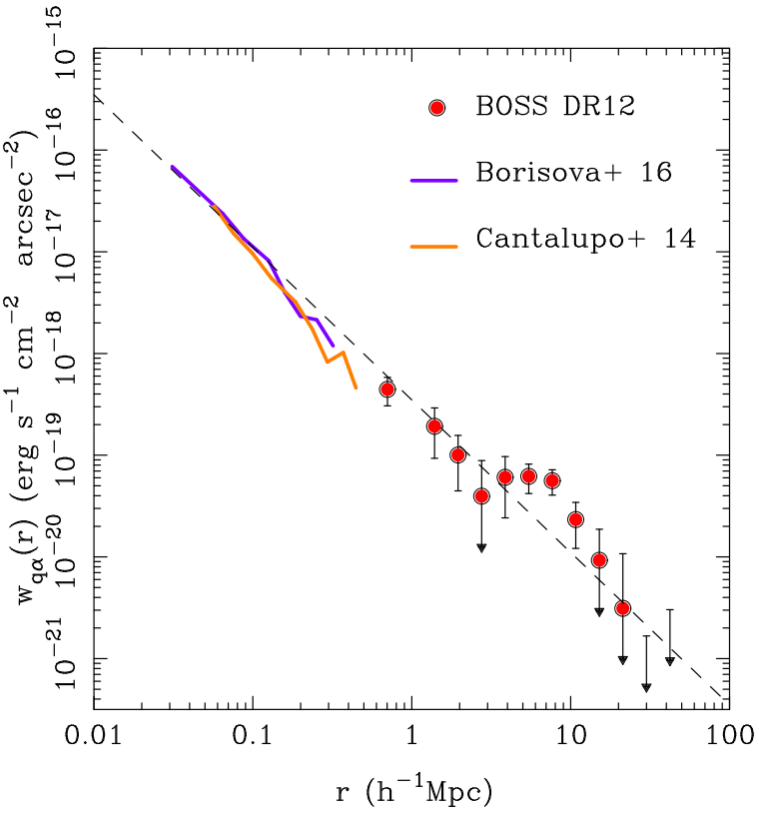

(b) Croft et al.

Figure 4.2: Comparison of figure 7 from [94] and figure 4 from [95]. Despite different nomenclature the y axis use the same units. Note a small difference in the x axis however, as the figure below uses h, meaning the axis has to be multiplied by ~ 0.7 to compare. Despite this, significant discrepancy can be easily seen.

the movement of charges within their pixels, and can convert it to a digital value. With a semiconductor layer that converts any incoming photons into a moving electron and thus a moving charge, these devices allow a direct conversion from photons to a numerical value, bypassing a most of the problems of photographic imaging.

One of the aspects where it has proven remarkably useful is to obtain deep images. Saturation of a pixel however remains a problem, as charges spill on other pixels and thus affect the whole image, but long exposures are needed to ascertain the characteristic of the faintest objects. There exists alternatives though, like the stacking of images.

Stacking consists on adding one image on top of the other, adjusting for differences in position and calibration. On paper it is very similar to just having an image with an exposition time twice of the previous one, but there are some important differences.

The first is that we avoid the problem of saturation: a bright emission that would saturate the pixel in a long exposure would appear as normal and not affect the surrounding pixels in the 2 individual images. The second is about the type of uncertainty we are working with. In a long exposure, the shot/Poisson noise is less relevant as the number of photons we are working with increases, but the thermal noise (ambient photons getting mistaken for signal photons) increases with time. Thus the thermal noise, which is a systematic very hard to model, becomes dominant. With stacking, the sources of error of a single image remain. This means the Poisson noise dominates, and while it is more important than in a long exposition, we can use statistics to model it pretty well.

$$\mathrm{SNR} = \frac{\mathrm{N_{images}}}{\sigma}\mathrm{SNR_{image}} = \frac{\mathrm{N_{images}}}{\sqrt{\mathrm{N}}}\mathrm{SNR_{image}} = \frac{1}{\sqrt{\mathrm{N}}}\mathrm{SNR_{image}}\ , \tag{4.3}$$

where SNR is the signal to noise ratio of the stack, the one with the subindex being the signal to noise ratio of an individual image, and N_{images} the number of images we are stacking.

Thus, for a stacked image our uncertainty goes as the square root of the number of images we are stacking. This allows us to study very faint objects below the nominal limit of the telescope we are working with.

It is relevant to also ask about the scientific purpose of stacking. Its basis is to improve the images we have of fainter objects when we stack that same object, which besides minor differences shares the same purpose as longer exposures. However, its uses are not limited to this. We can stack different images of different objects.

This can seem absurd, as joining 2 different images distorts them. If we join enough random images we would end with a mess of random pixels following a gaussian distribution. But following that same property, if the images are not random and they share some characteristics the resulting image would enhance these shared properties while the rest of the image would end a random distribution.

How it would work is that pixels outside the shared characteristic would follow a random distribution, as the same pixel in different images could hold a bright object, a faint star, complete void, etc. By the central limit theorem, this would end as a Gaussian distribution. Pixels affected by the shared characteristic however would add up with each other, maintaining their original distribution as they are not random. This happens even if this shared characteristic is below the noise threshold of one of the original images. The relation between this signal and the rest of the image, which now is effectively noise, follows the signal to noise ratio equation mentioned before; the normal distribution noise raises as square of the number of images, but the signal (if there is any) improves linearly,

which results in an overall square root of the number of images enhancement of the original signal[2].

Thus, if we stack a high enough number of images we believe to be similar in an aspect but cannot confirm individually, the resulting stack would end with that aspect clear to see while everything else that could detract or overshadow it in individual images would fade out in the long run of stacks.

This properties of stacking can be very useful for a relatively new field in astrophysics, intensity mapping. In intensity mapping we do not care only for an astrophysical object and its emission spectra, but also from the emission coming from its surroundings (thus the term mapping), even when this emission is diffuse enough that we cannot associate any object to it. This diffuse emission can have many origins, be it a background light coming from extremely far objects to fluorescence from gas in the surrounding to diffraction and even gravitational lensing.

Normally distinguishing between these possible origins or even types of existence for this emission is extremely hard. As this diffuse emission is faint the degree of uncertainty is large and the characteristics and parameters we assign to them uncertain. Very high and careful exposures can be done for particular objects to resolve these issues, but are impracticable for large surveys where we want to observe as many of a certain subtype of object as possible.

In those cases stacking can be extremely useful. If the diffuse emission is characteristic of the type of objects whose surroundings we are looking at, then the stacking will give a much more accurate image of it. This would allow improved physical insights on its origin and a better grasp of how much of the original signal was noise for future survey strategies. Even in the case where such emission could not be found in the stacking, we could assign it a maximum magnitude much more stringent than in the initial survey. Even this would also result in a better understanding of how much of the diffuse emission from the images are random backgrounds and inform future endeavours.

4.2.1 Point spread function

It is important to take into account that even as we aim to stack hundreds of images, these images share similar origins and instrument. All typical defects present in CCD cameras will be shared among all the images, and thus survive through the stacking. Even if different cameras and telescopes were to be used, as the systematic errors would be similar they would not simply create a normal distribution as the rest of the image.

One particular defect present in any kind of light instrument is the Point Spread Function (PSF). This describes the shape that appears on the camera when the telescope observes a single point of light. As the mirrors and instrument are not perfect, those defects would result in this single point appearing spread out on the camera, thus the name. Modern instrument attempt to minimize this effect as much as possible, but its presence is unavoidable and accepted in all types of surveys.

This is double for observatories on Earth. While the intrinsic PSF of an instrument comes from the mentioned optical inperfections, the fact we are observing objects through the Earth's atmosphere, the sky, adds up to the problem. As the light comes from the source to the telescope, it crosses patches of the sky that are in constant change,

[2]If the signal to noise ratio of the original images used in the stack differs between them this improvement becomes much harder to compute. Fortunately, modern surveys take care to keep the signal to noise consistent and put warnings on images when external factors do not allow it

minute differences in temperature and velocity occurring continuously. Each of these small changes brings its own small change on how the light refracts in the atmosphere. While stacking allows for shorter exposition times, a minimum is still needed to reach at least a perfunctory depth. In this minimum time countless of these changes have happened, the same patch of the sky refracting photons in different ways. As a result, even without taking into account the instrument, we would see the image as blurry. This effect is what we call the seeing of the sky.

As the seeing comes from countless minute but independent small changes[3], we can apply the central limit theorem in turn. Therefore the seeing can overall be approximated as a gaussian, but the parameters of the gaussian will depend on the region, altitude and even the particular day. The seeing overall dominates the PSF of Earth telescopes and it is one of the major reasons even optic telescopes like the Hubble have a major advantage from being being space-borne.

On Earth or space regardless, the PSF is unlike the thermal noise in that it works by distorting a source, rather than just being a flat background. The uncertainty is thus a percentage of brightness of the central source rather than just a limiting magnitude.

The PSF is thus rather troublesome for any kind of intensity mapping or work in diffuse backgrounds. Long exposures will increase the brightness of the central source and thus the magnitude of the effect, resulting in the PSF overshadowing the diffuse emission in its surroundings. As the PSF is a systematic effect stacking will also not erase it, rather, similarly to the long exposure, magnify it.

The only real way to deal with the PSF is to compute it and subtract it from images. As the PSF depends mostly on the instrument and the seeing can be approximated as a gaussian, once modelled it can be subtracted from the image of that instrument no matter the central object we are observing. Modelling the PSF can be done through both previous work with the instrument or directly through the images. In fact, a stacking is perhaps one of the easiest and more pragmatic way to obtain it.

As mentioned before, continuous stacking results in the enhancement of the shared characteristics of images and the dilution of everything else. The PSF always will come through when stacking, and it is a major limitation of the technique. But conversely, if we stack images of objects that we know do not have any extra diffuse radiation or similar non-instrument systematics around them, then the final stack will contain only the purest form of the PSF. This model of the PSF would also have the advantage of being the one on the image directly rather than theoretical, and so would automatically take into account any possible change in the systematics of the instrument.

Of course, in practice things are not as simple. A more extended object will have a different PSF than a point source by definition, and strictly the PSF also depends in a lesser way on a variety of other factors, like the pixel position within the CCD. The seeing changing for each day will also carry a minimum dispersion we cannot avoid. The type of objects which fulfill the requirements needed, mostly being as point-like as possible, also tend to be limited to stars, and the stacking improves with numbers of images so we will want as many of them as is possible. Even then, some level of systematics will always be present around all objects, which would limit our uncertainty even with infinite images. Still, at our usual numbers (thousands of images) and limiting magnitudes, the level of uncertainty will roughly follow the initial relation of square root of the number

[3]Patches in the sky are very distant from each other despite looking adjacent. Even relatively close by sections of the sky will have countless changes on the span of a small exposure, with the distance between being larger than their sound speed, thus ensuring they are dynamically disconnected.

of images. Therefore, as long as both modelling and subtraction are done properly, the initial limiting magnitude of the images can be greatly lowered, keeping the advantages of stacking.

4.2.2 Potential issues

Even without the PSF, stacking is not a trivial process and problems commonly arise that must be solved or worked with:

Position Stacking requires for the objects of the various images to be perfectly centered on each other. This goes even beyond stacking the adequate pixels: If for example an object is nearer the limit towards the left of the pixel, then even if their nebula is perfectly symmetrical stacking various of them with other properly centered objects will result in an abnormally strong left side and a weaker right for the final stacked image. This bipolar signal would come only from systematic effects that could easily mislead us. Even if we assume that the emission is circular and try to average the signal at each radius, there will be mismatch coming from the emission at differing distances being averaged as being from the same one. This would at best increase the deviation and lower the validity of the results. Obviously, this is not an issue that can be completely resolved, however from the brightness distribution and the shape of the PSF an approximation of the position of the object within the pixel can be obtained in the process of photometric reduction. Using these, we can try to adjust the various images so that they add precisely where the objects center each other, but we would need to go below the pixel resolution. For this, an easy workaround is to interpolate the images, but this brings its own set of new issues.

Interpolation The easiest way to adjust the positions of the objects so they align even below the resolution of a pixel is interpolating. It does complicate things in other ways however. From the start, we are interpolating in a single image, where the uncertainty and the dispersion of the values is relatively high. The end result could be fuzzier than we hoped. The major problem however is again the Point Spread Function (PSF) of the objects. Accurately resolving the PSF is an important step in determining the characteristics of faint objects, especially when we want to find emission surrounding them. However, as the PSF of faint objects can be of the same order as the dispersion in the image, they become entangled when interpolating. This means there is a good chance of the interpolation changing or altering in a minor way the shape of the PSF. While we can model the average PSF through the methods mentioned previously, if we use interpolation to obtain the PSF through stacking then our model PSF will be affected by this too. The differences between real and the changed PSFs could induce systematic errors of the order of the PSF in the final image, that would put in question any results. There are ways to interpolate points between pixels while maintaining the shape of the PSF, the most famous of which is drizzling, but all require the use of weight maps in addition to the images, which adds another layer of complexity. Another alternative is to just avoid interpolating. Using nearest neighbour for pixels will most likely result in a higher degree of error due to the position issue mentioned above, but another possibility is just to abandon the pixels and use real distances. Instead of trying to make a standard stacked image, we relate the values in the pixels with their distance to the central object, which can include decimals thus avoiding the position issue. We bin these

values within various ranges, ensuring that each bin has the same amount of values that would normally correspond to our stacking, and then do the median in each bin. This method makes the assumption that the PSF's shape is radial, which is not completely true for minor details, thus some degree of extra care is needed when analyzing non-radial results. However, for diffuse emission which is expected to be so, it is a much simpler and easier way that allows us to use a higher number of images that otherwise would require excessive computational cost.

Artifacts While the central objects might be perfectly aligned, the surroundings might not. This can happen because we are stacking different examples of the same type of object to find generic properties, but these same type of objects can have wildly different surrounding third objects. If all the cases are very isolated and we only care about the object in itself then we do not need to worry, but in most cases we will have numerous other objects in our field and we will also want information about diffuse haloes or other extensive effects. If we just stacked without doing anything else, those third objects would end up as part of the normal distribution surrounding the central object but also increasing its average, creating artifacts that are not part of the signal we are searching and increasing the dispersion. To avoid those third objects biasing the final stacked image, some kind of masking is required to remove those pixels from the stacking. However, depending on the number of images we are working with manual masking can be impractical. Some kind of automatized masking is helpful but not perfect, and will still result in some smaller artifacts. The easiest solution to all this conundrum is using the median instead of the mean when stacking. This would also remove other unknown singular effects and systematics affecting only a fraction of the images that might slip through. While overall using some form of masking is still preferable, working with the median lowers the risk and effects of any third object interfering with our signal.

4.3 J-PLUS

The Javalambre-Photometric Local Universe Survey [97], known as J-PLUS, is a wide area survey of the sky from the Observatorio Astrofísico de Javalambre, in Aragon, Spain. Using an 80 cm telescope it is planned to observe up to $8,500\text{deg}^2$ with a set of 12 different optical filters. One of the main characteristics of the survey is the large field of view (FOV), each image being 2 deg^2 and thus containing a lot of astrophysical objects in it. The limiting magnitude is modest, but the resolution pairs very well with the wide FOV, each pixel being $0.55''$.

It is a survey very well suited to projects that require working with large amount of objects, both within an image and on the broader sky. The set of 12 different filters also allows for the use of pseudo-spectral methods, as it contains a good number of narrow and intermediate bands among the typical 5 broadbands. We showcase the various set of bands in figure 4.3

Each filter only catches the radiation within a wavelength range, separating the magnitudes found in each different filter to their respective wavelengths. This allows an estimate of the spectra of the observed object. While very low resolution, this is enough to capture the most common and bright emission lines, like Lyman α or $H\alpha$. This information can be extremely valuable for unknown objects, and a lot of work has been put into using this information to create a set of reliable photometric redshift estimates for all observed

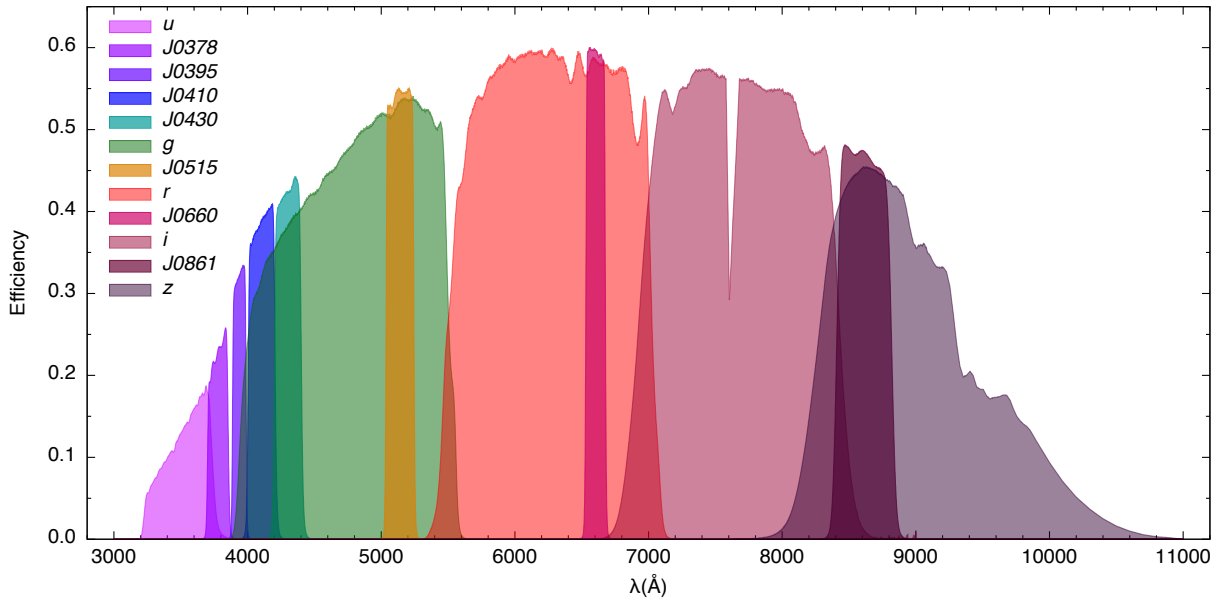

Figure 4.3: Set of filters used in J-PLUS. From [97], but similar information available at `http://www.j-plus.es`. On the y axis is the efficiency in terms of light absorbed by the filter, and x is the wavelength in amstrongs.

Filter	$m_{\rm lim}^{\rm J-PLUS}$	$m_{\rm lim}^{\rm EDR}$	$m_{\rm lim}^{\rm DR1}$
u	20.5	21.1	20.8
J0378	20.5	21.1	20.7
J0395	20.5	21.0	20.7
J0410	20.7	21.0	20.9
J0430	20.7	21.0	20.9
g	21.5	21.7	21.7
J0515	20.7	21.0	20.9
r	21.5	21.4	21.6
J0660	20.7	20.8	20.9
i	21.2	20.3	21.1
J0861	20.0	20.2	20.2
z	20.2	20.0	20.3

Table 4.1: Planned limiting magnitudes of J-PLUS for point-like sources in a circular aperture of 3 arcsec and SNR > 5 for each filter in J-PLUS, together with the averaged limiting magnitudes obtained in the Early Data Release (ERL) and Data Release 1 (DR1). Reproduced from table 4 in [97] .

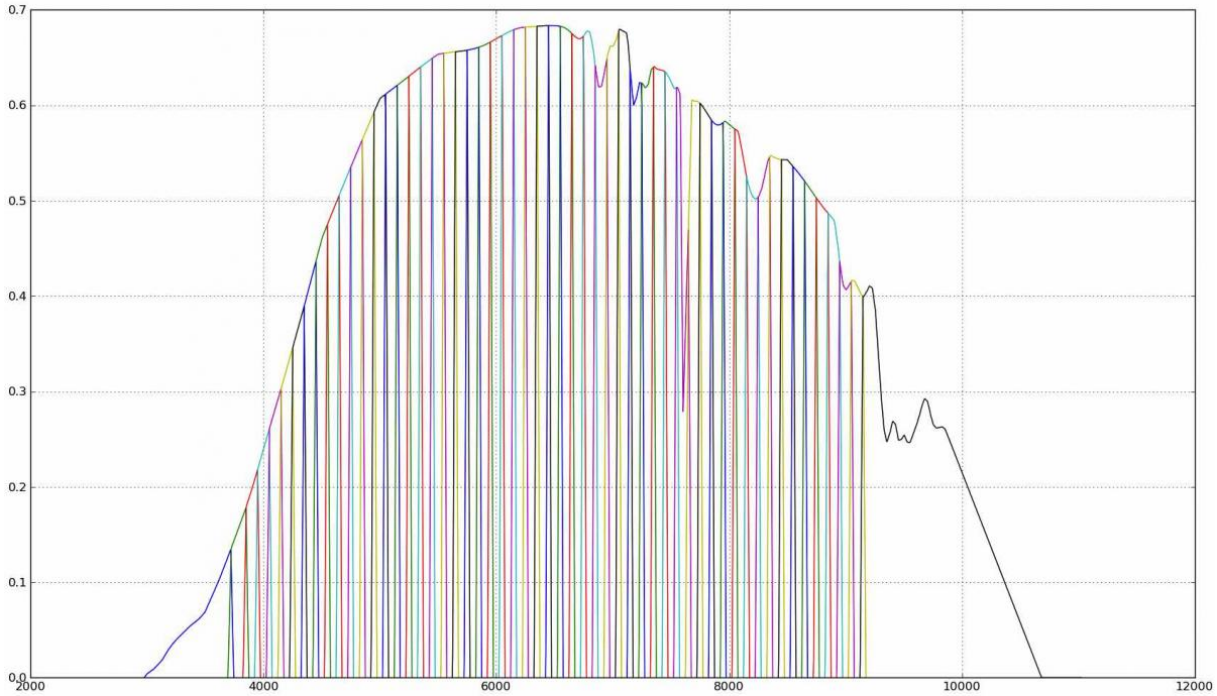

Figure 4.4: Set of filters used in J-PAS. From `http://www.j-pas.org`. On the y axis is the efficiency in terms of light absorbed by the filter, and x is the wavelength in amstrongs.

objects.

The worth of these filters is equally high when observing already known objects though. With a known redshift, the exact emission lines that fall within each filter can be easily computed for much better understanding and a more accurate pseudo-spectra. At first glance this might seem trivial, as for already known objects specialized spectroscopy will give all this information and more with better accuracy. Finding spectra for objects however is time costly, and spectral surveys that cover a large part of the sky, like SDSS [98], are very complex and thus very rare and expensive. If we have objects from which we have a reliable redshift but only a few broadbands, objects from GAIA for example, J-PLUS can give us good estimates of some emission lines without needing a spectra for each. Due to the aforementioned wide area of the survey, J-PLUS excels working with these kind of more common objects and using statistical methods on them.

The limiting magnitude for each filter is shown in Table 4.1, obtained from [97]. While they differ for various filters, especially the wider broadbands, the narrow bands do have very similar limiting magnitudes making the pseudo-spectra we are discussing feasible. The variability of the limiting magnitude between various observation campaigns also serves as a good estimate of the uncertainty.

Another advantage of J-PLUS is that it is meant to work as calibration for J-PAS [99]. The Javalambre Physics of the Accelerating Universe Astrophysical Survey surveys the same $8,500\text{deg}^2$, using an improved 255cm telescope in the same observatory, and also featuring an improved camera and a set of 59 narrow filters. We show the bands in figure 4.4. While they cover a similar frequency range, the improved spectral resolution and limiting magnitudes are a marked improvement.

This makes all the pseudo-spectral methods mentioned before much more powerful. Because this survey is seen as a natural continuation to J-PLUS, all the photometric reduction and data handling methods will have continuity. This allows any kind of work

started in J-PLUS to have a natural and much more powerful continuation with J-PAS.

For our concrete case of stacking, the wide area and number of filters are very helpful. With such a big fraction of the sky covered there are a very high number of objects, which make stacking more accurate and robust. The number of filters also allows for useful checks; we do not expect the PSF to change much if at all for different filters.

Even the size of the images are helpful, as the high resolution means we have luxury of avoiding borders of images or other positions which can be unreliable due to subtler effects and still have a high number of objects. Furthermore, as J-PAS is expected to have a very similar PSF to J-PLUS due to sharing the observatory (and so the sky and portion of the instruments), almost all our work can be similarly applied to the later survey. Indeed, with the improved limiting magnitude and a much higher number of filters, stacking with J-PAS will be an even more powerful tool than with J-PLUS.

4.3.1 Calibration

In order for the stacking to be meaningful, a minimum accuracy on the single images is needed. Thus, it is necessary to have a good understanding of the possible biases and correlations present in the calibration of J-PLUS' photometry [100]. There are various possible ways for these kind of large scale surveys to be calibrated. Here we make a brief summary of each of them, but for detailed analysis we refer to [100, 101].

The first and simplest would be through standard stars. Ideally, J-PLUS would use known and catalogued spectro-photometric standard stars (SSSs) to calibrate every single tile and filter, allowing for an independent measure of the absolute flux in each of them. However, there were several problems. First is that a major proportion of those stars could appear saturated in a normal exposure. Another would be that calibration could only be performed in perfect photometric nights, with a stable and clear sky through all the observations, and even then the number of reference stars would be low compared to the wide area surveyed by J-PLUS. Similarly, calibrating by comparing with SDSS and Pan-STARSS 1 photometry also runs into shortcomings, as neither covers fully the 12 different filters used by J-PLUS, and the SDSS spectroscopy does not reach the redder bands either. Instead, other type of methods are needed.

An alternative is using stellar locus regression (SLR). This was indeed the initial calibration method used on DR1. Rather than using a single calibration type, the SLR depends on both an initial calibration through other ways and statistics. First, a reference filter is calibrated using one of the previously mentioned methods, mostly a combination of SDSS/PS1 photometry and spectroscopy. Then, using that reference filter (the i band was the one that gave the best results), a median stellar locus is constructed in all 2145 possible colour-colour combinations using all the stars in that image. The stellar locus is structure in color-color diagrams, similar in a way to how susbsets of stars appear grouped in more standard Hertzsprung–Russell diagrams. The calibration is obtained from an iterative process that minimizes the distance of the 2145 stellar locii to the median locii. This type of calibration still has a few shortcomings, not only it needs an initial method to calibrate at least one band, but also does not include corrections of the reddening due to the Milky Way's dust, which would affect all the colours of the locii including the median.

To try to correct this issue, a third calibration way is the stellar white dwarf locii (SWDL). The SWDL calibration will be set as the default calibration procedure in subsequent J-PLUS data releases and is present as corrections in DR1 [101]. First high quality stars in the pointing using Gaia information are defined. Using these pointings, the images

are de-reddened using Milky Way dust maps of Bayestar17 [102] and the extinction law by [103]. Then the gri broad bands are calibrated with PS1 photometry. This includes a plane correction depending on the position of the pixels: this position-dependent effect impacts the photometry of the sources at the 2% level. Moreover, this gradient is not universal and depends on the pointing, and so the paramters change for each image. The origin of this gradient is still unclear and is under investigation, but possibilities include the differential variation of the airmass across the observation, the presence of scattered light in the focal plane, or the change of the effective filter curves with position. Then, the instrumental stellar locus can be computed, a step very similar to the SLR, but allowing for offsets between different pointings/tiles.

Finally, another correction comes from White Dwarf locii. The emission of white dwarf (WD) can be modelled at the ~ 1 % flux level from parameters easily obtained through their spectra. One for one calibration is both too time consuming and depends heavily on having already catalogued WDs on the images. However, we can use previous white dwarves from [104] and [105], modeling various colour-colour diagrams and comparing with the observed WDs locii. Because the models give absolute (and not relative) flux levels, this resolves any further ambiguity about the locii being displaced by reddening and transforms instrumental magnitudes to calibrated AB magnitudes outside the atmosphere.

For our stacking we use DR1 data, but after helpful conversation with the author of [101] we were able to manually add the SWDL corrections, meaning our photometry should match the expected J-PLUS specifications.

4.4 Stacking with J-PLUS

Knowing the issues we will face, we can proceed. But first of all, is it even feasible to see anything with J-PLUS?

Fortunately it is not hard to make such calculus, as long as we take some approximations. First of all J-PLUS usual depth is $AB \sim 21.25$ mag [97], and we have it for each filter in Table 4.1. Then we can use figure 4.2 to approximate the surface brightness we should see at a radius. The images would be in pixels, which in J-PLUS each correspond to 0.55", same in J-PAS. At redshift ~ 2, an arcsecond corresponds to ~ 8.5kpc. This means 70 kpc already are close to 8 arseconds or 15 pixels, and given the presence of near objects and imperfect masking we do not expect anything beyond 20 pixels to be useful, so it is a good initial value. For 70 kpc [94] would give a value of $\sim 2 \cdot 10^{-19}\mathrm{erg}/(\mathrm{s\,cm^2\,arcsec^2})$. The values around 70 kpc cited in [95] are found in giant Ly α nebulaes in very bright QSOs rather than averages, so they serve as maximum value.

With all this, we can compute:

$$\mathrm{m_{AB}} \sim 20.5 \longrightarrow \mathrm{f_\lambda} = \frac{10^{-0.4(\mathrm{m_{AB}}+48.6)}}{3.3[\lambda]^2 \cdot 10^{-19}} \longrightarrow \mathrm{f} \sim \mathrm{f_\lambda} \cdot 30 \sim 10^{-15}\mathrm{erg}/(\mathrm{s\,cm^2}) \,, \tag{4.4}$$

where we have taken the wavelength of the band where we expect Lyman α emission coming from $z \sim 2$ to fall, roughly around $3,950$ Å, and so the characteristics of J395 narrow band, both its amplitude and the limiting magnitude of 20.5 for SNR=5. The efficiency of the filter varies, but it averages at ~ 0.3 for FWHM of 100 Å, so the integral would be roughly equivalent to multiplying by 30. As we are only looking for an estimate we drop decimals and do not bother with more extensive calculations, $10^{-15}\mathrm{erg}/(\mathrm{s\,cm^2})$ works for us. Now, this was for an aperture of 3 arcseconds, which corresponds to an area

$A = \pi r^2 = (1.5)^2\pi \approx 7\text{arcsec}^2$. Then we only have to remember equation 4.3 and the diffuse value we are aiming for:

$$2 \cdot 10^{-19}\text{erg}/(\text{s}\,\text{cm}^2\,\text{arcsec}^2) \cdot 7\text{arcsec}^2 \longrightarrow \sqrt{\text{N}} = \frac{10^{-15}}{1.4 \cdot 10^{-18}} \longrightarrow \text{N} \sim 5 \cdot 10^5\ . \qquad (4.5)$$

An important subtlety however is that we are dealing with the surface brightness at a certain radius. In an image, each pixel will only stack with ones corresponding to the same exact position. However, the surface brightness at a certain radius measures all the pixels that are at that radius. Therefore, multiple pixels will contribute per image. At farther radius therefore the number of pixels that will contribute will be more than the initial circumference of 3 arcseconds of diameter. If we take N to include also a factor coming from that added area, this could reduce the number of images we need to work with by a lot. Making the simplest of assumptions, the surface brightness comes from a circumference at that radius with a width of 1 pixel, we can simply apply $A \sim 2\pi R \cdot 0.55$ and compare it to the initial area of 7arcsec^2. For the 70 kpc, this gives roughly $\sim 28\text{arcsec}^2$ pixels for each QSO image, meaning we could need as low as $\text{N} = (5 \cdot 10^5) \cdot (7/28) \sim 1.25 \cdot 10^5$ images.

This is fairly optimistic however, as we would be assuming adjacent pixels and areas are completely independent. The power of stacking comes from independent images lowering the Poissonian noise, but for pixels of the same image they are in fact correlated and therefore the signal to noise ratio would not exactly follow equation 4.3. We expect the contribution of larger areas per image to the surface brightness to help in some way, the result being between the optimist projection of 10^5 and the pessimistic of $5 \cdot 10^5$ images, but we cannot rely on just taking an assumption and will need an independent way to check the final error.

Unfortunately, both the pessimistic or the optimistic projection still require hundreds of thousand quasars and are completely impracticable for J-PLUS. Candidate QSO catalogues have reached millions, but reliably confirmed quasars are harder, some of the last catalogues having more than $3 \cdot 10^5$ [106], but those are still spread over the entire sky and multiple redshifts. J-PLUS does neither cover a large enough footprint nor enough wavelengths, on top of the existence of uncertainties and systematics resulting from stacking images on different filters that could worsen the noise.

For J-PAS in comparison the situation vastly improves. With an expected average depth of $\text{m}_{\text{AB}} \sim 24$:

$$m_{AB} \sim 24 \longrightarrow f = \frac{10^{-0.4(m_{AB}+48.6)}}{3.3\,[\lambda]^2 \cdot 10^{-19}} \cdot 30 \sim 5 \cdot 10^{-17}\text{erg}/(\text{s}\,\text{cm}^2) \qquad (4.6)$$

$$1.4 \cdot 10^{-18}\text{erg}/(\text{s}\,\text{cm}^2) \longrightarrow \sqrt{\text{N}} = \frac{5 \cdot 10^{-17}}{1.4 \cdot 10^{-18}} \longrightarrow \text{N} \sim 1275\ . \qquad (4.7)$$

This ends up being around 300 quasars for the optimistic projection, both much more feasible numbers. It is fairly easier to find quasars too given J-PAS also has a much higher number of filters covering multiple redshifts. Therefore with J-PAS we expect to be able improve on current results of Lyman α diffuse emission fairly easily. This however also means we must absolutely make as sure as possible that our main uncertainty comes from the thermal noise, so we will need to have a lot of care for systematics that could worsen that uncertainty. Given the wide range between cases an independent way to estimate our

dispersion is also extremely important. While we will have to wait for J-PAS, stacking shows promise.

4.4.1 Error control

While our aims are now set, there remains a few issues to still solve. The first about how we will be able to determine our grade of error independently of our previous estimation.

As mentioned, despite its use and overall usefulness, stacking bring its own share of problems that can raise the overall uncertainty of our final result above the Poisson noise we expect. While trying to apply the various workarounds that exist we always want a way to check the final result, to avoid the worst case scenario of finding misleading signals that were only artifacts of the stacking. There exists various way of trying to find the standard deviation of our final stacked image, but one of the biggest advantages of stacking is that it gives us access to statistical methods and thus to one of the most robust ways of estimating our error, resampling.

Resampling is a broad definition of various methods, including the more famous bootstraping and jackknife estimator, used to estimate the uncertainty on the statistical parameters of a distribution, like our collection of images. Resampling consists on shuffling a number of the individual values, in our case single images, with other either estimated or repeated from the same distribution, and then calculating the parameter we are interested in again. The idea is that if one the images is significantly biasing our final value, then we will see a big jump in some of the resampled results, as the parameter of the distribution not having that particular image will change greatly.

If all the individual values behave as expected, then the result of changing a few will only result in a variation within the standard deviation of the distribution. We can repeat this method as many times as variations within the distribution are possible, meaning we can do resampling thousands of times with thousands of individual values. This way we can both catch the offending singular image by looking for the odd value but also get a very robust estimate of the standard deviation of our distribution.

For our stacking, we use resampling through substituting random images with a repeated but also random image, though a jackknife estimator would work equally well. The biggest advantages of this method, shared with other resampling types, is that it gives both the variance while also catching problems with individual images that could otherwise escape our attention. We are working with a collection of roughly 450 very wide images, which we will subdivide in many more as we look for individual objects, so this a great help, especially as the process is almost completely automated. Furthermore, we can estimate the Poisson noise to a certain point from our stacking as mentioned in the previous section, so any value significantly higher is a strong warning that there is an issue, be it a lot of troublesome images or some subtler systematic error that we had not though of.

While these kind of estimators are not perfect, the biggest issue with resampling are systematic effects present in all images, which would be completely ignored as the images simply switch with themselves. However our computation of the PSF will catch all these systematics that are present in all images, as the same stacking that obtains the PSF will also naturally give us this type of ever present systematic, allowing us to take them into account. Thus resampling complements very well our overall approach.

Our method is to use the resampling first with our PSF stack. As we only need some of surroundings of the star (in our case maximum of 50 pixel radius) we will actually have

a lot of adequate stars per image. Indeed, while we are working with hundreds of images, the numbers of stars we have access to for the PSF is in the hundreds of thousands. With this number we can not only obtain a great final result but also do thousands of resamplings to make our results very robust. As mentioned, all ever present systematics including the PSF, will not influence the standard deviation, thus after resampling we will have both the median value of these systematics and the standard deviation of them, all of which will inform our final Quasar stack.

We will also use resampling on this Quasar stack, but the much lower number of QSOs compared to all other objects means we do not expect the method to provide much additional information besides the standard deviation. In contrast, it is likely that the standard deviation of our PSF stack will gives us the variation within these systematic and thus the maximum accuracy we could achieve through stacking. After all, even if we subtract the PSF correctly we expect the variance within the PSF we have found to be higher than the Poisson noise of our final PSF stack. That is because the PSF has minor variation even within the same instrument due to differences in the night sky, very small physical changes of the telescope between the taking 2 different images and even the pixel position[4]. In summary, the resampling in our QSO stack will only give us an estimate of the Poissonian noise within the stack while the error bars in our PSF will show us how well behaved the overall PSF is and if it is feasible to reach high depths with the stacking.

4.4.2 Methods

For the stacking we have made a custom program, one for the stars and one for the quasars. While they share most of the code, there are several differences to to account for both numbers of the object and accuracy.

We start by cross-mapping which of the SDSS quasars would be present on J-PLUS and in which filter would their Lyman α emission fall on, if at all. With the help of various members of Centro de Estudio de Física del Cosmos de Aragon (CEFCA), who man the unit of data management of J-PLUS, we end with a list of 1539 quasars in Data Release 1 for the J0395 band filter spread in roughly 450 images.

We also need a list with the images, in a FITS format, the program needs to access for the QSOs and a catalogue with all the data of J-PLUS objects. Note that this catalogue is not the one associated with each image, as it contains all objects in all the images used in one place and has been especially compiled using the data services given by CEFCA. This is because the act of accessing the catalogue of each image and later replacing it adds up, and it was both more efficient and easier to work with a single big catalogue. The information on the unified catalogue is the same as the dual type catalogues for each image, and uses the r-band (RSDSS) of J-PLUS for object identification, as it is the deeper one. For more information on the specifics of how to access and format of J-PLUS catalogues we defer to the data access manual in `http://www.j-plus.es`.

The program starts by opening the image, and from its header obtain all the necessary data to identify it. The name is used to crossmatch with a tile catalogue, that contains all the parameters pertinent to the image overall, like the zero points needed to calibrate each image. The units of the image are Analog Digital Units (ADU), something that scales with photon counts but needs to be properly calibrated to be turned into proper photometric flux units. As DR1 uses by defect only Stellar Locus regression, we also

[4]The pixel position has in fact to be taken into account for the calibration, so we expect that the PSF will differ in a similar way.

add the extra corrections given Stellar White Dwarf Locii, the additional parameters of which also in the catalogue. With all the information, we then convert ADU into flux units (concretely erg/(scm^{2}Hz) as they are a more straightforward conversion into AB magnitudes) for the whole image.

As we expect few QSO for images we make a cut of a 200x200 pixels with the QSO exactly at the center for the following parts. This also involves interpolating the image so the QSO falls exactly at the center. By waiting until after the cut for the interpolation we get more than enough scale for our purposes and also save a lot of computational time.

Then we identify objects within the cut that are not the quasar and mask them. The mask consists on a number of pixels within a set radius forcefully put to 0, the radius depending on the Kron radius parameter of the catalogue and if it is a point-like or extended object as determined by the CLASS_ STAR parameter, which we will explain in detail later. We tried other methods, included making the mask scale with the brightness of the object, but as the Kron radius already includes an indirect measure of the flux of the object they did not help and were worse in a a number of ways. While at first glance setting the mask to 0 might look like it biases towards lower values, poissonian noise already causes there to be negative ADU values, and in practice masking should only barely affect the image, as our selection includes flags for objects that are too close. An improvement would be to use weight maps and change the weight of those mask to 0, but that is an added layer of complexity not required for our current aims.

Once all this is done, the cut image with the quasar is saved and subsequently stacked with each new cut until the program has gone through all the images, though we are careful to save a copy of each individual cut for both savekeeping and later bootstrapping.

The stacking for the stars is slightly different. First, rather than start with a list of QSOs we simply look at all the objects within the image once we opened it. Of course, we must use the same images we used for QSOs for consistency's sake, though admittedly when using such a large fraction of DR1's image we expect the difference to be minimum. Each object is classified using the CLASS_ STAR parameter given by the SExtractor software [107], used in the photometric reduction of the image. CLASS_ STAR is multilayer feed-forward neural network trained using supervised learning, it estimates the a posteriori probability for a detected object to be a point source or an extended object.

More details on CLASS_ STAR are present in [107], but while not perfect it works well when using large statistics. CLASS_ STAR ranks the probability of an object being a point source or extended on a 0 to 1. We choose a 0.96 cut as it works well while still giving a large amount of objects. Tests using 0.97 and 0.95 did not reveal any large changes, but also not marked improvements. After this first selection, we make a magnitude cut and we take only objects between 18.3 and 20.3 AB magnitude. This is because we want objects bright enough to be properly catalogued and so we can see the PSF clearly, but we do not want too bright objects that would bias the PSF, as most of the QSOs we are working with are faint. Indeed, the average brightness of our QSOs falls near $m_{AB} \sim 20$, which works well enough for our aims.

After those selections, we calibrate and mask the whole image. Unlike with quasars, the number of stars taken by image is big, so it is more computationally efficient to mask every not selected star this way at the beginning, as cuts will likely overlap between them. Of note is we avoid the interpolation, as it both could affect the PSF and it is too computationally expensive. Rather, as mentioned in section 4.2.2 we simply take the 2D profile for each star, as we do not expect any asymmetry from stars and it simplifies

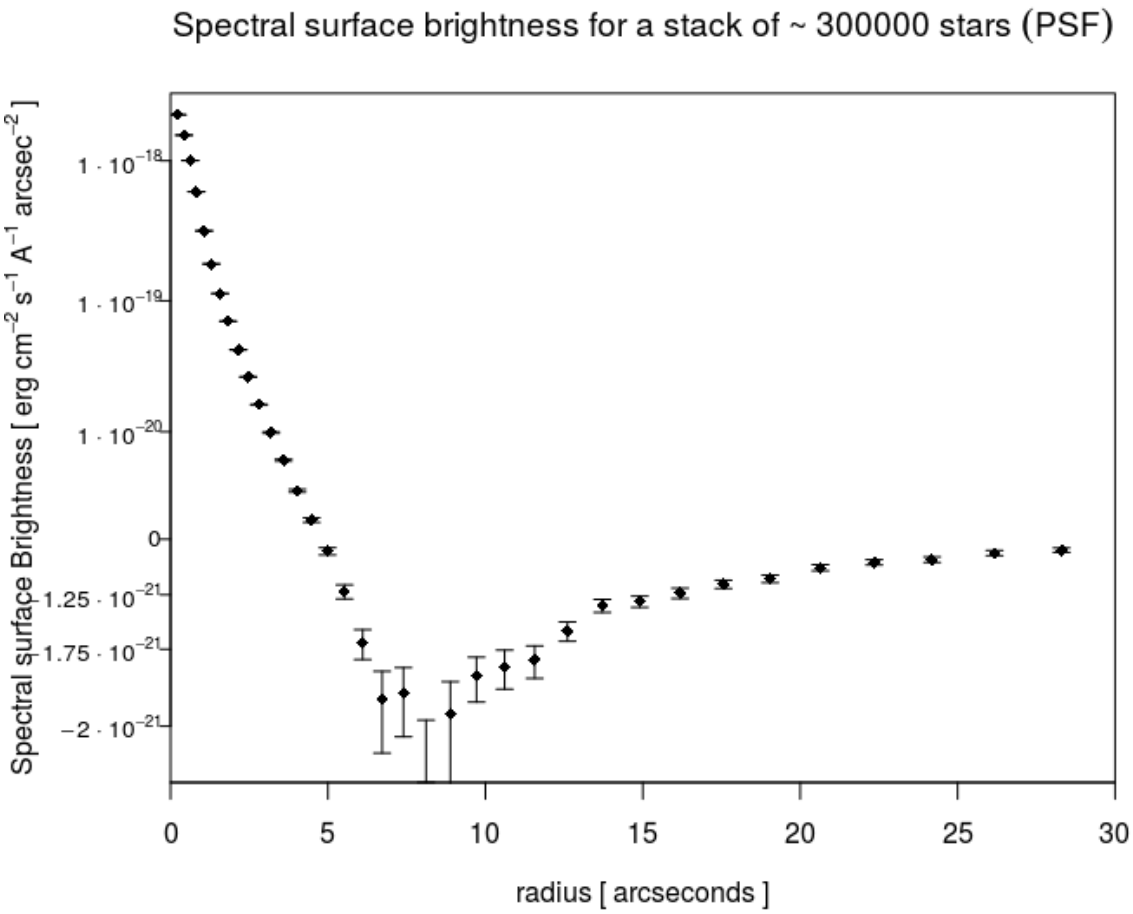

Figure 4.5: Stack of $\sim 300,000$ stars in J-PLUS. The logarithm scale makes the gaussian attributes of the PSF difficult to appreciate, but we can see the error bars are very low, far below the level of flux we want to reach.

things a lot. This also means we do not save individual images from stars, rather just a 2D profile, but using this process also saves a lot of memory.

In total, we found roughly $320,590$ stars in the J0395 filter band that fulfilled all our conditions. We also added a number of flags to the program to make biased selections in case we want to check for systematic issues, an example being one that only took the brightest ($m_{AB} < 18.6$) or faintest ($m_{AB} > 20$) stars for our selection, with $41,249$ and $66,487$ stars respectively for the J0395 band.

4.4.3 Results

We proceed to the stacking. First we start by stacking around $300,000$ stars to obtain a good estimate of the PSF and the level of dispersion we can reach with a great number of objects. The stack with background subtracted is shown in figure 4.5. While hard to appreciate in the current log scale, the PSF follows a smooth gaussian curve. As expected with the great number of stars we found we can get a very good determination of the PSF. Furthermore, the error bars of the star stack are very small, showing the PSF to be very well behaved, the final uncertainty being very close to the one expected from only the Poissonian noise. Indeed, remembering section 4.4 the number of stars

we are using is pretty in between the pessimistic and optimistic projections: error bars $\sim 10^{-21}$erg/(s Åcm^2 arcsec^2) correspond roughly to $\sim 3\cdot10^{-20}$erg/(s cm^2 arcsec^2), which is almost ten times more depth than the signal we are aiming for, $2\cdot10^{-19}$erg/(s cm^2 arcsec^2), fitting with high SNR at that flux level. Overall the PSF seems to have little variance and can be very well determined.

Also interesting perhaps are the negative values at the scales of 5-15 arcseconds. They are very small ($< 10^{-21}$erg/(s Å cm^2 arcsec^2)) and have the highest degree of uncertainty, so we do not assign physical meaning to those negative fluxes, but it could be some kind of systematic effect. Could indicate either the background is overvalued for some reason or also that the PSF has some strange properties at those ranges maybe moving a small portion of the flux that at medium scale to long scales, thus overestimating the background and underestimating emission at $5-15$ arcseconds. Another possibility is the masking having undue effects on closer distances, as masking sets the pixels to 0 which when subtracted the background would bias the pixels towards negative. This effects should be in theory spread evenly, but we might have subestimated the importance of clustering which could bias closer ranges more.

As a safety check we compare the total stack with two subpopulations of stars within it, the brightest and the faintest ones, as seen in figure 4.6, both around $\sim 50,000$ stars. The gaussian nature of the PSF is much more clearly seen once normalised, but can also be appreciated in the surface brightness case. The negative values remain for the faint stars, though the new scaling makes it hard to see for the graph in erg/(s Å cm^2 arcsec^2), showing how small the deviation is in fact.

Even then, a more interesting part is that the negative values of the PSF are more relevant for fainter stars while they are absent on brighter ones, as can be easily seen in the normalised case. In part this is expected, because the background will not depend on the star but for the stack of brighter stars the PSF will also naturally be brighter, thus a smaller chance of negative results once the background is subtracted. Overall, that the effect is gone or lessened with higher magnitudes is helpful but does not help differentiate between any of its possible origins.

We do try to go for another safety check using an entirely new filter. The r broadband is considered the standard in J-PLUS, as it has the best depth (see Table 4.1) and also corresponds to the same r-band as in SDSS, which makes double-checking calibration issues or weird objects much easier. Taking into account the increased depth of the band we can we go for a slightly different magnitude spread in our selection with $19.3 < m_{AB} < 21.3$, otherwise following the exact same selection process for stars as in the J0395 filter. The selection ends up with $316,615$ stars, only slightly less than J0395

We show the results of the stack in figure 4.7. Having only slightly less stars than the stack with the J0395 filter the PSF is similarly well behaved, though the negative values seem more prominent relative to the error bars. This seems to confirm the relation with the brightness of the source, as the median brightness of this stack is lower, though again makes hard to guess the proper origin. It however looks undeniable that there is a systematic effect making the medium ranges a bit smaller or the background brighter

However, an advantage of stacking is that we were able to find this systematic effect directly on our PSF. As the effect seems to depend on the magnitude, we expect our quasar stack to have the systematic on a similar degree as same magnitude stars, if probably with much higher dispersion due to the much lower number of quasars.

Finishing our determination of the PSF, we can move on the quasars. We use a cross match list to find $\sim 1,550$ quasars both on SDSS and J-PLUS catalogues. We showcase

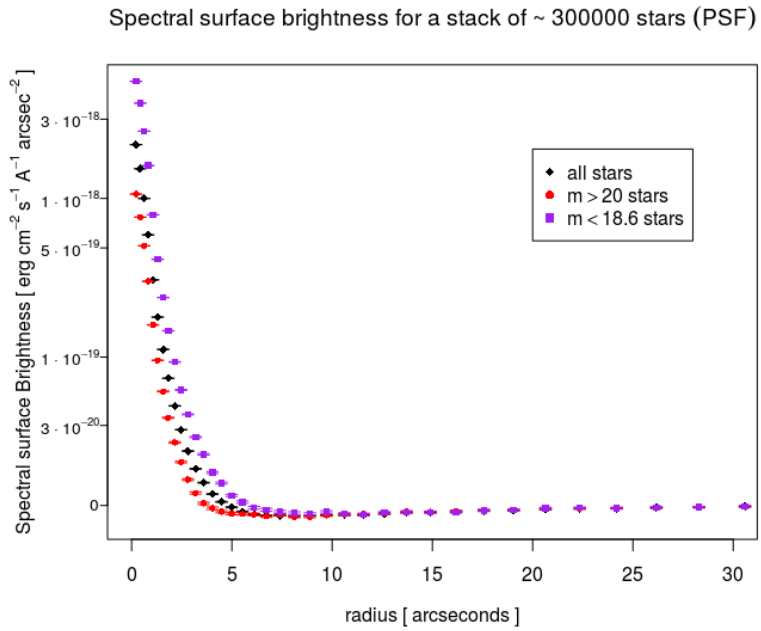

(a) Comparison between stacks of stars of differing brightness

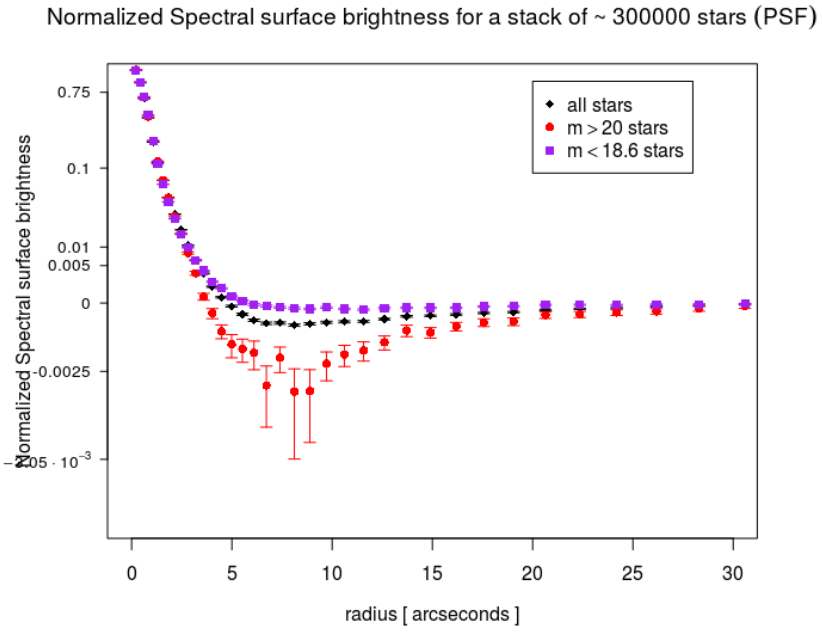

(b) Comparison between stacks of stars normalised

Figure 4.6: Comparison of the stack of $\sim$ 300.000 stars with smaller subsets of $\sim$ 40.000 and $\sim$ 66.000 stars with $18.3 < m < 18.6$ and $20 < m < 20.3$ respectively. Above is the plot in astronomic units, while below we have normalized their surface brightness by their integrated flux within 10 arcseconds. The gausssian nature of the PSF can be very easily appreciated.

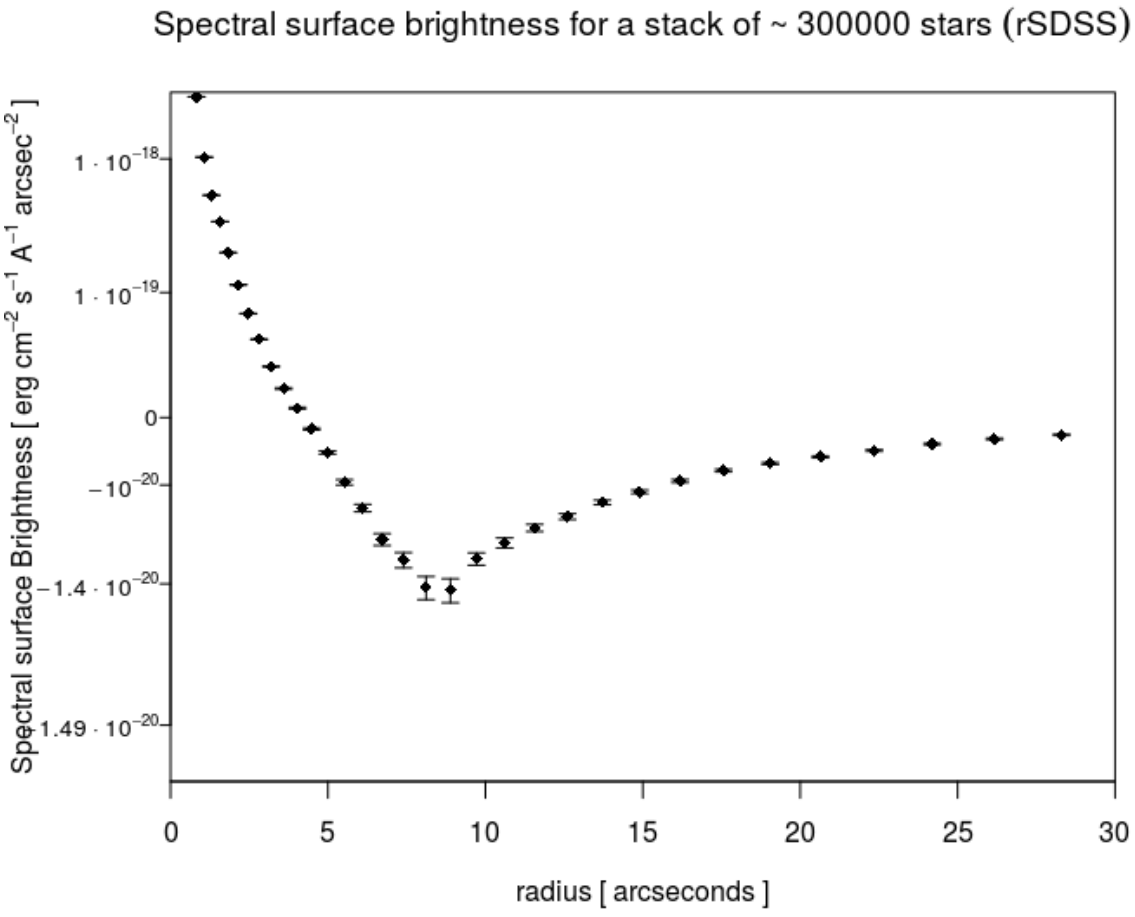

Figure 4.7: Stack of $\sim 300,000$ stars in J-PLUS for the r band. We see a very similar case as in the PSF of J0395, though the negative values are slightly more prominent. Note that as the units used on the y axis contain information of the wavelength, they are not directly comparable to previous graphs, though the relative changes within the flux are.

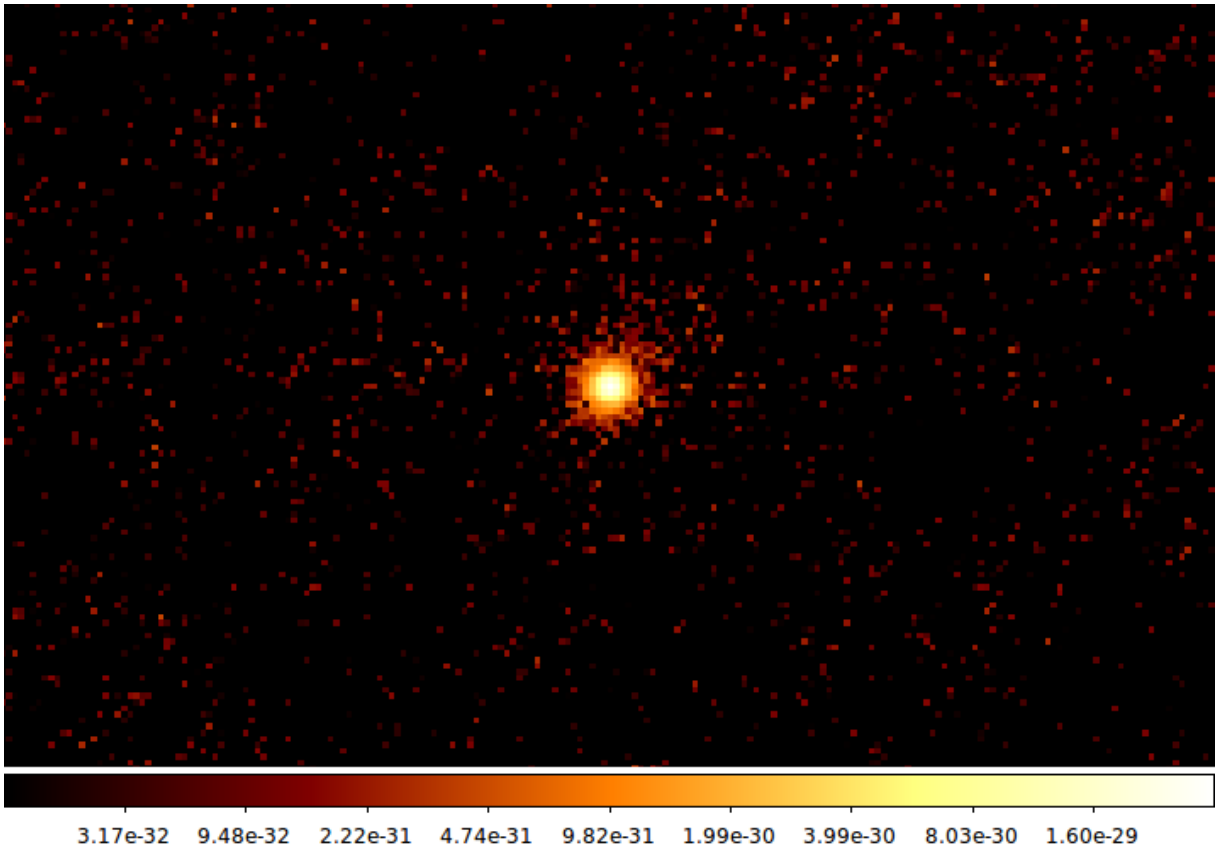

Figure 4.8: Stack of 1,550 QSOs in J-PLUS. As expected, we are unable to see any extended emission, and even some assymetry still remains. Units are erg/(scm^{2}Hz).

the resulting stacked QSO image in figure 4.8. As expected, it is extremely hard to see any kind of extended emission. Even the PSF is very faint at single glance. In this image we have not yet subtracted the background for clarity, nor changed the units yet, but the relative differences are clear to see.

A more useful comparison of the surface brightness of the quasar stack with the PSF coming from the star stack is shown in figure 4.9, with the background subtracted for both spectral surface brightness units and a normalised case, same as before. All extended emission in the quasar stack seems to correspond to the PSF, with any possible slight excess more than compensated by the large error bars.

The lack of signal was expected in J-PLUS, taking into account that the stack is too small to be accurate for this kind surface brightness. Overall, on the flux we see a variability of roughly $\sim 5 \cdot 10^{-21}$erg/(s cm^2 Å, arcsec^2), so it would roughly correspond to $1.5 \cdot 10^{-19}$erg/(s cm^2 arcsec^2), making very hard to discern the $2 \cdot 10^{-19}$erg/(s cm^2 arcsec^2) signal. It is however encouraging that the degree of the undervalue systematic seems to be almost exactly the same for PSF, as expected and showing that whatever origin we can account for it.

The large error bars themselves come from the difference in number of objects stacked. To compare with figure 4.2 we make figure 4.10, where again we have approximated the integration of the filter by multiplying for 30. This suits our purposes, as we only want to check the order of magnitude we reach for the error bars in each of the cases. With N in the star stack reaching $300,000$, it is on the same level as the projection of images we needed to reach the 10^{-19}erg/(s cm^2 arcsec^2), and indeed we can see that on the star stack we do reach that level of flux, even if for stars we do not expect any signal. For the number of quasars we stacked, we expect error bars roughly 15-20 times bigger than for the star case, which is also similar to what we get.

Overall, despite the issues with possible uncertainties, the levels of flux reached for both quasar and star stacks are satisfactory and fit our expectations. In particular the error bars are very small for the star case, so this means PSF can be obtained very reliably, and despite the larger dispersion the quasar stack also acts like we expected. In J-PAS, following these same methods, the PSF can be computed well enough so that it does not interfere with the signal of the expected extended emission. Given the systematic effect we see also seems to depend on the magnitude of the central object, we expect the increased depth of J-PAS will also help with more accurate luminosities and improved background accuracy, though even in the worst case it is also shown that the PSF replicatesthe systematic so we can subtract it anyway.

4.5 Discussion and future prospects:

We have stacked up to 1,550 QSOs and more than 300,000 stars in J-PLUS. As expected, with only 1,550 QSOs is not enough to distinguish any kind of diffuse emission beyond the PSF. The expected value of $2 \cdot 10^{-19}$erg/(s cm^2 arcsec^2) is roughly the same size of the error bars of our quasar stack, making saying anything about the signal we seek impossible.

It is also remarkable that we appear to have found some sort of systematic within our stack. Star and quasars stacks share similar magnitudes and a similar undervalue, but using biased star selections we found the systematic appaers to be smaller for higher magnitude stars despite a lower number of stacks, but also not depend on the filter. This undervalue could have various possible origins. One is that the mask we use biases the flux we see towards lower values, and due to clustering this is felt closer to the star. Another

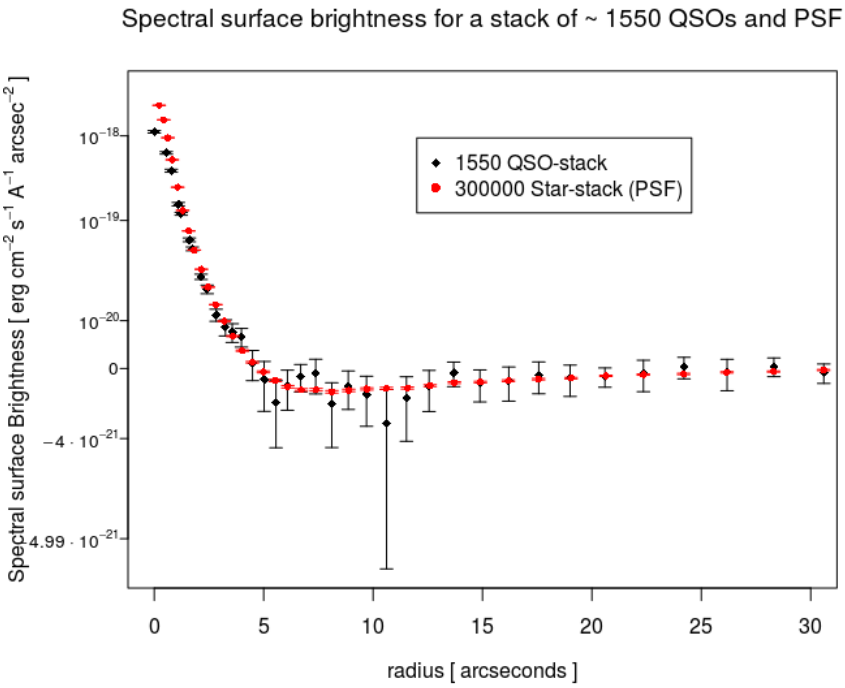

(a) Comparison of QSO and star stack

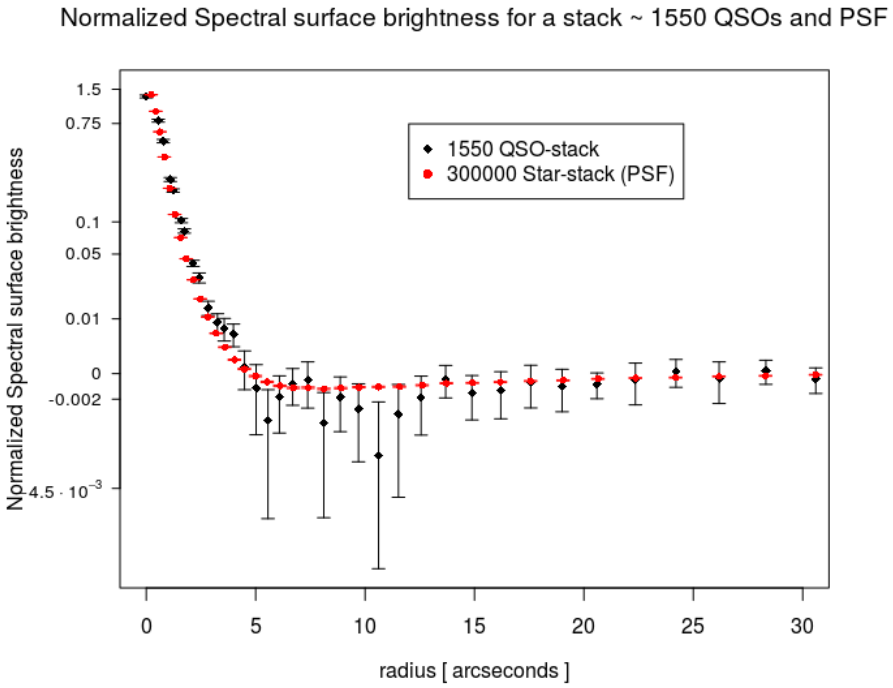

(b) Comparison of both stacks normalised

Figure 4.9: Comparison of the extended emission of the stack of 1,550 QSOs with a stack of 300,000 stars in the same filter. The error bars of the stars are remarkably low, showing that the stack in itself is effective and we find the PSF with high accuracy, while the systematic we saw before is also matched by the quasars. Note that the background has been subtracted from both in this graph.

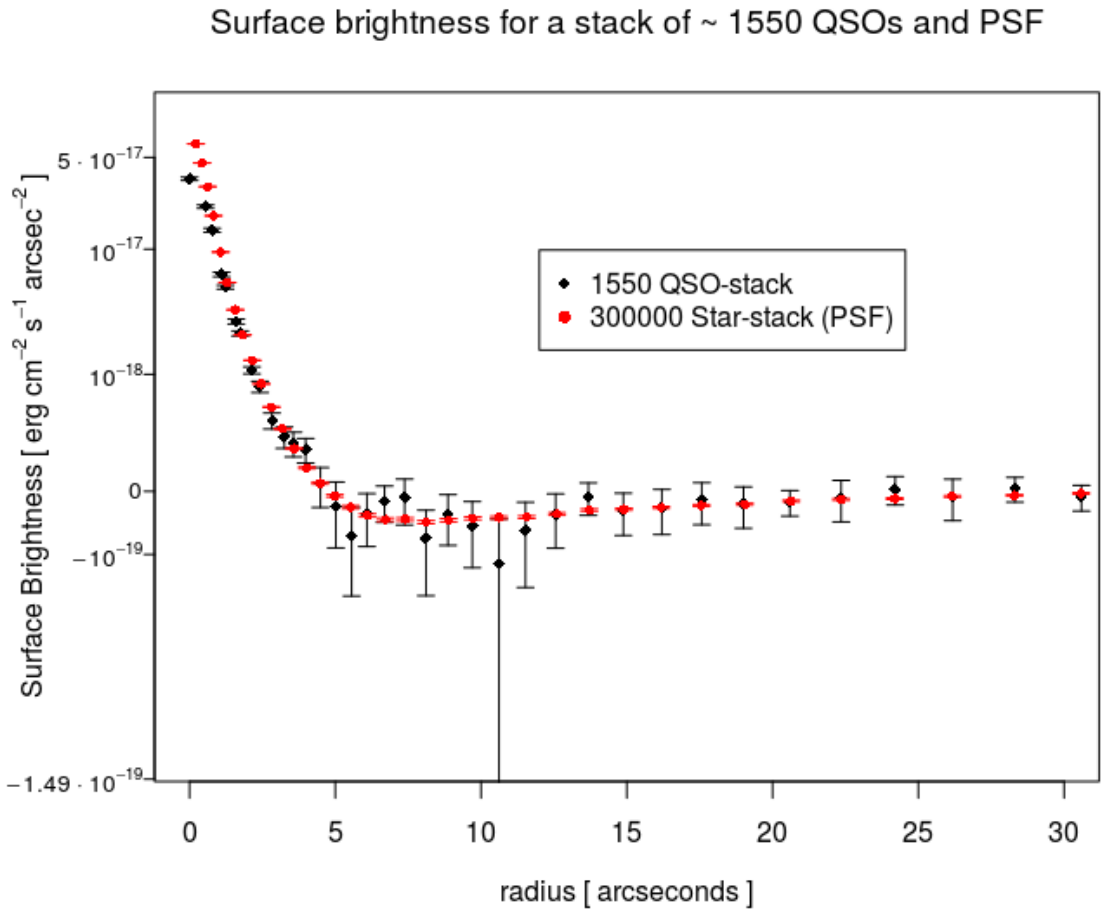

Figure 4.10: Stack of 1,550 QSOs in J-PLUS compared with the star stack of 300,000 stars using the same units as Figure 4.2. We again remark that this is a result of an approximation, and so its purpose is orientative, to show the depths were reaching with each of the stacks.

is that is simply a peculiarity of the PSF in the bigger scales. The last is that we are overvaluing the background in some unknown way.

While the systematic is worrying the PSF reproduces it, and so we can eventually subtract it from our quasar stack. Overall, as the systematic effect seems to become less important with higher luminosities too, we also expect that the improved depth of J-PAS will help, at least ensuring more accurate background. Rather, the dispersion is the main issue for the quasar stack, due to the low number of quasars compared to images. This is still as expected, as from the beginning J-PLUS did not have the limiting magnitudes to reach the depths the signal we are looking at is.

The error bars in the star stack in comparison are very well behaved. It is partly as expected, as it is the result of a selection of stars within certain magnitude bins and that do not trigger any other flag. Nonetheless the depth we reach and the small size of the error bars even there fit with our expectations of Poissonian noise, which means the dispersion due to the PSF itself is negligible for the magnitudes we are interested in. This is fantastic, as it means we can stack without major worries.

Even more encouraging is that for the star stack we reached depths even further that the the signal of $10^{-19}\mathrm{erg}/(\mathrm{s\,cm^2\,arcsec^2})$ we are looking for. Because our number of stars fit the projection we made for J-PLUS to reach those depths, this means that as long as J-PAS maintains its supposed characteristics our projection for J-PAS is similarly valid. Stacking the number of QSOs we have in J-PLUS ($\sim 1,550$) in J-PAS should be more than enough to reach the depths the signal we are looking for. Overall the PSFs obtained are all an excellent showing of the power of stacking, and give us a lot of hope for J-PAS.

In conclusion, while with J-PLUS we are unable to improve on the extended Lyman α emission of quasars, we have showcased that our methods to both achieve lower fluxes and obtain the PSF with stacking work. Given the many similarities between J-PLUS and J-PAS we expect applying our current methods to the later should work smoothly, even recycling parts of the programs used, and would finally allow us to easily reach the flux levels we wanted and at least improve bounds on Lyman α diffuse emission around quasars.

CHAPTER 5

SUMMARY AND CONCLUSIONS

This thesis main work is focused on looking for observational signatures of the most extreme of Black holes, in both big and small mass ranges. A main portion of these extremes would come from primordial black holes (PBHs), and would give the very interesting possibility of being the majority or all of the dark matter (DM).

In Chapter 2 we have explored the idea of PBHs being the dark matter. We have summarized their main formation path, where primordial quantum fluctuations would be enhanced during inflation to the point where they would naturally form black holes [42]. The exponential expansion of inflation would mean that the black hole would not form immediately, but rather have to wait until the fluctuations cross the horizon again. The PBH would form with a mass roughly the one in the horizon when that happens, resulting in PBHs being able to form with almost any mass. This opens a lot of windows where PBHs escape the current MACHO constraints.

We have then analyzed the further constraints that have emerged since, and various methods. The biggest contribution comes from microlensing, which looks for small fluctuations in a star's brightness as a compact object crosses our line of sight and their gravitational force affects the light beams slightly deflecting them. While helping in creating constraints of more than 10 orders of magnitude in mass (see Figure 2.1), microlensing seems to have reached its limit as finite source effects make it extremely hard to constraint lighter masses [56]. PBH evaporation is in a similar state. Hawking radiation is incredibly important for low mass PBHs, assuring us that any PBH smaller than 10^{15} grams would have evaporated by today, and giving strong bounds on 10^{16-17} grams PBHs through the expected increase in extra-galactic background light we should see. But larger masses are almost completely unaffected by it, and its dependence on spin means the weaker constrains are uncertain. Finally, gravitational waves (GW) are incredibly promising, but current LIGO and Virgo sensitivity is only capable of detecting events of $1 - 100\,\mathrm{M}_\odot$ mergers and closer than $z \sim 1$. While those are very valuable for confirming PBHs, a lot of constraints for the $1 - 100\,\mathrm{M}_\odot$ mass range already exist forcing them to be below even a small part of the DM. There is hope that next generation detectors, like LISA might be able to detect the stochastic GW background that the formation of PBHs as DM would cause [70], but those are at least 15 years away and subject to the uncertainty of formation models.

Of importance also is remembering that almost all the constraints assume that PBHs will come from a single mass rather than an extended mass distribution. As taking into

account the later is extremely complex [34] and we expect a peak in the mass distribution, this a good approximation, but one that has to be taken with caution for fringe cases. Similarly, the possibility that PBHs could be born with a greater degree of clustering than the standard matter distribution exists, and is a prominent part of more exotic formation models of PBHs. This degree of clustering changes all known constraints and also creates new ones.

Throughout this, a known window remains where PBH could be the majority of the DM, centered around $10^{-14}\,M_\odot$. The upper end of this window, $10^{-12}\,M_\odot$ is particularly interesting, as they are big enough they could be probed by their interactions with common objects, like stars. They are massive enough that they would accrete a solar mass star if they fall to their core, even faster if the core was that of an ultradense neutron star. There was previous work on these ideas [40, 41], but their constraints suffer from uncertainties in the environments they work with. On Chapter 3 we improve on this work through our own model, set in the early universe.

We work around $z \sim 20$, with extremely poor metal stars but just after the formation of the very first stars and in a more common $10^7\,M_\odot$ DM halo. In those high redshifts the DM density of the universe is very high and standard velocity dispersion fairly low, so if they were the DM then PBHs of $10^{-12}\,M_\odot$ would be interacting a lot with other objects. As a proto-star forms from a gas cloud, the adiabatic contraction that accompanies it would end up bounding a lot of these PBHs to the just born star. These PBHs would have random orbits, and there is a chance some cross the star outright. Assuming the star has a mass lower than $1\,M_\odot$ and so survives for a long time then the PBH could go through this orbit to this day.

Despite their weird properties, the PBH would still be affected by dynamical friction. The collisionless variant is purely gravitational [74], while gaseous friction depends more on the medium its crossing [82, 83]. In this thesis we study both and compare the results for this particular case. While gaseous friction is slightly stronger, both are very weak and the difference is negligible for statistical results. Despite the weakness of the friction, as the orbit of the PBH starts being affected then it will drop closer to the center of the star, meaning shorter orbits, higher density and stronger friction. We have studied carefully the evolution of the bound orbits, and we have determined a starting critical eccentricity for each radius. Above this critical eccentricty, we expect the PBH to fall to the core of the star within 10^{10} years.

Despite being so small, once it falls to the core the PBH has no problem accreting the entire star within 10^9 years. We however also take into account that the galaxy could interfere with the process, as because of the high eccentricity some of the orbits could be extremely long closing even to the parsec. Without need for third objects, tidal forces of the galaxy alone would be enough to perturb these orbits, so we use them to set a maximum radius beyond which the orbits will not contribute to the PBH capture rate. We then integrate all the orbits with high enough eccentricity up to this maximum radius, and we parametrize the result of the numeric integral with a new dimensionless variable we call Ξ.

Knowing this, we can relate this whole process with the galaxy dark matter density and velocity dispersion to estimate the average number of stars who will suffer this fate. Further, Ξ contains all the information about the orbits, but not about the Dark matter density. This means that with a few caveats Ξ can be used for computing this process for any redshift, we just need to shift the DM density and velocity dispersion accordingly, as can be seen in equation 3.20. We provide a table with all the values of Ξ we computed

for a variety of r_{max} and stellar models in table 3.3.

Working with $z \sim 20$ as we started gives surprising results. If $10^{-12}\,M_\odot$ PBHs were all the DM we would expect extremely few low mass stars to survive in the center of the galaxy. As can be seen in figure 3.9, the average lowers with distance from the centers, but even at $0.1R_{\text{Virial}}$ we would expect between 10 to 1 % of the stars to end as black holes. If PBHs of $10^{-12}\,M_\odot$ are all the dark matter, not only could they help explain the lack of detections of low mass extremely metal poor stars, but also we would expect there to be many sub solar mass black holes, but still big enough for us to detect, awaiting to be discovered.

While distinguishing sub solar mass black holes as being from $10^{-12}\,M_\odot$ PBHs will be hard, just that we expect their existence could help constrain that window as being all of the dark matter. In contrast, the detection of subsolar mass black holes would definitely prove PBHs existence, but our mechanism is one of the few ways in which those sub solar mass black holes could exist and they would still explain all the dark mater.

Having worked this window, we moved on to the other extreme in Chapter 4. SMBHs despite being more familiar are still full of uncertainties. One in particular is the emission of Lyman α by QSOs, especially the creation of giant nebulae of such radiation. This diffuse emission could be powered by different ways, but recombination cascades should be the most common, allowing us to relate directly the brightness of the nebula with the density of ionized Hydrogen.

The brightest quasars seem to have Lyman α diffuse emission almost invariably [90], but we can not detect them for fainter ones. As one of the other uncertainties of quasars are also their contribution to the reionization of the universe, and Lyman α emission is one of the most important sources helping that contribution. On top of that of nebulae also help us understand the depth of the process through the ionized density, making studying these Lyman α nebulae a fairly relevant matter.

A way to solve this could be through stacking, but earlier work presents differing results [94,95]. Stacking itself is a a method that relies on joining images of the same type of objects. By taking advantage that Poissonian noise of each image is independent but the rest of the signal is not, the signal to noise ratio improves that of the original image by $\sqrt{N}$, N being the number of images used. Stacking is very well suited to working with diffuse emission, and in a lot of ways it is one of the very few way to work with such faint radiation. Stacking also carries its own share of issues, particularly that the Point Spread Function (PSF) of the images will be similarly magnified, and that systematic uncertainties will remain.

A survey that could make very good use of stacking is J-PAS and its predecessor J-PLUS. A very wide survey with a fairly big footprint, but also importantly a good number of narrowband filters for J-PLUS, and an incredibly good number of filters for J-PAS. Filter bands are important because the Lyman α emission of the QSOs is redshifted, meaning even if we know a lot of quasars we cannot do anything if their emission is not covered by a filter. While we expect only J-PAS to have enough depth to improve the current results on Lyman α emission, J-PLUS shares many of its characteristics so we can use it as a proof of concept to check for the PSF and other systematic issues.

We do that, and the results are satisfactory. While the QSO stacked image does not reach enough depth to appreciate any kind of extended emission in figure 4.8, and we have an overall undervalue that appears to be a systematic, the former was something expected and the later can be accounted for as is also present in the PSF. In comparison the star stack does give the PSF very reliably and with very low uncertainty in figure 4.5,

one that matches the one we would need for our computation with QSOs.

Indeed, in Figure 4.10 we show that the start stack reaches the flux level the Lyman α signal should be, and with a number that matches our projection for J-PLUS. Given that our projection for J-PAS is we would need even less QSO images than the ones we have used for J-PLUS, just applying this same chapter to J-PAS with no changes should already give at least improved results in the Lyman α surface brightness surrounding quasars. Once J-PAS starts releasing data all, we are confident it should be easy to apply all the previous work done in this thesis.

Overall, our aim in this thesis has been to seek possible observational consequences for what normally are very theoretical and abstract objects, both extremes of the mass range for black holes. For PBHs we achieved a surprising observational result that could help either confirm or deny their existence as the dark matter, while for quasars we have done a proof of concept and all the previous work needed so that when future surveys are ready we can improve on current observational results of Lyman α nebulae.

To conclude, there a number of exciting prospect in the future:

J-PAS: The most immediate, J-PAS is expected to start this same year, and to begin releasing data in another year or two. Our expectations are that with as maybe as low as $\sim 1,000$ quasars it could be enough to improve current values of extended Lyman α emission. Considering our proof of concept stack alone had more than 1,500 QSOs, the expectation would be to be able to improve upon them by a lot. With a lot of the work already done in J-PLUS and familiarity with its systematics, we expect the transition of the work to J-PAS should be smooth.

LIGO: GWs are one of the most novel detectors we have, and while its novelty means it still does not reach all the ranges we want, it also means each new discovery improves our understanding by leaps and bounds. Further detection of BHs in the supposed mass gap could make stellar origin only black holes models unable to explain mergers for example. While unlikely, the discovery of subsolar mass black hole merger would be the final proof of the existence of PBHs too. Even simple merger events with nothing out of the oridinary improves our statistics and can help set out constraints.

LISA: While LIGO is already a big success, LISA is a realistic hope to discover PBHs. The improved detection already makes it so it could catch a subsolar merger more easily, but LISA can also prove or disprove the existence of a stochastic GW background. While in this thesis our focus has been on $10^{-12}\,\mathrm{M}_\odot$ PBHs, which if produced the standard way should leave a similar bakcground for LISA to detect, other low mass PBHs are also expected to contribute this background if they exist, meaning constraints will improve over all the mas ranges. Overall LISA should resolve a lot of the current doubts within the community.

Appendices

APPENDIX A

CHANGE OF VARIABLES

With the dynamical friction, we can find the lost energy. However, just computing the change in the speed and from it the energy will not work: the potential of the star acts on the velocity of the PBH during its crossing, meaning the change in velocity would be increased by the change in gravitational potential the same way the velocity of the PBH is. Thus, if computed this way, the change in energy would depend on where we modify the PBH's speed, which is obviously false. By computing the energy loss directly we can avoid this conundrum. We can also make a change of variables so we integrate for the radius rather than time, simplifying the problem.

$$\Delta u = \int_{t1}^{t2} a_{df}\, v dt = 2\int_{r_{min}}^{R_*} a_{df}\, v dr \frac{dt}{dr}$$

Where $r_m in$ is the smallest radius the PBH will reach during its orbit. As the Keplerian orbit breaks down when the PBH enters the star, as the potential becomes non-linear inside the star, an alternative way to obtain the pericenter is needed. It can be found both through energy and angular momentum, but we focus on the later.

$$\sin\theta = \frac{l}{vr} \longrightarrow \sin\left(\frac{\pi}{2}\right) = \frac{l}{vr_{min}} \longrightarrow l = r_{min}\, v(r_{min})$$

Returning to the energy:

$$\frac{dt}{dr} = \frac{dt}{d\lambda}\frac{d\lambda}{dr} = \frac{1}{v}\frac{1}{\cos\theta} = \frac{1}{v}\frac{1}{\sqrt{1-\frac{l^2}{r^2\, v^2}}}$$

$$\Delta u = 2\int_{r_{min}}^{R_*} a_{df}\, v \frac{1}{\sqrt{1-\frac{l^2}{r^2\, v^2}}}\frac{1}{v} dr = 2\int_{r_{min}}^{R_*} \frac{a_{df}}{\sqrt{1-\frac{l^2}{r^2\, v^2}}} dr$$

By assuming the modification to the angular momentum of a single pass is negligible, we have $l = r_{min} v(r_{min})$, as only r_{max} and r_{min} will be completely perpendicular to the trajectory (the radial velocity will be 0). However, this means that the integral above will diverge for $r \to r_{min}$, which is its lower limit. A change of variables is required if we want to compute it. Recovering the θ we used for r_{min}:

$$\sin\theta = \frac{l}{vr} \longrightarrow r = \frac{l}{v(r)\sin\theta}, \quad \theta = \arcsin\left(\frac{l}{v(r)r}\right) \longrightarrow \cos\theta(r_{min}) = 0$$

$$\left(\frac{-\mathrm{l}}{\mathrm{v(r)^2 r^2}}\right)\left(\mathrm{v(r)} + \mathrm{r}\frac{\mathrm{d\,v}}{\mathrm{dr}}\right)\mathrm{dr} = \cos\theta \mathrm{d}\theta$$

$$\Delta \mathrm{u} = 2\int_{\theta(\mathrm{r_{min}})}^{\theta(\mathrm{R_*})} \frac{\cos\theta \mathrm{a_{df}}(\theta)}{\cos\theta}\left(-\frac{\mathrm{v^2 r^2}}{\mathrm{l}}\right)\left(\mathrm{r}\frac{\mathrm{d\,v}}{\mathrm{dr}} + \mathrm{v}(\theta)\right)^{-1}\mathrm{d}\theta$$

$$\Delta \mathrm{u} = -2\int_{\frac{\pi}{2}}^{\theta(\mathrm{R_*})} \frac{\mathrm{a_{df}}(\theta)\,\mathrm{l}}{\sin^2(\theta)}\left(\frac{\mathrm{l}}{\mathrm{v}(\theta)\sin\theta}\frac{\mathrm{d\,v}}{\mathrm{dr}}(\theta) + \mathrm{v}(\theta)\right)^{-1}\mathrm{d}\theta$$

Which despite looking more complex, it is not particularly harder to compute. r_{min} can be found iteratively for each energy and angular momentum, and we can compute every other variable from the stellar model.

APPENDIX B

FALLING INTO THE CORE OF THE STAR

It is straightforward to see that once the PBH orbits within the star, it will eventually settle into the core even with the most conservative approximations:

$$\mathrm{a_{target}} \sim 10,000\ \mathrm{km} \longrightarrow \mathrm{u_{target}} = \frac{-\mathrm{GM}}{2\mathrm{a}} \sim -7 \cdot 10^{6} \mathrm{km}^2/\mathrm{s}^2$$

$$\mathrm{u_{loss}} > 10^{-5} \mathrm{km}^2/\mathrm{s}^2 \cdot \mathrm{orbit}.$$

A look at both Figures 3.4 and 3.3 shows the energy loss is if anything and underestimation. Even keeping it like this:

$$\mathrm{T_{orbit}} = 2\pi\sqrt{\frac{\mathrm{a}^3}{\mathrm{GM}}} \sim 2\pi\sqrt{\frac{(500,000\mathrm{km})^3}{\mathrm{G\,M_{\odot}}}} \approx 2 \cdot 10^{-4}\mathrm{yrs}$$

$$\frac{\mathrm{u_{target}}}{\mathrm{u_{loss}}} = 7 \cdot 10^{11}\mathrm{orbits} \longrightarrow \mathrm{t} = 7 \cdot 10^{11} \cdot 2 \cdot 10^{-4} \sim 10^{8}\,\mathrm{yrs}.$$

Where we have approximated the whole of the mass being in the core (which is overall conservative, reducing the orbital period but affecting the e_{target} even more), taken a much lower limit of the e_{loss} (which should increase even more by the core) and used a single orbital period from when the PBH has just been captured (while we expect the orbital period would get smaller as it gets closer to the core).

CHAPTER 6

BIBLIOGRAPHY

[1] S. Hawking, "Gravitationally collapsed objects of very low mass," *Monthly Notices of the Royal Astronomical Society*, vol. 152, p. 75, Jan. 1971.

[2] B. J. Carr and S. W. Hawking, "Black holes in the early Universe," *Monthly Notices of the Royal Astronomical Society*, vol. 168, pp. 399–416, Aug. 1974.

[3] R Core Team, *R: A Language and Environment for Statistical Computing*. R Foundation for Statistical Computing, Vienna, Austria, 2021.

[4] A. Friedmann, "Über die Krümmung des Raumes," *Zeitschrift fur Physik*, vol. 10, pp. 377–386, Jan. 1922.

[5] G. Lemaître, "Un Univers homogène de masse constante et de rayon croissant rendant compte de la vitesse radiale des nébuleuses extra-galactiques," *Annales de la Société Scientifique de Bruxelles*, vol. 47, pp. 49–59, Jan. 1927.

[6] E. Hubble, "A Relation between Distance and Radial Velocity among Extra-Galactic Nebulae," *Proceedings of the National Academy of Science*, vol. 15, pp. 168–173, Mar. 1929.

[7] P. J. E. Peebles, "Primeval helium abundance and the primeval fireball," *Phys. Rev. Lett.*, vol. 16, pp. 410–413, Mar 1966.

[8] A. G. Riess *et al.*, "Observational Evidence from Supernovae for an Accelerating Universe and a Cosmological Constant," *The Astrophysical Journal*, vol. 116, pp. 1009–1038, Sept. 1998.

[9] R. Peccei and H. Quinn, "Cp conservation in the presence of pseudoparticles," *Physical Review Letters - PHYS REV LETT*, vol. 38, pp. 1440–1443, 06 1977.

[10] S. Weinberg, "A new light boson?," *Phys. Rev. Lett.*, vol. 40, pp. 223–226, Jan. 1978.

[11] F. Wilczek, "Problem of strong P and T invariance in the presence of instantons," *Phys. Rev. Lett*, vol. 40, pp. 279–282, Jan. 1978.

[12] L. Di Luzio, M. Giannotti, E. Nardi, and L. Visinelli, "The landscape of QCD axion models," *Physics Reports*, vol. 870, pp. 1–117, July 2020.

[13] F. Chadha-Day, J. Ellis, and D. J. E. Marsh, "Axion Dark Matter: What is it and Why Now?," *arXiv e-prints*, p. arXiv:2105.01406, May 2021.

[14] J. Hart *et al.*, "The Telescope System of the MACHO Program," *Publications of the Astronomical Society of the Pacific*, vol. 108, p. 220, Feb. 1996.

[15] C. Alcock *et al.*, "The MACHO Project: Microlensing Results from 5.7 Years of Large Magellanic Cloud Observations," *The Astrophysical Journal*, vol. 542, pp. 281–307, Oct. 2000.

[16] K. Schwarzschild, "On the gravitational field of a sphere of incompressible fluid according to Einstein's theory," *arXiv e-prints*, p. physics/9912033, Dec. 1999.

[17] B. Balick and R. L. Brown, "Intense sub-arcsecond structure in the galactic center.," *The Astrophysical Journal*, vol. 194, pp. 265–270, Dec. 1974.

[18] R. Genzel, D. Hollenbach, and C. H. Townes, "The nucleus of our Galaxy," *Reports on Progress in Physics*, vol. 57, pp. 417–479, May 1994.

[19] B. P. Abbott *et al.*, "Observation of Gravitational Waves from a Binary Black Hole Merger," *Phys. Rev. Lett*, vol. 116, p. 061102, Feb. 2016.

[20] R. C. Tolman, "Static solutions of einstein's field equations for spheres of fluid," *Phys. Rev.*, vol. 55, pp. 364–373, Feb 1939.

[21] J. R. Oppenheimer and G. M. Volkoff, "On massive neutron cores," *Phys. Rev.*, vol. 55, pp. 374–381, Feb 1939.

[22] R. J. Foley, D. A. Coulter, C. D. Kilpatrick, A. L. Piro, E. Ramirez-Ruiz, and J. Schwab, "Updated parameter estimates for GW190425 using astrophysical arguments and implications for the electromagnetic counterpart," *Monthly Notices of the Royal Astronomical Society*, vol. 494, pp. 190–198, May 2020.

[23] R. H. Cyburt, B. D. Fields, K. A. Olive, and T.-H. Yeh, "Big bang nucleosynthesis: Present status," *Reviews of Modern Physics*, vol. 88, p. 015004, Jan. 2016.

[24] S. W. Hawking, "Black hole explosions?," *Nature*, vol. 248, pp. 30–31, Mar. 1974.

[25] F. Wang *et al.*, "A Luminous Quasar at Redshift 7.642," *The Astrophysical Journal*, vol. 907, p. L1, Jan. 2021.

[26] F. Pacucci, M. Volonteri, and A. Ferrara, "The growth efficiency of high-redshift black holes," *Monthly Notices of the Royal Astronomical Society*, vol. 452, pp. 1922–1933, Sept. 2015.

[27] H. Deng, J. Garriga, and A. Vilenkin, "Primordial black hole and wormhole formation by domain walls," *Journal of Cosmology and Astroparticle Physics*, vol. 2017, p. 050, Apr. 2017.

[28] K. Hashino, S. Kanemura, and T. Takahashi, "Primordial black holes as a probe of strongly first-order electroweak phase transition," *arXiv e-prints*, p. arXiv:2111.13099, Nov. 2021.

[29] W. E. East and L. Lehner, "Fate of a neutron star with an endoparasitic black hole and implications for dark matter," *Phys. Rev. D*, vol. 100, p. 124026, Dec. 2019.

[30] A. Abramovici, W. E. Althouse, R. W. P. Drever, Y. Gursel, S. Kawamura, F. J. Raab, D. Shoemaker, L. Sievers, R. E. Spero, K. S. Thorne, R. E. Vogt, R. Weiss, S. E. Whitcomb, and M. E. Zucker, "LIGO: The Laser Interferometer Gravitational-Wave Observatory," *Science*, vol. 256, pp. 325–333, Apr. 1992.

[31] V. De Luca, V. Desjacques, G. Franciolini, P. Pani, and A. Riotto, "GW190521 Mass Gap Event and the Primordial Black Hole Scenario," *Phys. Rev. Lett*, vol. 126, p. 051101, Feb. 2021.

[32] P. Amaro-Seoane *et al.*, "Laser Interferometer Space Antenna," *arXiv e-prints*, p. arXiv:1702.00786, Feb. 2017.

[33] T. D. Brandt, "Constraints on MACHO Dark Matter from Compact Stellar Systems in Ultra-faint Dwarf Galaxies," *The Astrophysical Journal*, vol. 824, p. L31, June 2016.

[34] N. Bellomo, J. L. Bernal, A. Raccanelli, and L. Verde, "Primordial black holes as dark matter: converting constraints from monochromatic to extended mass distributions," *Journal of Cosmology and Astroparticle Physics*, vol. 2018, p. 004, Jan. 2018.

[35] B. Carr, F. Kühnel, and M. Sandstad, "Primordial black holes as dark matter," *Phys. Rev. D*, vol. 94, p. 083504, Oct 2016.

[36] B. Carr, M. Raidal, T. Tenkanen, V. Vaskonen, and H. Veermäe, "Primordial black hole constraints for extended mass functions," *Phys. Rev. D*, vol. 96, p. 023514, July 2017.

[37] V. Atal, A. Sanglas, and N. Triantafyllou, "LIGO/Virgo black holes and dark matter: the effect of spatial clustering," *Journal of Cosmology and Astroparticle Physics*, vol. 2020, p. 036, Nov. 2020.

[38] S. Sugiyama, T. Kurita, and M. Takada, "On the wave optics effect on primordial black hole constraints from optical microlensing search," *Monthly Notices of the Royal Astronomical Society*, vol. 493, pp. 3632–3641, Apr. 2020.

[39] A. M. Green and B. J. Kavanagh, "Primordial black holes as a dark matter candidate," *Journal of Physics G Nuclear Physics*, vol. 48, p. 043001, Apr. 2021.

[40] F. Capela, M. Pshirkov, and P. Tinyakov, "Constraints on primordial black holes as dark matter candidates from capture by neutron stars," *Phys. Rev. D*, vol. 87, p. 123524, Jun 2013.

[41] F. Capela, M. Pshirkov, and P. Tinyakov, "Constraints on primordial black holes as dark matter candidates from star formation," *Phys. Rev. D*, vol. 87, p. 023507, Jan 2013.

[42] A. Escrivà, "PBH formation from spherically symmetric hydrodynamical perturbations: a review," *arXiv e-prints*, p. arXiv:2111.12693, Nov. 2021.

[43] M. Sasaki, T. Suyama, T. Tanaka, and S. Yokoyama, "Primordial black holes—perspectives in gravitational wave astronomy," *Classical and Quantum Gravity*, vol. 35, p. 063001, Mar. 2018.

[44] A. Escrivà, C. Germani, and R. K. Sheth, "Universal threshold for primordial black hole formation," *Phys. Rev. D*, vol. 101, p. 044022, Feb. 2020.

[45] K. Inomata, M. Kawasaki, K. Mukaida, and T. T. Yanagida, "Double inflation as a single origin of primordial black holes for all dark matter and LIGO observations," *Phys. Rev. D*, vol. 97, p. 043514, Feb. 2018.

[46] B. Carr, S. Clesse, J. Garcia-Bellido, and F. Kuhnel, "Cosmic Conundra Explained by Thermal History and Primordial Black Holes," *arXiv e-prints*, p. arXiv:1906.08217, June 2019.

[47] J. Fuller and L. Ma, "Most black holes are born very slowly rotating," *The Astrophysical Journal*, vol. 881, p. L1, aug 2019.

[48] S. Ekström *et al.*, "Grids of stellar models with rotation. I. Models from 0.8 to 120 $M_\odot$ at solar metallicity (Z = 0.014)," *Astronomy & Astrophysics*, vol. 537, p. A146, Jan. 2012.

[49] T. Harada, C.-M. Yoo, K. Kohri, and K.-I. Nakao, "Spins of primordial black holes formed in the matter-dominated phase of the Universe," *Phys. Rev. D*, vol. 96, p. 083517, Oct. 2017.

[50] Planck Collaboration, "Planck 2018 results. X. Constraints on inflation," *Astronomy & Astrophysics*, vol. 641, p. A10, Sept. 2020.

[51] S. Bird, H. V. Peiris, M. Viel, and L. Verde, "Minimally parametric power spectrum reconstruction from the Lyman alpha forest," *Monthly Notices of the Royal Astronomical Society*, vol. 413, pp. 1717–1728, 05 2011.

[52] "Pbhbounds." `https://github.com/bradkav/PBHbounds`. Accessed: 2022-01-08.

[53] F. De Paolis, M. Giordano, G. Ingrosso, L. Manni, A. Nucita, and F. Strafella, "The scales of gravitational lensing," *Universe*, vol. 2, no. 1, 2016.

[54] M. Sasaki, "Cosmological Gravitational Lens Equation: Its Validity and Limitation," *Progress of Theoretical Physics*, vol. 90, pp. 753–781, 09 1993.

[55] H. Niikura *et al.*, "Microlensing constraints on primordial black holes with Subaru/HSC Andromeda observations," *Nature Astronomy*, vol. 3, pp. 524–534, Apr. 2019.

[56] A. Katz, J. Kopp, S. Sibiryakov, and W. Xue, "Femtolensing by dark matter revisited," *Journal of Cosmology and Astro-Particle Physics*, vol. 2018, p. 005, Dec 2018.

[57] J. A. Dror, H. Ramani, T. Trickle, and K. M. Zurek, "Pulsar timing probes of primordial black holes and subhalos," *Phys. Rev. D*, vol. 100, p. 023003, Jul 2019.

[58] M. C. LoPresto, "Some simple black hole thermodynamics," *The Physics Teacher*, vol. 41, no. 5, pp. 299–301, 2003.

[59] G. Ballesteros, J. Coronado-Blázquez, and D. Gaggero, "X-ray and gamma-ray limits on the primordial black hole abundance from Hawking radiation," *Physics Letters B*, vol. 808, p. 135624, Sept. 2020.

[60] A. Coogan, L. Morrison, and S. Profumo, "Direct detection of hawking radiation from asteroid-mass primordial black holes," *Phys. Rev. Lett.*, vol. 126, p. 171101, Apr 2021.

[61] J. H. MacGibbon, "Can Planck-mass relics of evaporating black holes close the Universe?," *Nature*, vol. 329, pp. 308–309, Sept. 1987.

[62] W. M. Farr, S. Stevenson, M. C. Miller, I. Mandel, B. Farr, and A. Vecchio, "Distinguishing spin-aligned and isotropic black hole populations with gravitational waves," *Nature*, vol. 548, pp. 426–429, Aug. 2017.

[63] M. Safarzadeh, W. M. Farr, and E. Ramirez-Ruiz, "A trend in the effective spin distribution of LIGO binary black holes with mass," *The Astrophysical Journal*, vol. 894, p. 129, may 2020.

[64] B. P. Abbott *et al.*, "GW150914: Implications for the Stochastic Gravitational-Wave Background from Binary Black Holes," *Phys. Rev. Lett.*, vol. 116, p. 131102, Apr. 2016.

[65] P. A. Rosado, P. D. Lasky, E. Thrane, X. Zhu, I. Mandel, and A. Sesana, "Detectability of gravitational waves from high-redshift binaries," *Phys. Rev. Lett.*, vol. 116, p. 101102, Mar 2016.

[66] J. Baker *et al.*, "The Laser Interferometer Space Antenna: Unveiling the Millihertz Gravitational Wave Sky," *arXiv e-prints*, p. arXiv:1907.06482, July 2019.

[67] S. Mukherjee, M. S. P. Meinema, and J. Silk, "Prospects of discovering sub-solar primordial black holes using the stochastic gravitational wave background from third-generation detectors," *arXiv e-prints*, p. arXiv:2107.02181, July 2021.

[68] D. Baumann, P. Steinhardt, K. Takahashi, and K. Ichiki, "Gravitational wave spectrum induced by primordial scalar perturbations," *Phys. Rev. D*, vol. 76, p. 084019, Oct 2007.

[69] S. S. Bavera, G. Franciolini, G. Cusin, A. Riotto, M. Zevin, and T. Fragos, "Stochastic gravitational-wave background as a tool to investigate multi-channel astrophysical and primordial black-hole mergers," *arXiv e-prints*, p. arXiv:2109.05836, Sept. 2021.

[70] N. Bartolo, V. De Luca, G. Franciolini, A. Lewis, M. Peloso, and A. Riotto, "Primordial Black Hole Dark Matter: LISA Serendipity," *Phys. Rev. Lett*, vol. 122, p. 211301, May 2019.

[71] A. M. Green, "Microlensing and dynamical constraints on primordial black hole dark matter with an extended mass function," *Phys. Rev. D*, vol. 94, p. 063530, Sept. 2016.

[72] P. Montero-Camacho, X. Fang, G. Vasquez, M. Silva, and C. M. Hirata, "Revisiting constraints on asteroid-mass primordial black holes as dark matter candidates," *arXiv e-prints*, June 2019.

[73] F. Capela, M. Pshirkov, and P. Tinyakov, "Adiabatic contraction revisited: Implications for primordial black holes," *Phys. Rev. D*, vol. 90, p. 083507, Oct 2014.

[74] S. Chandrasekhar, "Brownian Motion, Dynamical Friction, and Stellar Dynamics," *Reviews of Modern Physics*, vol. 21, pp. 383–388, Jul 1949.

[75] J. F. Navarro, C. S. Frenk, and S. D. M. White, "A Universal Density Profile from Hierarchical Clustering," *The Astrophysical Journa*, vol. 490, pp. 493–508, Dec. 1997.

[76] E. L. Łokas and G. A. Mamon, "Properties of spherical galaxies and clusters with an NFW density profile," *Monthly Notices of the Royal Astronomical Society*, vol. 321, pp. 155–166, Feb. 2001.

[77] A. Stacy, V. Bromm, and A. T. Lee, "Building up the Population III initial mass function from cosmological initial conditions," *Monthly Notices of the Royal Astronomical Society*, vol. 462, pp. 1307–1328, Oct. 2016.

[78] J. Dutta, S. Sur, A. Stacy, and J. S. Bagla, "Modeling the Survival of Population III Stars to the Present Day," *The Astrophysical Journal*, vol. 901, p. 16, Sept. 2020.

[79] L. R. Prole, P. C. Clark, R. S. Klessen, and S. C. O. Glover, "Fragmentation induced starvation in Population III star formation: a resolution study," *arXiv e-prints*, p. arXiv:2112.10800, Dec. 2021.

[80] B. Paxton *et al.*, "Modules for Experiments in Stellar Astrophysics (MESA): Binaries, Pulsations, and Explosions," *The Astrophysical Journal*, vol. 220, p. 15, Sept. 2015.

[81] M. A. Abramowicz *et al.*, "No Observational Constraints from Hypothetical Collisions of Hypothetical Dark Halo Primordial Black Holes with Galactic Objects," *The Astrophysical Journa*, vol. 705, pp. 659–669, Nov 2009.

[82] E. C. Ostriker, "Dynamical Friction in a Gaseous Medium," *The Astrophysical Journal*, vol. 513, pp. 252–258, Mar 1999.

[83] D. Thun, R. Kuiper, F. Schmidt, and W. Kley, "Dynamical friction for supersonic motion in a homogeneous gaseous medium," *Astronomy & Astrophysics*, vol. 589, p. A10, May 2016.

[84] M. Roncadelli, A. Treves, and R. Turolla, "Primordial black holes are again on the limelight," *arXiv e-prints*, p. arXiv:0901.1093, Jan 2009.

[85] C. Bambi, D. Spolyar, A. D. Dolgov, K. Freese, and M. Volonteri, "Implications of primordial black holes on the first stars and the origin of the super-massive black holes," *Monthly Notices of the Royal Astronomical Society*, vol. 399, pp. 1347–1356, Nov 2009.

[86] D. Markovic, "Evolution of a primordial black hole inside a rotating solar-type star," *Monthly Notices of the Royal Astronomical Society*, vol. 277, pp. 25–35, Nov. 1995.

[87] M. Cappellari, "Structure and Kinematics of Early-Type Galaxies from Integral Field Spectroscopy," *Annual Review of Astronomy and Astrophysics*, vol. 54, pp. 597–665, Sept. 2016.

[88] D. F. Torres and L. A. Anchordoqui, "Astrophysical origins of ultrahigh energy cosmic rays," *Reports on Progress in Physics*, vol. 67, pp. 1663–1730, Sept. 2004.

[89] M. J. Rees, "Black Hole Models for Active Galactic Nuclei," *Annual Review of Astronomy and Astrophysics*, vol. 22, pp. 471–506, Jan. 1984.

[90] S. Cantalupo, "Gas Accretion and Giant Lyα Nebulae," in *Gas Accretion onto Galaxies* (A. Fox and R. Davé, eds.), vol. 430 of *Astrophysics and Space Science Library*, p. 195, Jan. 2017.

[91] H. Nussbaumer and W. Schmutz, "The hydrogenic 2s-1s two-photon emission," *Astronomy & Astrophysics*, vol. 138, p. 495, Sept. 1984.

[92] S. Cantalupo, C. Porciani, and S. J. Lilly, "Mapping Neutral Hydrogen during Reionization with the Lyα Emission from Quasar Ionization Fronts," *The Astrophysical Journal*, vol. 672, pp. 48–58, Jan. 2008.

[93] S. Cantalupo, F. Arrigoni-Battaia, J. X. Prochaska, J. F. Hennawi, and P. Madau, "A cosmic web filament revealed in Lyman-α emission around a luminous high-redshift quasar," *Nature*, vol. 506, pp. 63–66, Feb. 2014.

[94] F. A. Battaia, J. F. Hennawi, S. Cantalupo, and J. X. Prochaska, "THE STACKED LYαEMISSION PROFILE FROM THE CIRCUM-GALACTIC MEDIUM OFz$\sim$ 2 QUASARS," *The Astrophysical Journal*, vol. 829, p. 3, sep 2016.

[95] R. A. C. Croft, J. Miralda-Escudé, Z. Zheng, M. Blomqvist, and M. Pieri, "Intensity mapping with SDSS/BOSS Lyman-alpha emission, quasars, and their Lyman-alpha forest," *Monthly Notices of the Royal Astronomical Society*, vol. 481, pp. 1320–1336, 08 2018.

[96] R. A. C. Croft *et al.*, "Large-scale clustering of Lyman alpha emission intensity from SDSS/BOSS," *Monthly Notices of the Royal Astronomical Society*, vol. 457, pp. 3541–3572, 01 2016.

[97] A. J. Cenarro *et al.*, "J-PLUS: The Javalambre Photometric Local Universe Survey," *Astronomy & Astrophysics*, vol. 622, p. A176, Feb. 2019.

[98] D. J. Eisenstein *et al.*, "SDSS-III: Massive Spectroscopic Surveys of the Distant Universe, the Milky Way, and Extra-Solar Planetary Systems," *The Astronomical Journal*, vol. 142, p. 72, Sept. 2011.

[99] N. Benitez *et al.*, "J-PAS: The Javalambre-Physics of the Accelerated Universe Astrophysical Survey," *arXiv e-prints*, p. arXiv:1403.5237, Mar. 2014.

[100] J. Varela and D. Cristóbal-Hornillos, "Calibration Procedures Of J-Plus Images," in *Early Data Release and Scientific Exploitation of the J-PLUS Survey*, p. 4, Oct. 2017.

[101] C. López-Sanjuan *et al.*, "J-PLUS: photometric calibration of large-area multi-filter surveys with stellar and white dwarf loci," *Astronomy & Astrophysics*, vol. 631, p. A119, Nov. 2019.

[102] G. M. Green *et al.*, "Galactic reddening in 3D from stellar photometry - an improved map," *Monthly Notices of the Royal Astronomical Society*, vol. 478, pp. 651–666, July 2018.

[103] E. F. Schlafly *et al.*, "The Optical-infrared Extinction Curve and Its Variation in the Milky Way," *The Astrophysical Journal*, vol. 821, p. 78, Apr. 2016.

[104] P. E. Tremblay, H. G. Ludwig, M. Steffen, and B. Freytag, "Spectroscopic analysis of DA white dwarfs with 3D model atmospheres," *Astronomy & Astrophysics*, vol. 559, p. A104, Nov. 2013.

[105] E. Cukanovaite, P. E. Tremblay, B. Freytag, H. G. Ludwig, and P. Bergeron, "Pure-helium 3D model atmospheres of white dwarfs," *Monthly Notices of the Royal Astronomical Society*, vol. 481, pp. 1522–1537, Dec. 2018.

[106] I. Pâris, P. Petitjean, *et al.*, "The Sloan Digital Sky Survey Quasar Catalog: Fourteenth data release," *Astronomy & Astrophysics*, vol. 613, p. A51, May 2018.

[107] Bertin, E. and Arnouts, S., "Sextractor: Software for source extraction," *Astron. Astrophys. Suppl. Ser.*, vol. 117, no. 2, pp. 393–404, 1996.